CESSNA 182B WINDSCREEN MATERIAL MODEL DEVELOPMENT AND FULL SCALE UAS TO AIRCRAFT IMPACT TESTING FACILITY

by

Forrest Jacob Arnold

A thesis submitted in partial fulfillment
of the requirements for the degree

of

Master of Science

in

Mechanical Engineering

MONTANA STATE UNIVERSITY
Bozeman, Montana

May 2020

ACKNOWLEDGEMENTS

I would like to thank Dr. Douglas Cairns and Robb Larson for their guidance through the research process. Dan Samborsky for sharing his material testing expertise. Dr. Kyeongsik Woo for his advice in creation of a material model. I would like to thank ASSURE and the FAA for their support of this research. Finally, I would like to thank my family for their support and encouragement.

TABLE OF CONTENTS

TABLE OF CONTENTS CONTINUED

LIST OF TABLES

LIST OF FIGURES

Figure Page

LIST OF FIGURES CONTINUED

Figure Page

LIST OF FIGURES CONTINUED

Figure Page

LIST OF FIGURES CONTINUED

ABSTRACT

Unmanned Aircraft Systems (UAS) have become popular in the last decade. More than 1.5 million have been registered by the Federal Aviation Administration (FAA) since 2015. In order to understand the risk UAS pose to manned aircraft and make informed regulation decisions, the FAA has created air to air collision studies. As a part of the FAA general aviation air to air collision research, a Cessna 182 windscreen material model and a full scale impact testing facility were required.

A Finite Element Crash Model of a Cessna 182 is in development as a part of the general aviation air to air collision research. The National Institute for Aviation Research at Wichita State University is managing development of the model. In support of that work, an LS-DYNA material model of the Poly(Methyl methacrylate) windscreen was developed. Results from tensile testing at multiple strain rates were used to develop material models using MAT_124 and MAT_187. A model of an impact tower was created to compare the material models to test results. The material models were tuned to better fit the impact tower test results. MAT_187 has more flexible material inputs, which allowed it to outperform MAT_124.

A full scale impact testing facility was developed to support Finite Element model validation and direct testing of UAS to aircraft impact. A slingshot style launcher was designed and built to launch common quadcopter style UAS. Testing has shown that the launcher is capable of 120 knots with the accuracy required to repeatably hit the leading edge of a wing. Additionally, the launch site required a system for instrumented testing to compare experimental results with finite element results. A system was developed to allow flexible fixturing, impact speed and orientation measurement, and inclusion of load cells and strain gauges.

INTRODUCTION

Unmanned Aircraft Systems (UAS) have become popular in recent years. Since starting a registration program in December of 2015, the Federal Aviation Administration (FAA) has registered more than 1.5 million UAS's, with recreational users accounting for 1.1 million registrations [1], [2]. This sudden rise of consumer UAS's has brought questions of their safety. The FAA responded on two fronts; rules and regulations on the use of UAS, and research of the risks UAS pose.

As UAS's first emerged, the FAA created a set of rules and regulations for UAS flight aimed at public safety, including the following rules. UAS users owning a system between 0.55 lbs and 55 lbs must register with the FAA. UAS's must be flown below 400 ft above ground level, within line of sight of the pilot, and not after civil twilight. UAS's have airspace restrictions and must not fly near aircraft, airports, groups of people, or near emergencies. The FAA [2] provides the full set of regulations and free resources informing users of where it is safe and legal to fly.

UAS pilots who follow FAA rules pose little risk to public safety; however, UAS pilots break these rules. The FAA receives more than 100 reports per month of UAS's flying in violation of FAA regulations, often nearby to aircraft. In the published report for October through December of 2019, most of the sightings were reported by pilots flying near an urban area and were often flying above 400 ft or near an airport [2]. UAS sighting have been reported near emergencies as well. The Los Angeles Times [3] reported a UAS sighting which grounded firefighting aircraft fighting the Maria fire in 2019, adding to the more than 20 times that year that UAS had interrupted firefighting. With so many close

encounters between UAS and aircraft, aircraft are increasingly being grounded due to risk of collision.

With a new set of challenges to managing the airspace, the FAA created the UAS Center of Excellence Alliance for System Safety of UAS through Research Excellence (ASSURE). ASSURE is responsible for conducting research providing the FAA with the information required to safely integrate UAS into the National Airspace [4]. Knowing that collisions between aircraft and UAS will likely occur, ASSURE has created air to air collision research projects for commercial aircraft, rotorcraft, and general aviation aircraft. This research will provide important information to the FAA on the risk the UAS pose to manned aircraft. Allowing the FAA to make an informed decision on managing regulation of UAS flight.

Due to the high cost of full scale testing, ASSURE air to air collision studies use a combined approach of finite element analysis and full scale testing. Finite element models are developed of aircraft and UAS using a component level approach. That is, models are developed and validated for individual components, and assembled virtually. Full scale testing is used to confirm the performance of the finite element models. With a database of confirmed models for UAS and aircraft, new combinations of aircraft and UAS can be analyzed virtually, reducing the number of needed full scale tests. This has the added advantage that already developed aircraft models can be used in crash simulation with new UAS designs.

As a part of the ASSURE general aviation air to air collision study, the National Institute of Aviation Research (NIAR) at Wichita State University is managing

development of a finite element model of a Cessna 182. Their work includes reverse engineering of aircraft geometry, generation of meshed component models, virtual assembly of components with contact definition, implementation of material models within the model, and comparing model results with full scale testing for confirmation of the model. In support of model development, Montana State University was tasked with development of an LS-DYNA material model for the windscreen and full scale impact testing. The work presented here focuses on these two major needs in researching crash between general aviation aircraft and UAS.

For use in the finite element model of a Cessna 182 in development, a material model of the windscreen was developed. After extensive research of LS-DYNA material models, two were selected for development and required material testing was identified. For material testing, a windscreen was cut into coupons. Tensile testing was performed across 4 log decades of strain rate, and impact tower testing was performed across the full range of capable impact velocities. Using the tensile testing data, two material models were created. A model of the impact tower was then developed to compare the material models to test data. The two material models were then tuned and validated using the impact tower test data. The models were compared, and the better performing model was provided to NIAR for implementation in a windscreen finite element model. Along with NIAR's work in creating the windscreen model, the final step in the material model development will be validation through full scale crash testing of the windscreen.

A full scale crash test facility was developed in order to perform necessary full scale testing and support finite element model validation. The full scale test facility needed to be

capable of launching quadcopter style UAS velocities common for general aviation aircraft. The facility needed the flexibility to allow for test articles such as wings, struts, tail structure, windscreen, or any other aircraft part of concern. This flexibility required an accurate launcher capable of hitting low profile test articles, and a test fixture capable of easy modification. In support of finite element model validation, the facility needed a flexible instrumentation system to be implemented on the test articles as needed.

THEORETICAL BACKGROUND

Finite Element Method

The Finite Element Method (FEM) is a method for solving engineering problems and mathematical models which can be expressed with partial differential equations. The method has a wide range of application, including heat, fluid, magnetism, and structural analysis. FEM is commonly used in problems where a direct solution is not possible, such as structures with complex geometry. Complex systems are broken down into smaller, finite elements which can be modeled with simple equations. The equations for each finite element are assembled into a system of equations based on their interaction for solution.

Governing Equations for Structural Dynamics

A force balance is generally used for structural problems. For structural dynamics problems, the forces are from acceleration, damping, an internal force, and an external force. For each element, the force balance takes the form of Equation 1. The stiffness matrix [k] and damping matrix [c] may depend on several factors including strain rate and temperature. The system is then assembled into a global system, which takes the form of Equation 2. [5]

$$[m]\{\ddot{d}\} + [c]\{\dot{d}\} + [k]\{d\} = \{f_{ext}\} \quad (1)$$

$$[M]\{\ddot{D}\} + [C]\{\dot{D}\} + [K]\{D\} = \{F_{ext}\} \quad (2)$$

Implicit and Explicit Formulations

Implicit and Explicit formulations are used in solving dynamic FE problems. Implicit formulations use matrix inversion to solve the system of equations together. Implicit solutions are unconditionally stable for linear problems and allow for large time steps [5]. Matrix inversion is computationally expensive and causes implicit formulations to be time consuming for nonlinear and dynamic problems [6]. Implicit formulations are well suited for quasistatic problems, steady state problems, and problems where strain rate does not affect the solution.

Explicit formulations solve each consecutive timestep individually. Explicit formulations are conditionally stable. The time step must be less than the Courant time step, defined as the time it takes an elastic wave to travel through a single element [6]. Time step restrictions cause explicit formulations to be time consuming for problems with highly refined mesh or problems with large time scales [5]. Explicit formulations are well suited for dynamic problems, especially when strain rate effects play a role in solution.

LS-DYNA

LS-DYNA is a commercial finite element solver that specializes in large deformation static and dynamic structural response. The solver has a wide range of capabilities, but is most often used for automotive crash, explosion, and manufacturing analysis. A large constitutive model library is available, allowing an accurate model of a variety of materials. Implicit and explicit solvers are available, though the implicit solver is limited, and the explicit solver is used by default.

In LS-DYNA, the governing equations take the form of Equation 3, where ρ is mass density, N is an interpolation matrix, a is nodal acceleration, B is the strain-displacement matrix, σ is the stress vector, b is the body force vector, t is the traction load vector, v is the volume, and ∂b_1 is the boundary. The summation is of all elements, m, in the system. The first term represents the force due to acceleration. The second term represents an internal force due to strain. The third term represents an internal force due to some body force. The fourth term represents an external force due to a traction on the boundary. Damping forces are not considered. [7]

$$\sum_{m=1}^{n}\left\{\int_{v_m}\rho N^t N a dv+\int_{v_m}B^t\sigma dv-\int_{v_m}\rho N^t b dv-\int_{\partial b_1}N^t t ds\right\}^m=0 \qquad (3)$$

Physical Testing

Finite Element models are data driven, requiring testing data in model input determination as well as confirmation of the results. In determination of the model inputs, material testing is required. Quasistatic tensile testing is usually required. Additional tensile testing at various strain rates is often necessary for materials with strain rate dependence. Some materials require compression, shear, or three point bend testing for accurate results. Additionally, it is an accepted engineering practice to develop a simple coupon scale test to initially validate the material model. A coupon scale test allows for a large data set, often at much lower cost than full scale testing. Full scale testing should also be applied to fully confirm the performance of the model. Once a model is fully

confirmed, it can be applied to new loading cases with a higher degree of confidence in the results.

CESSNA 182B WINDSCREEN IMPACT MODELING AND TESTING

LS-DYNA's explicit solver is being utilized for NIAR's Cessna 182 crash model. In creation of the model, an appropriate LS-DYNA material model was required for each component. This chapter focuses on development of the windscreen material model. Covering the process from determining appropriate material models through confirmation testing with a simple impact test.

PMMA Material Testing Literature Review

A literature review was performed for material testing of PMMA. Test data that included various strain rates of tensile and compressive testing was required.

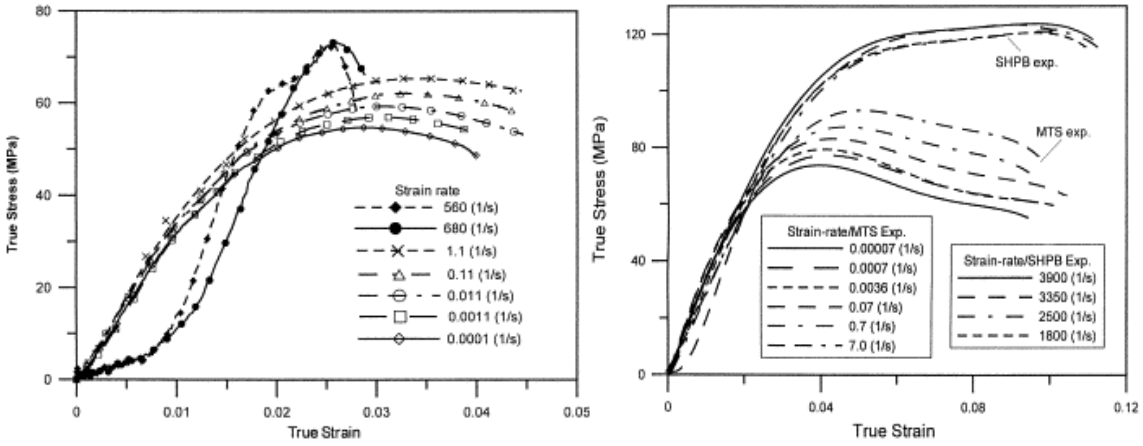

Figure 1. PMMA in tension (left) and compression (right) at various strain rate [8]

Chen [8] tested PMMA in tension and compression across a range of strain rates. Testing below strain rates of 10 1/s were performed with a hydraulically driven test frame. High strain rate testing was performed with a split Hopkinson pressure bar. Testing showed PMMA has different behavior in tension and compression as well as strain rate dependence. Ultimate strength in both tension and compression increased with increased

strain rate, as shown in Figure 2. Ultimate tensile strength increased in a linearly compared to log of strain rate, with an R^2 value on fit of 0.997. Ultimate compressive strength increased when compared strain rate, but a log linear fit did not fit the data as well with an R^2 value of 0.934. In tension, strain to failure did not change between quasi-static and a strain rate of 1.1 1/s; however, the breaking strain at strain rates of 580 1/s and 680 1/s were much lower than in testing at lower strain rates (Figure 1). In compression, strain to failure did not show relation to strain rate. The elastic behavior was nonlinear, and increased in stiffness with strain rate. Stiffness did not show dependence on loading direction.

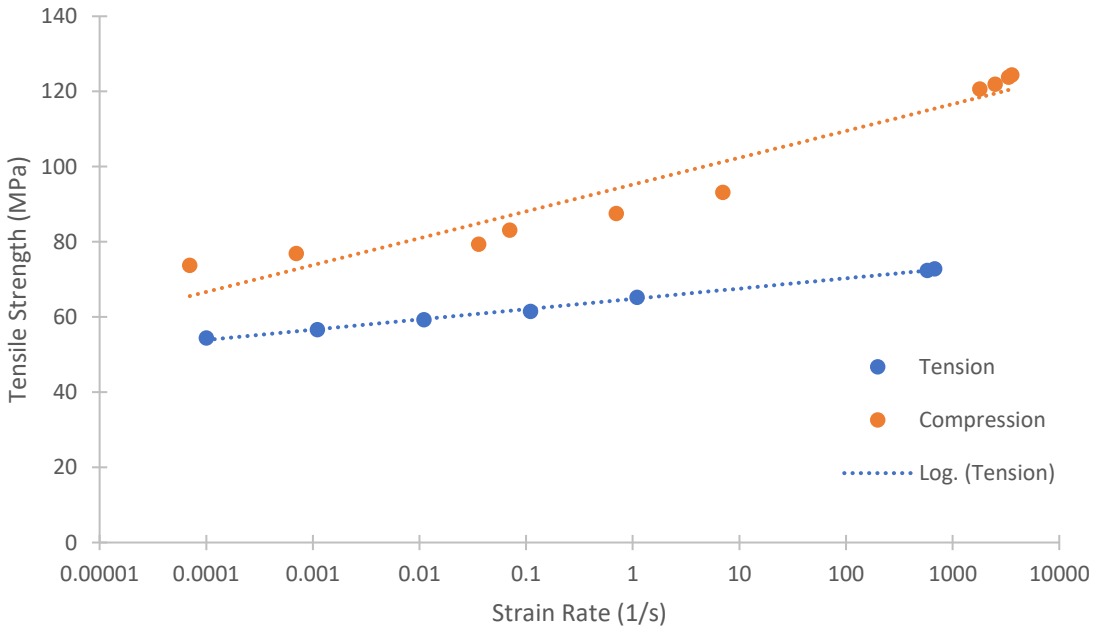

Figure 2. Ultimate tensile and compressive strength compared to natural log of strain rate (Chen, 2002)

LS DYNA Polymer Material Models

LS DYNA has more than 100 material models that defines the materials stress-strain response in the model. These material models vary greatly. Ranging from a linear elastic response without failure to complex strain rate dependent stiffness, yield, and failure responses. Due to the wide range of models, care must be taken to choose an appropriate model for the material. To begin selection, material behavior must be characterized. PMMA has a nonlinear elasto-plastic response with strain rate dependence, behavior that is important for the material model to accurately represent.

The literature review has shown that PMMA has nonlinear elastic behavior followed by nonlinear elasto-plastic behavior under loading. Few material models allow for input of nonlinear elastic behavior, so this behavior was not used to limit model selection. A number of material models are available that allow for input of nonlinear elasto-plastic behavior, so this behavior was used to limit model selection.

Within nonlinear elasto-plastic material models, LS-DYNA has many material models that have strain rate hardening inputs. Many of these models utilize a Cowper-Symonds hardening curve. Cowper-Symonds is commonly used in modeling metals; however, the hardening behavior does not match well with polymers [9]. In order to more accurately model the hardening behavior of PMMA, material model selection was limited to models that allow user defined hardening behavior.

Material models MAT_24, MAT_89, MAT_124, and MAT_187 meet these requirements and were investigated in depth as options to model PMMA. Behavior of the material models is outlined in the list below.

- MAT_24 – PIECEWISE_LINEAR_PLASTICITY
    - Linear elastic zone independent of strain rate
    - Three options for yield behavior with strain rate hardening
        - Single base yield curve with Cowper-Symonds hardening
        - Single base yield curve with user defined scaling factor on yield by strain rate
        - Independent yield curves as a function of strain rate
    - Three strain rate formulation options
        - Deviatoric strain rate
        - Total strain rate
        - Plastic strain rate
    - Plastic strain to failure independent of strain rate
    - Tension and compression behavior are the same

- MAT_89 – PLASTICITY_POLYMER
    - Non-linear elastic zone dependent on strain rate
    - Two options for yield behavior with strain rate hardening
        - Single base stress-strain curve with user defined scaling factor on yield by strain rate
        - Independent stress-strain curves as a function of strain rate
    - Total strain to failure as a function of strain rate
    - Total strain rate formulation
    - Strain rate filtering option
    - Tension and compression behavior are the same

- MAT_124 – PLASTICITY_COMPRESSION_TENSION
    - Linear elastic zone independent of strain rate
        - Separate tension and compression elastic modulus
    - Two options for yield behavior with strain rate hardening
        - Option 1

                - Single base yield curve in tension
                - Single base yield curve in compression
                - Cowper-Symonds strain rate hardening
            - Option 2
                - Single base yield curve in tension
                - Single base yield curve in compression
                - User defined scaling factor on yield by strain rate for tension
                - User defined scaling factor on yield by strain rate for compression
    - Three strain rate formulation options
        - Deviatoric strain rate
        - Total strain rate
        - Plastic strain rate
    - Plastic strain to failure as a function of strain rate of optional formulation
        - Plastic strain rate
        - Effective strain rate
    - Tension and compression behaviors are independent

- MAT_187 – SAMP-1 (Semi-Analytical Model for Polymers)
    - Linear elastic zone with strain rate dependence
    - Yield behavior with strain rate hardening
        - Independent tension yield curves as a function of strain rate
        - Additional optional yield curves inputs from quasistatic testing. A hardening curve is derived from the tension input table and applied to these inputs. Any combination of these can be used.
            - Compression
            - Shear
            - Biaxial

        - User defined plastic Poisson's ratio. Optional input of plastic Poisson's ratio as a function of strain rate.
        - Damage parameter as a function of plastic strain with option for dependence on triaxiality
    - Plastic strain to failure as a function of plastic strain rate
    - Strain rate filtering
    - Tension and compression yield behavior is different, but not completely independent

Ultimately, inputs for each of these material models were developed to understand how well the material model could represent the stress-strain response of PMMA. All of these material models were able to represent the behavior of PMMA in tension adequately to warrant further development; however, the material model was in development for PMMA in bending. Since PMMA is stronger in compression than tension, a material model based only on tensile data would underpredict strength in bending. A material model based only on compression data would overpredict strength in bending. A material model with independent tension and compression yield behavior would be able to accurately predict strength in bending. With that in mind, model choices were further limited to the material models with different tension and compression behavior, leaving MAT_124 and MAT_187.

As outlined above, MAT_124 and MAT_187 have different features. MAT_187 is a more flexible material model. Independent yield curves as a function of strain rate allowed with MAT_187 could be important if the material has a distinct ductile-brittle transition. This behavior is seen in PMMA tensile data, shown in Figure 1, between strain rates of 1.1 1/sec and 580 1/sec. Stiffness as a function of strain rate, also available only

with MAT_187 can also be observed in the tensile data, though the changes are small and may not affect results. MAT_124 allows for a separate hardening curve for tension and compression, while MAT_187 does not. Separate hardening curves could be important due to the loading direction dependent hardening behavior shown in Figure 2. MAT_187 has many other features that allow it to model complex behavior, but the extent of material testing to develop these inputs is prohibitive.

MAT_124 and MAT_187 have drawbacks that could make an accurate model difficult. For both material models, plastic strain to failure in tension and compression are equal. The tensile and compressive test data, shown in Figure 1, show that PMMA has a much higher strain to failure in compression. Additionally, PMMA is non-linear in the elastic zone, but both material models only allow linear inputs for elastic response. Meaning that the material model response is linear up to the beginning of yield. The only way to determine which of these features and drawbacks are critical is to perform material testing, and implement the model.

Stress-strain curves for the material being modeled are used to develop material model inputs. Material testing is required to develop these stress-strain curves. Quasistatic tensile testing is the minimum required for creation of a model. Tensile testing at various strain rates is required to implement rate dependent model options. For further improvement, compression and shear testing is useful. When possible, a manufactured part should be cut into coupons for testing. Ensuring that the material properties of a manufactured part are represented. In some cases, such as when part geometry does not

allow suitable sample creation, this is not possible. In these cases, a sheet of material from the same material manufacturer should be used for coupon level testing.

A coupon level impact test is standard practice for initial model confirmation. The coupon level impact test should represent the full scale problem to ensure that the correct material response is being confirmed. Simple impact testing is important for model validation since it removes model complexity connected to full scale validation testing. The small scale also allows for a large number of tests over a wide range of conditions. Producing a larger data set to compare with the model.

Material Testing

Coupon scale material testing was completed to support material model creation. Tensile testing was performed across a range of strain rates to aid in initial model creation. Three point impact testing was performed across a range of impact velocities to improve and confirm the material model.

Test Setup

Coupon Preparation. A new Cessna 182b windscreen destroyed for testing. The sides of the windscreen were determined to be suitably flat for sample creation. The left side, from a pilot's perspective, of the windscreen was cut into one inch wide strips parallel to the back side edges. The right side of the windscreen was cut into one inch wide strips perpendicular to the back side edges. The left and right sides were cut in orthogonal directions in order to determine whether the mechanical properties of the material showed any directionality. The strips were further divided into 18 tensile coupons and 33 impact

tower coupons. Tensile coupons were cut to 190 mm in length shaped into dog bone samples with 90 mm between the shoulders, a gauge width of 12.7 mm, a grip length of 50.8 mm, and grip width of 25.4 mm using a pin router and template. Impact tower coupons were cut to 127 mm in length and shaped into 22.7 mm wide samples using a pin router and template. Sample thicknesses were unaltered from the windscreen, which ranged in thickness from 5.78 mm to 6.4 mm. All cut surfaces of the samples were polished with 1200 grit sandpaper to remove surface flaws. Sample dimensions were then measured and recorded.

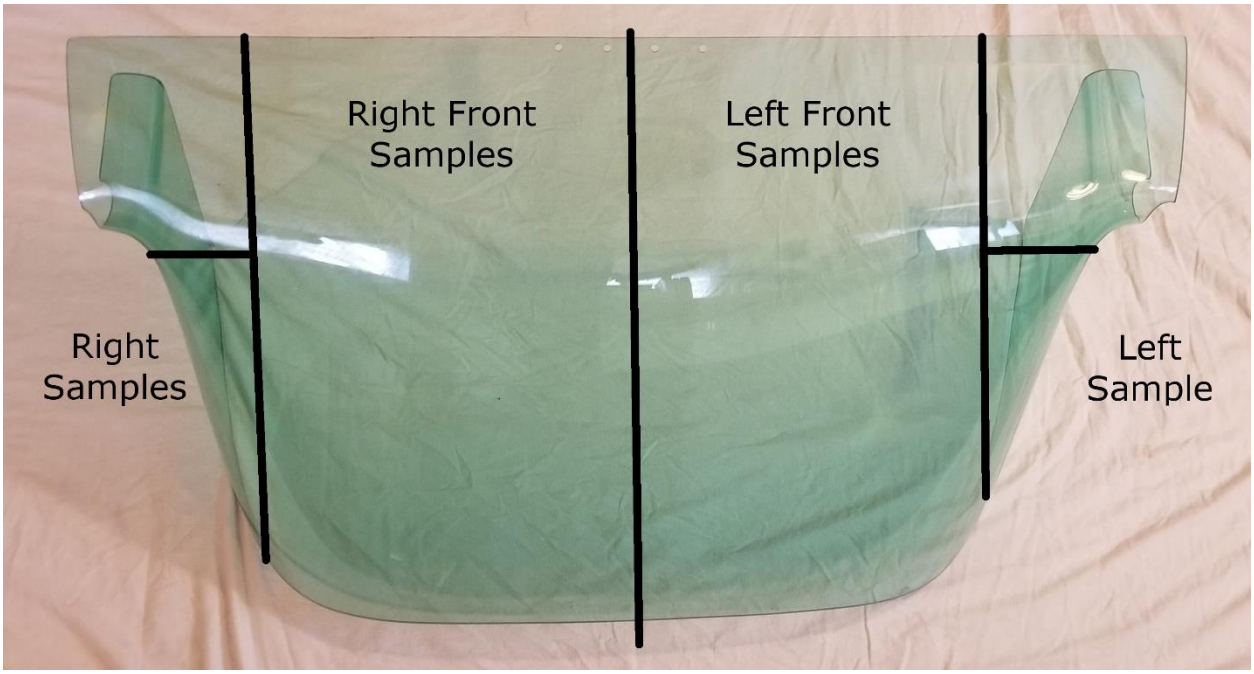

Figure 3. Windscreen with lines indicating sectioning cuts. Directions labeled from a pilot's perspective.

Tensile Testing. Tensile testing was performed with an Instron 8501 mechanical testing machine. A National Instruments NI-9205 was utilized for data acquisition. Load cell, crosshead location, extensometer, and strain gauge outputs were recorded. A sample rate of 1 kHz was used for quasistatic testing. A sample rate of 20 kHz was used for all

other tests. Eighteen tensile coupons were prepared. In all except two tests, a one half inch gauge length Instron dynamic axial clip-on extensometer was utilized. Hot glue was utilized to reduce stress concentration from the extensometer knife edge and reduce slippage. The remaining two samples were strain gauged. The samples were gripped with hydraulic parallel grips.

Figure 4. Tensile testing setup with an extensometer (left) and a strain gauge (right).

Tensile Testing Error. There were a number of factors that contributed to testing error, those sources of error are summarized below.

- NI 9205 DAQ: The NI spec sheet [10] reports a voltage measurement accuracy of 6.23mV. This results in the following possible error.
    - Stress: 0.82 MPa, Less than 1% of the lowest ultimate strength in testing
    - Strain: 25 microstrain, Less than 1% of the lowest strain to failure in testing
- Load Cell error: The load cell used for testing was designed specifically for axial material testing, however some small measurement error is expected.
- Strain Gauge error: The strain gauge used was also designed specifically for dynamic axial material testing, however some small measurement error is expected.

- Sample Geometry: Each sample had some level of curvature. The strain gauged samples give insight into the strain caused by gripping the sample. One of the strain gauged samples was one of the flattest samples, and had a clamping strain of 0.09%. The other strain gauged sample was one of the most curved samples and had a clamping strain of 0.26%. It is expected that the other samples fell somewhere within this range.

Though there was error in the measurement, variability in sample strength and sample curvature were likely the greater cause of variation in results.

Tensile Test Matrix. Eighteen samples were prepared for Tensile testing. The samples were tested at four machine rates, from quasistatic to the machine's maximum extension rate. 0.002 in/sec was selected for quasistatic testing. 5 in/sec was determined to be the maximum machine rate. 0.5 in/sec and 1 in/sec were then determined to fill an evenly spaced log strain rate dataset. Two samples at a machine rate of 5 in/sec were strain gauged, all other samples utilized the extensometer for strain measurement.

Table 1. Tensile Test Matrix

Machine Rate (in/sec)	Total Number of Samples	R Samples	L Samples
0.002	6	3	3
0.05	3	0	3
1	3	1	2
5	6	3	3

Impact Tower Testing. A Dynatup 8200 impact tower was utilized to perform coupon level three point bending impact tests across a range of impact velocities. The sliding impactor had a total mass of 7.762 kg. The impactor head below the force transducer

had a mass of 0.45 kg. The impactor head was wedge shaped with a radius of 3.175 mm on the leading edge was used. See Figure 5, Figure 6, and Figure 7 for test setup and dimensions.

Figure 5. Impact tower setup for testing

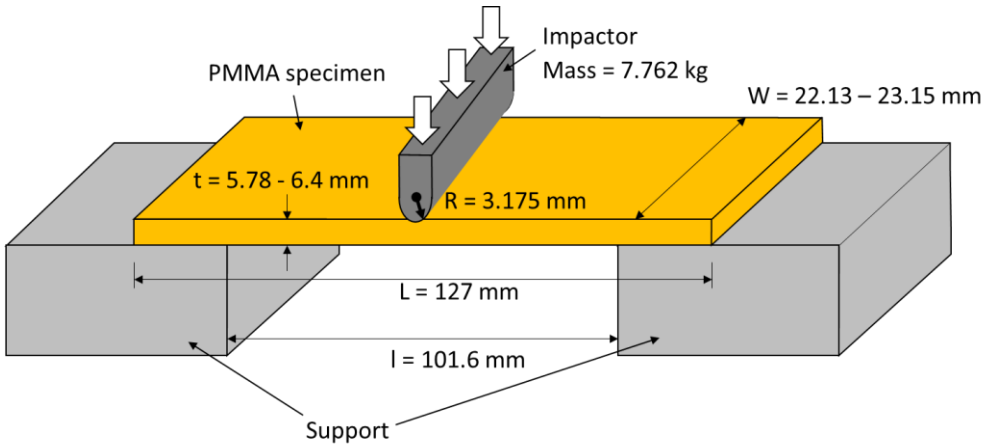

Figure 6. Impact tower dimensions [11]

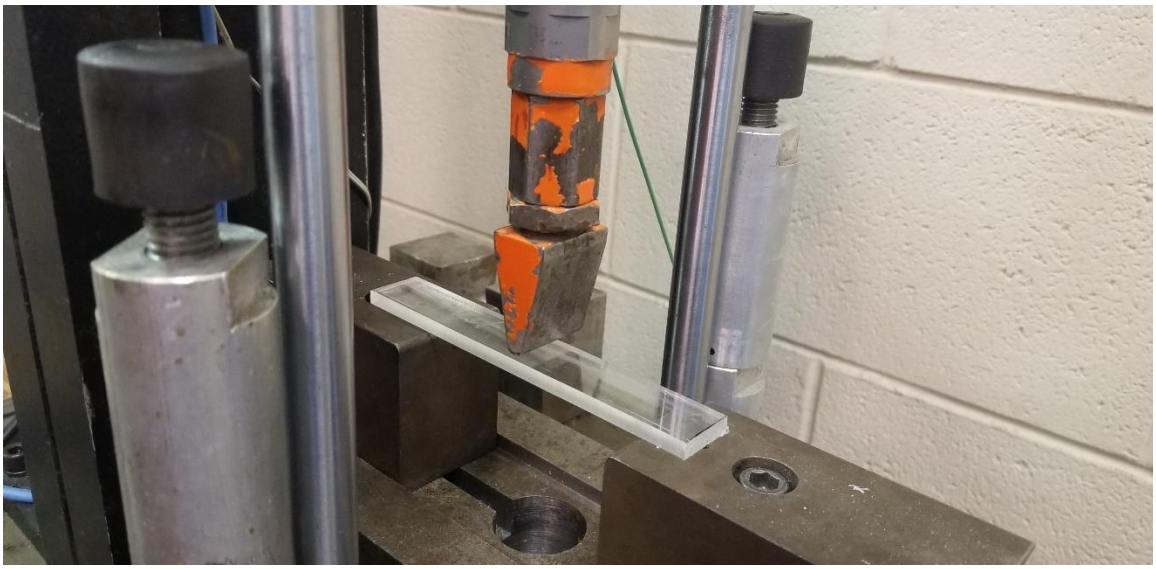

Figure 7. Closeup of Impact tower setup with the impactor head near the sample to show impact orientation

Instrumentation consisted of a Kistler 9041A piezoelectric force transducer placed in line between the impactor head and sliding frame was used to capture impact forces. A Kistler 5010 charge amplifier was used to condition the transducer charge output to a ±10V output. The amplifier time constant was set to medium. The charge conversion was set to 18 pC/lb, the calibrated value for the force transducer. The voltage amplification was set

by drop height, ranging from 30 V/lb to 100 V/lb. A National Instruments NI-9205 was used to record amplifier output voltage at 250 kHz.

Impact Tower Error. There were a number of factors that contributed to testing error, including measurement error and coupon geometry. Measurement error is outlined in the list below.

- Force Transducer Error. The Kistler does not publish accuracy information for their 9041A transducer, however; the force transducer was designed to measure impact loading of this style and magnitude. Since it was designed for testing of this style, error from the transducer was expected to be low. Confirmation testing further increased confidence in the accuracy of the measurement.
- Charge Amplifier Error. Kistler does not publish accuracy information for their 5010 charge amplifier, however; the charge amp was designed to work with this force transducer, for measurement of impact style loading. Since it was designed to work with the specified piezoelectric force transducer in testing of this style, error from the charge amplifier was expected to be low. Confirmation testing further increased confidence in the accuracy of the measurement.
- NI 9205. The NI spec sheet [10] reports a voltage measurement accuracy of 6.23mV. The load measurement error depends on the amplifier settings. For tests with the amp set to 100 lb/V, the voltage measurement accuracy equates to 2.8 N. For tests with the amp set to 30 lb/V, the voltage measurement accuracy equates to 0.8 N.
- Speed Measurement: This was likely the greatest source of error in Energy calculations for two reasons. Kinetic energy is dependent on velocity squared, and therefore error in velocity measurement is squared. Additionally, assumption was made that the impactor fell at constant acceleration, which may not have been the case.

These sources of measurement error were of concern. To increase confidence of the system, a confirmation test with an ERM-FA014o CHARPY V-notch test piece was completed, see Appendix E for the certificate of analysis. The calibrated coupon was certified at 58.7 J with an uncertainty of 1.5 J, the impact tower recorded an impact energy of 58.2 J. Tests were then performed on windscreen coupons.

In addition to measurement error, issues of sample geometry were a concern. All of the test samples had some level of curvature and twist. Placing a sample with center of curvature below the supports would effectively result in a change in length between supports as the sample begins to flex. To remove this variable, the samples were placed with the center of curvature above the supports. Due to coupon twist, it was not possible to have even contact on the supports for all samples. During the test, twisted samples would be straightened by the load of the impactor and supports, causing a mixed mode loading.

In order to account for variation in geometry, and therefore the mixed mode loading, each sample would need to be impact modeled individually. To do so, each sample would need to be 3D scanned and have a CAD model created. Each CAD model would then need to be meshed, and imported into the impact tower model. This would have an enormous time and computational expense. The resulting data set would also be difficult to use to validate the performance of the model, since there would be only one experimental result to compare each model. Due to the added complexity, the samples were treated as flat. This allowed a single model geometry to be run at a range of impact velocities, and compared to the full impact tower data set.

This decision was further supported by testing. While the majority of samples laid near flat on the impact tower supports, three samples were noted for having high levels of twist. If twist was a major issue, these samples would be expected to be outliers. Two of the three samples tested within one standard deviation, near the mean value of impact energy, displacement to failure, and average acceleration during impact. The other sample tested outside of 1 standard deviation for impact energy and average acceleration, but was within one standard deviation for displacement to failure.

Impact Tower Test Matrix. Tests were run with impactor drop heights from 40 mm up to 1800 mm. Based on the range of possible drop heights that caused failure to the sample. The approach used was to create a data set with evenly spaced groups of impact velocity. Three samples were intended to be tested at each group, but in some cases adjustments were made. Adjustments were made when the impact velocity spacing was not as expected, or to increase the sample size at drop heights with greater variance in results. Three samples were originally planned for 40 mm, but the drop height was determined to be too small to cause failure. The remaining two samples were tested at 50 mm. Table 2 includes the number of tests actually performed for each drop height group.

Table 2. Impact Tower Test Matrix

Drop Height (mm)	Number of Tests	Voltage Amplification (lb/V)
40	1	30
50	2	30
60	4	30
100	1	30
125	3	30
200	3	30
300	3	30
500	3	50
700	3	50
1000	3	50
1400	2	100
1800	3	100

Post-Processing

Tensile Testing. Tensile testing produced outputs of crosshead load, crosshead displacement, and strain from either the extensometer or strain gauge. True Stress vs True Strain for each test was required for use in material model creation. The postprocessing steps are laid out below.

1. Signal Processing - Output signals include data before loading began and after coupon failure.
    a. Start of loading was determined by the crosshead displacement reaching 0.001”, data points were added before based on data sampling rate and test crosshead speed to ensure no data points were lost. For example, if the crosshead speed was 1 in/sec and the sample rate 10kHz. The crosshead would move 0.001” in 10 samples; however, the crosshead must accelerate from rest during this period. Assuming that the crosshead accelerates at a

constant rate from rest to the intended speed in 0.001”. The crosshead would move 0.001” in 20 samples. Additionally, an inspection of each signal was conducted, to ensure the crosshead was stationary at that point. Additional data points were included if necessary.

b. The end of loading was found in separate ways for quasistatic and higher rate tests.

    i. For quasistatic tests, the load cell was under low load after failure of the sample, and therefore output a low voltage. The end of loading was determined by a large voltage in load cell output, searching from the end of the signal, moving toward the beginning. Each signal was inspected, and adjustments were made when necessary.

    ii. For higher rate tests, vibration of the load cell at sample failure causes noise in the signal. Two filter options were applied to the signals based on a quick inspection of the signal.

        1. The time of maximum load was used for samples that did not show softening just before failure. Each signal was inspected, and adjustments were made when necessary.

        2. In many tests, failure caused a spike in the extensometer output. In these samples, the time of maximum strain was just after failure. Failure generally occurred two data points

prior to the maximum. Each signal was inspected, and adjustments were made when necessary.

c. Load, displacement, and strain values are zeroed to the average of the 100 data points prior to the start of loading.

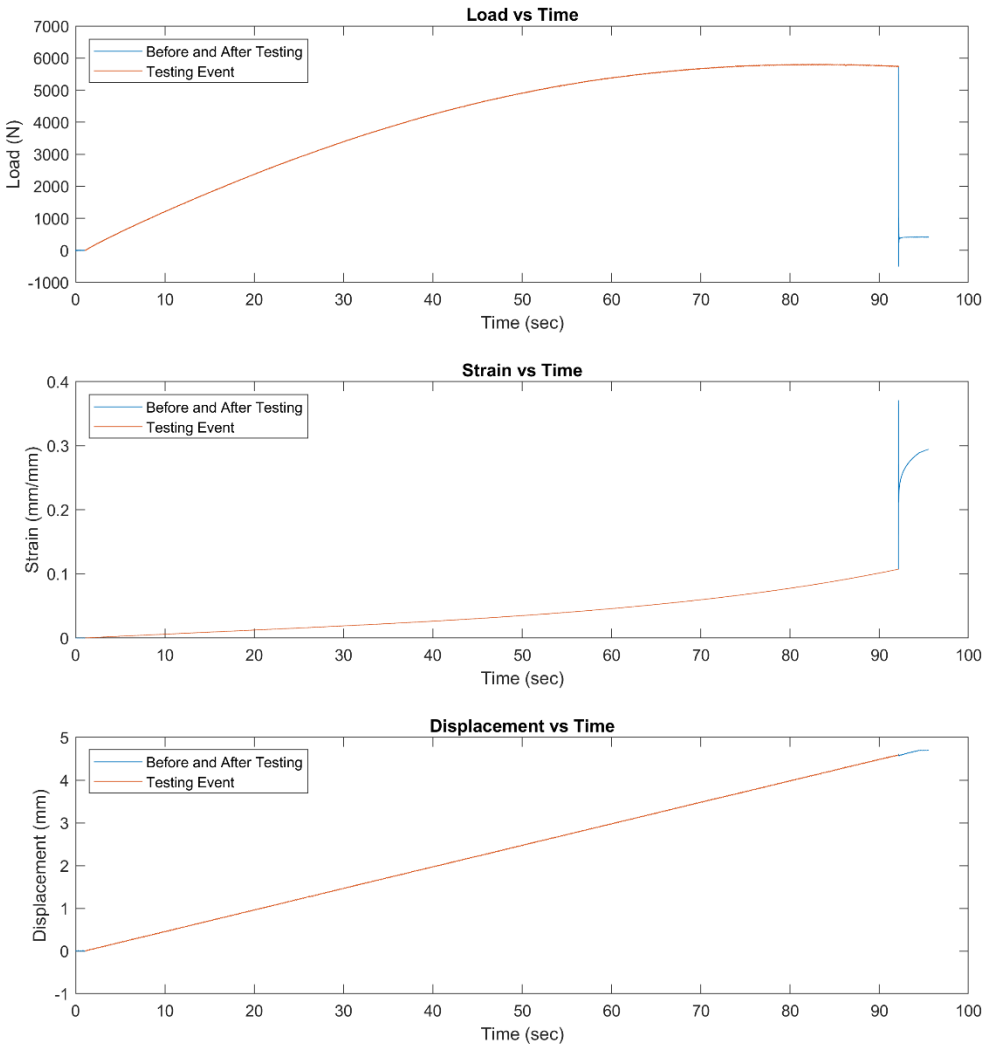

Figure 8. Tensile testing outputs

2. True Stress vs True Strain

    a. Sample dimensions along with load and strain data are used to produce engineering stress-strain curves.

$$\sigma_{\mathrm{eng}} = \mathrm{F}/\mathrm{A}_{\mathrm{cross-sectional}} \quad (4)$$

    b. The analytical solution for true stress and true strain can be used up the ultimate engineering tensile stress of a material [12]. In testing, all samples except for two failed at the ultimate engineering stress, so the analytical solution can be used for those curves. The analytical solution was used for the remaining two curves, with an understanding that the solution is not accurate beyond the engineering ultimate stress.

$$\sigma_{true} = \sigma_{eng}\left(1 + \varepsilon_{eng}\right) \quad (5)$$

$$\varepsilon_{true} = ln\left(1 + \varepsilon_{eng}\right) \quad (6)$$

Impact Tower Testing. Impact tower testing produces a force transducer output. The DAQ maximum sample rate of 250 kHz was selected to provide as much loading data a possible. Energy absorbed during impact for each test is desired. To determine the energy absorbed, kinetic and potential energy of the impactor during impact was analyzed. Acceleration, velocity, and displacement of the impactor were determined through analysis of the force transducer output. The postprocessing steps are laid out below.

1. Signal Processing – Important events in the output signal must be found. The events of interest are the moment freefall begins, the moment of first contact, and the end of the loading event.

    a. A 500 point moving average filter is applied to the signal to reduce noise and make finding voltage changes easier. This filter is used only to find loading events, not for further calculation.

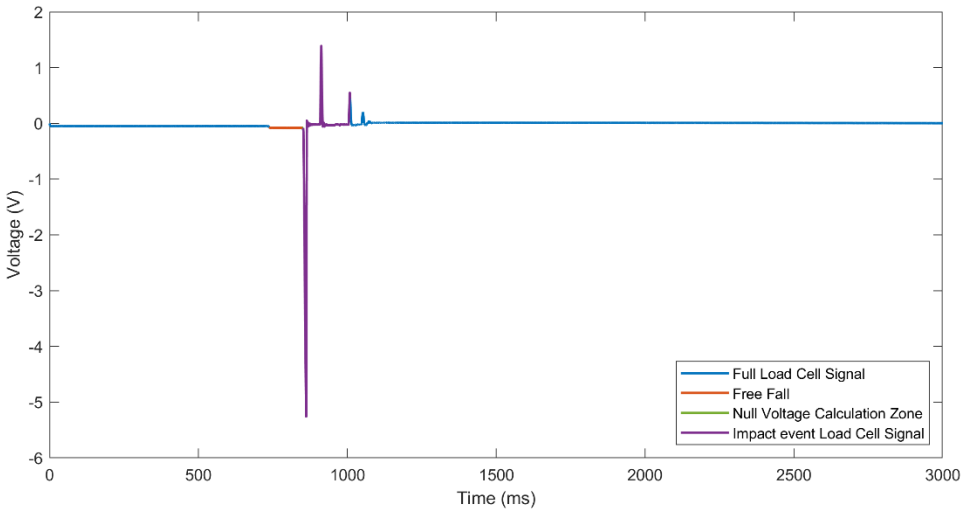

Figure 9. Impact tower force transducer output voltage with moving average filter

    b. The impactor has a striking head below the load cell. The mass of the head causes a tensile load on the load cell while hanging. The tensile load is relieved with freefall, causing a small drop in voltage output, see Figure 10. The voltage was compared to the average of the first 300 data points, when the voltage difference represented a load of 3 N that datapoint was selected as the drop time.

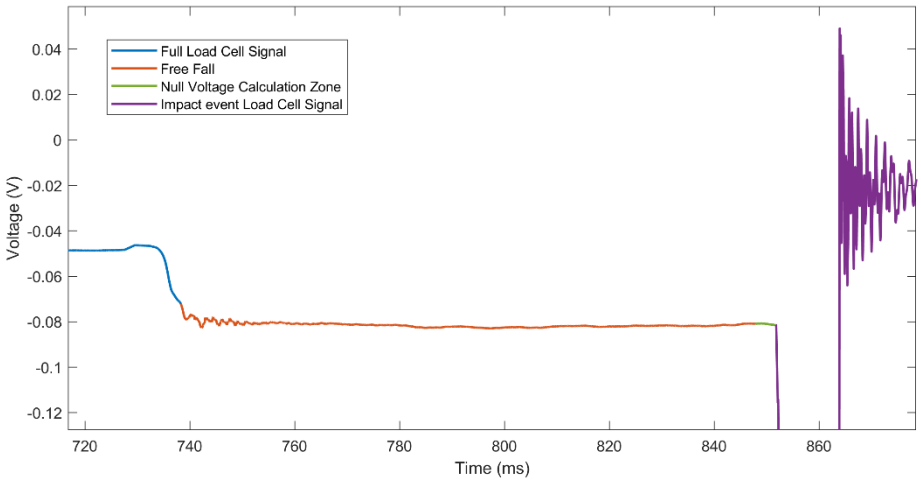

Figure 10. Impact tower force transducer output voltage from free fall to impact

c. Impact causes a large drop in output voltage. A search is conducted for a drop in voltage representing 45 N. The start of impact is marked as 25 data points before the drop in voltage to ensure no data is lost. The load cell is zeroed to the mean of the 100 datapoints prior to impact.

d. A voltage spike occurs as the shoulder of the impactor strikes the rubber stoppers, and the striking head puts a tensile load on the force transducer as it decelerates. A search is conducted for a spike in voltage representing 45 N, starting at the end, moving toward the start. The end of the loading event is marked at that point. The accuracy of this point is not important, it is simply used to trim extra data in further calculations.

2. Energy Absorbed during impact

a. Since the impactor is on slide rails acceleration on release is not equal to gravity. The impactor was assumed to accelerate at a constant rate over the

drop height for the length of free fall, determined in signal processing. The impact velocity was then determined.

$$a_{drop} = 2 * h_{drop}/t_{drop}^2 \quad (7)$$

$$v_{impact} = a_{drop} * t_{drop} \quad (8)$$

Calculated acceleration was compared to gravity, as it should be within 20%, but never greater.

b. Acceleration of the impactor was then calculated. The mass of the full impactor and the impactor head were measured. Due to the arrangement of the impactor, acceleration of the impactor head from impact does not exert a load on the force transducer. Only the mass above the load cell is used in acceleration calculation. Since the force transducer falls with the impactor, and was zeroed during free fall, the total acceleration of the impactor was the acceleration due to the force plus the acceleration due to gravity.

$$F(t) = m * a(t) + m * g \quad (9)$$

$$a(t) = F(t)/m + g \quad (10)$$

c. Velocity and displacement of the impactor was then calculated. The velocity through impact was calculated through cumulative numeric integration of acceleration through impact, with an initial velocity of the impact velocity. Displacement of the impactor through impact was calculated through cumulative numeric integration of velocity through

impact, with an initial displacement of zero. Failure of the sample was determined to be at the time of minimum velocity.

$$v(t) = \int_{t_{impact}}^{t} a(t)dt + v_{impact} \tag{11}$$

$$d(t) = \int_{t_{impact}}^{t} v(t)dt \tag{12}$$

d. Energy absorbed by the sample during impact was the sum of the change in kinetic and potential energy from the beginning of impact until sample failure. The entire impactor was being accelerated by the sample, so the mass used included the impactor head.

$$E_{absorbed} = \Delta E_{kinetic} + \Delta E_{potential} \tag{13}$$

$$E_{absorbed} = \frac{1}{2}m\left(v_{impact}^2 - v_{failure}^2\right) + mg\left(d_{impact} - d_{failure}\right) \tag{14}$$

Results and Discussion

Tensile Testing. Focus of tensile testing results was placed on material behavior that influences material model selection and implementation. Strain rate dependent behavior was of high importance in material model creation. The coupons tested showed strain rate dependence of strength, strain to failure, and elastic modulus.

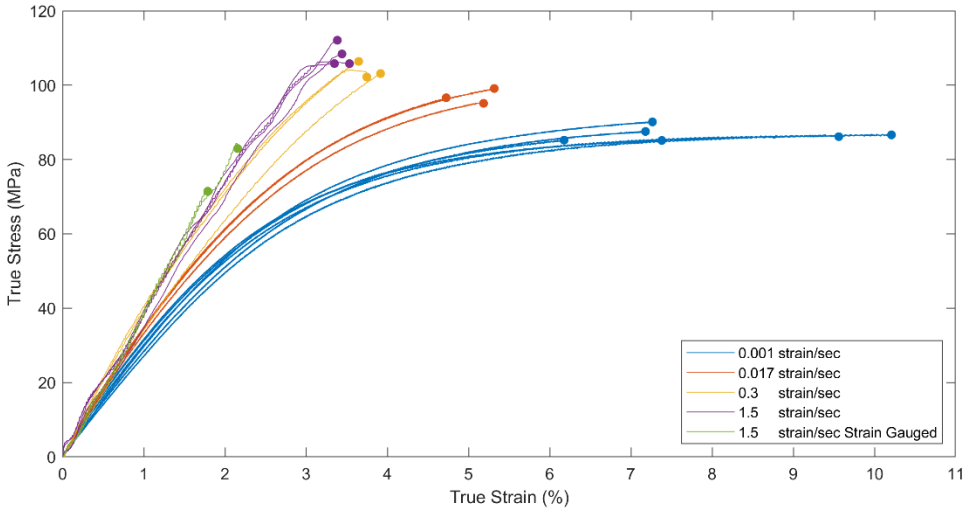

Figure 11. Tensile testing of PMMA at varied strain rate

Two of the eighteen samples were strain gauged. The strain gauged samples failed at a much lower stress and strain than the samples tested with an extensometer. The strain gauged samples followed the same behavior as the extensometer samples of the same strain rate until failure. The strain gauged samples are the only outliers in the data set, and for that reason, they will not be included in discussion of strain rate dependent behavior of the material. The reason for decreased strength of these samples is unknown. More testing would be required to determine the cause of these outliers.

The ultimate tensile strength as well as elastic modulus increased with increased strain rate. A linear fit of ultimate tensile strength vs log strain rate, shown in Figure 12, illustrates the relation. Strain to failure decreased with increased strain rate. Failure occurred between 6% and 11% strain at quasi-static, and transitioned to failing at about 3.5% strain at 1.5 strain/sec.

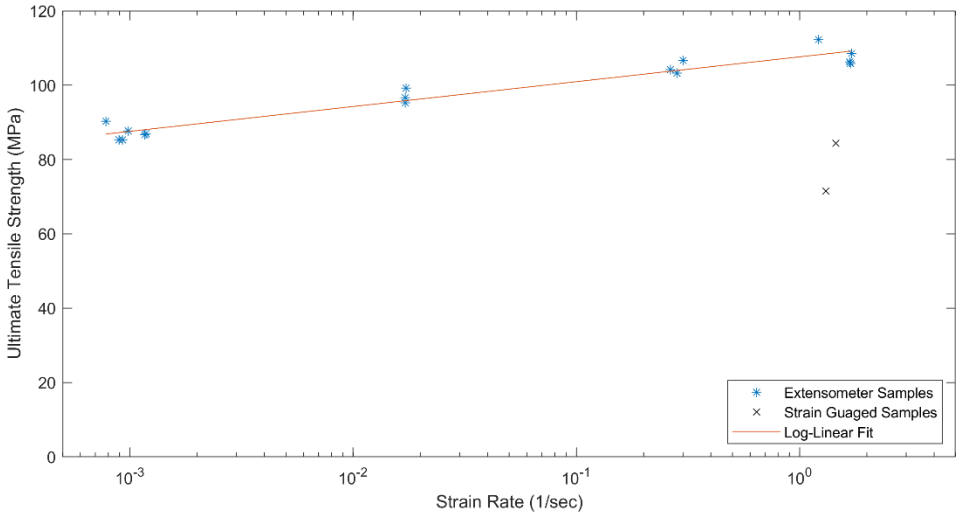

Figure 12. Ultimate tensile strength of PMMA vs strain rate

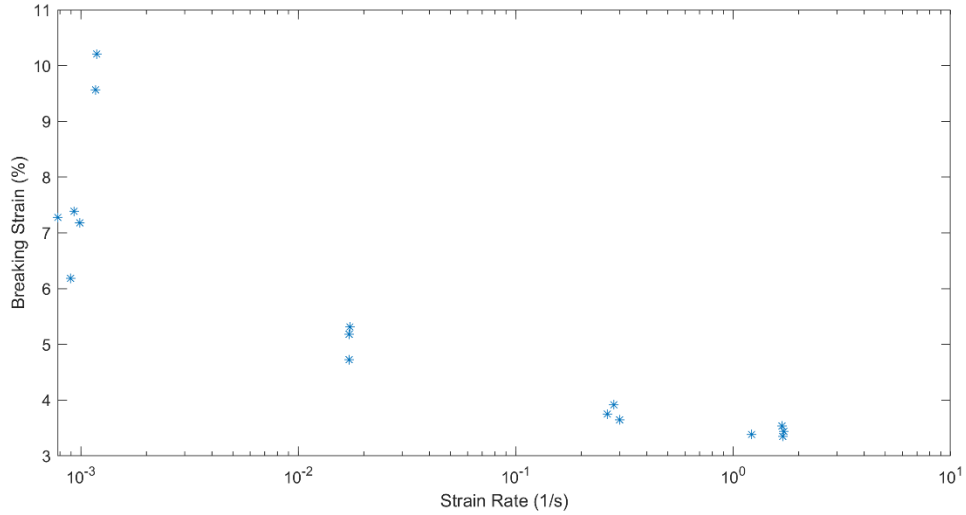

Figure 13. Strain to failure of PMMA vs strain rate

The material did not show directionality. That is, the material did not have any mechanical properties with dependence on orientation as a consequence of the manufacturing of the windscreen. Eleven samples from the left and seven samples from the right were tested. When compared in Figure 14, there is no discernible difference in strength, stiffness, or strain to failure between the right and left samples.

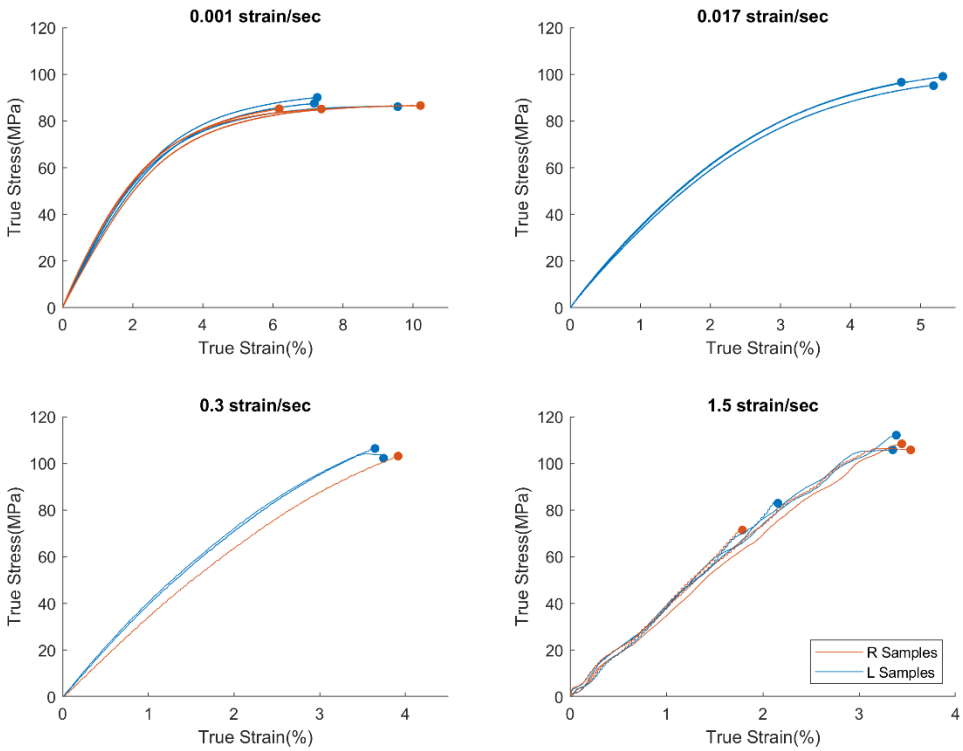

Figure 14. Tensile tests at various strain rates comparing Right samples and Left samples

Impact Tower Testing. Focus of impact tower testing was placed on validation and tuning of the material model. Energy absorbed by the coupon, average acceleration of the impactor, and displacement were used to compare the model to the coupons. Each was plotted against impact velocity, shown in Figure 15. See Appendix B for load cell force vs time and impactor velocity vs time plots for each sample. Coupons tested did not show a correlation between impact velocity and any of these values.

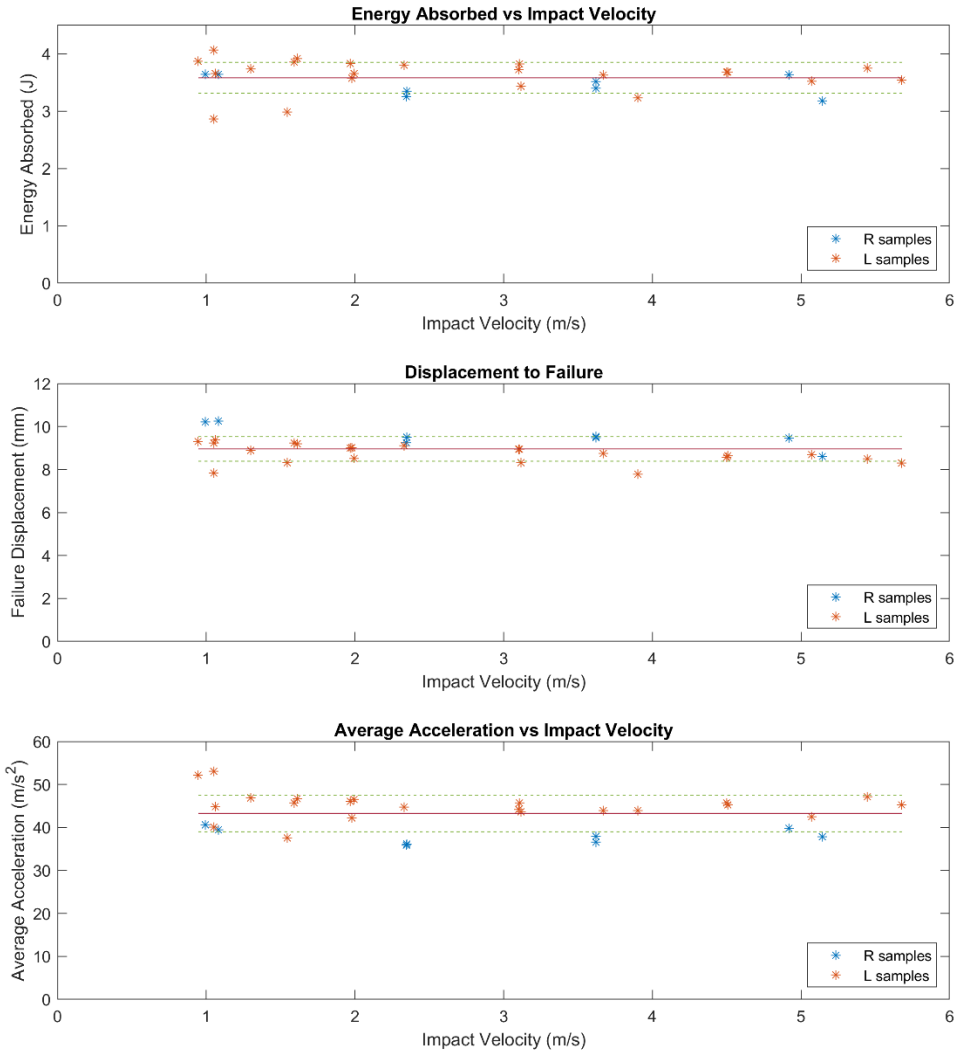

Figure 15. Energy absorbed by the sample during impact (top), displacement of the impactor at sample failure (middle), and average acceleration of the impactor through impact (bottom) with the average and one standard deviation marked

All impact tower samples had crack initiation along the top surface. About two thirds of the coupons had a chip form along the top surface, with a crack propagating downward through the coupon from the chip. The rest had a crack initiate just away from the striker and propagate toward below the striker, then down through the coupon. Impact velocity did not correlate to the failure mode.

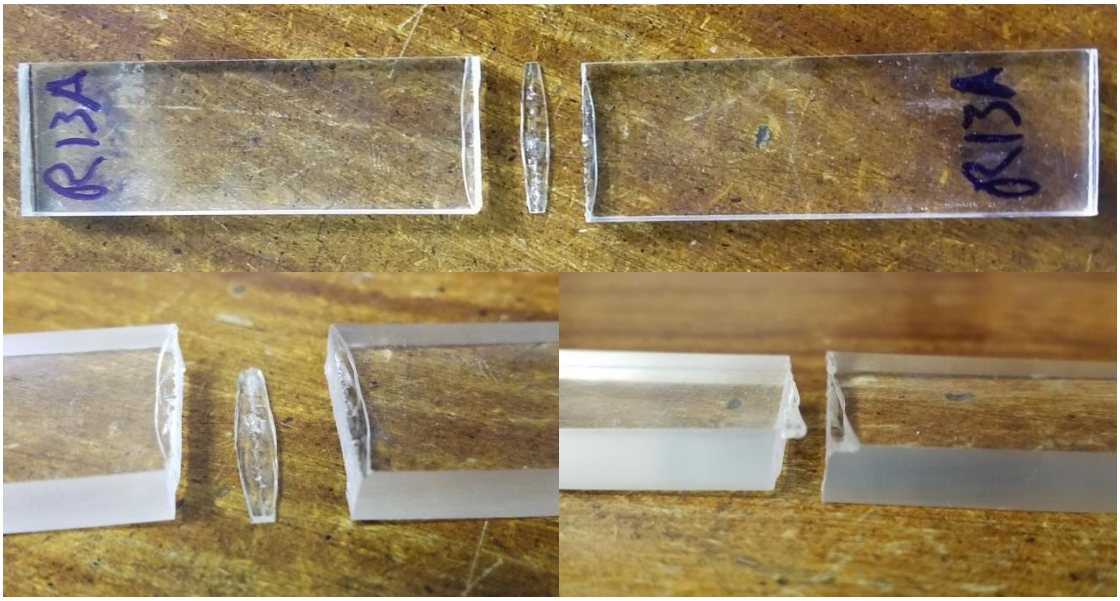

Figure 16. Impact tower coupon failure surfaces

Impact tower samples from the left and right were tested. The right samples showed a lower average acceleration during impact as well as a larger displacement at failure. The left side samples had an average thickness of 6.34 mm while the right side samples had an average thickness of 5.82 mm. The difference in sample thickness was likely the cause of differences in these quantities. There was no clear correlation between energy absorbed in impact and sample group.

Material Model Creation

Material models were developed with both MAT_124 and MAT_187. Required and important inputs for each were identified, outlined in Table 3. Performance of the models was compared with single element tests as well as an impact tower model.

Table 3. Required and important material model inputs [13]

MAT_124	MAT_187
• Mass Density • Poisson's ratio • Elastic Modulus – constant • Yield stress vs Plastic strain base curve in compression • Yield stress vs Plastic strain base curve in tension • Scaling factor of yield stress vs strain rate in compression • Scaling factor of yield stress vs strain rate in tension • Strain rate formulation • Plastic strain at failure vs strain rate	• Mass Density • Poisson's ratio • Bulk Modulus - Time step calculation only • Shear Modulus - Time step calculation only • Elastic Modulus – Base value when strain rate dependent curve is not in effect • Elastic Modulus vs Effective strain rate • Table of Yield stress vs Plastic strain curves in tension with respective strain rates • Yield stress vs Plastic strain in compression at quasistatic • Plastic Poisson's ratio • Plastic strain at failure vs plastic strain rate • Decay constant in viscoelastic law – bug does not allow this value to be 0 when strain rate dependent elastic modulus option is selected • Strain rate filtering factor

Calculation of Inputs from Tensile Data

Inputs of Mass Density and Poisson's ratio were determined from material property databases. A Viscoplastic strain rate formulation, which is used by MAT_187, was selected for MAT_124 due to recommendations for modeling polymers. All other inputs had to be

calculated. The MATLAB code that was used to calculate these inputs appears in Appendix B.

Tensile Test Data Processing. Tensile testing data needed to be processed before being used for model input. Noise in the tensile data needs to be removed to create a stable material model. Processing began with true stress – true strain curves created after tensile testing. Stress – Strain curves for each test were interpolated onto a single equally spaced strain vector. For each strain rate, a mean of the curves was taken to create a single stress – strain curve. At this point, calculations differed for MAT_124 and MAT_187.

MAT_124. Selecting an elastic modulus for a material that is not linear elastic requires compromise. A balance must be struck between stiffness and yield point. No matter the stiffness selected, the model will predict yield before it would occur, and/or underpredict stiffness [9]. Choice of elastic modulus determines the degree of these errors. More issues arise when selecting an elastic modulus for materials where stiffness is strain rate dependent. For example, the elastic modulus in Figure 17 predicts yield of the 0.001 strain/sec curve at ~ 17 MPa and does not intersect the 1.5 strain/sec curve. A range of elastic modulus was tried in further calculations.

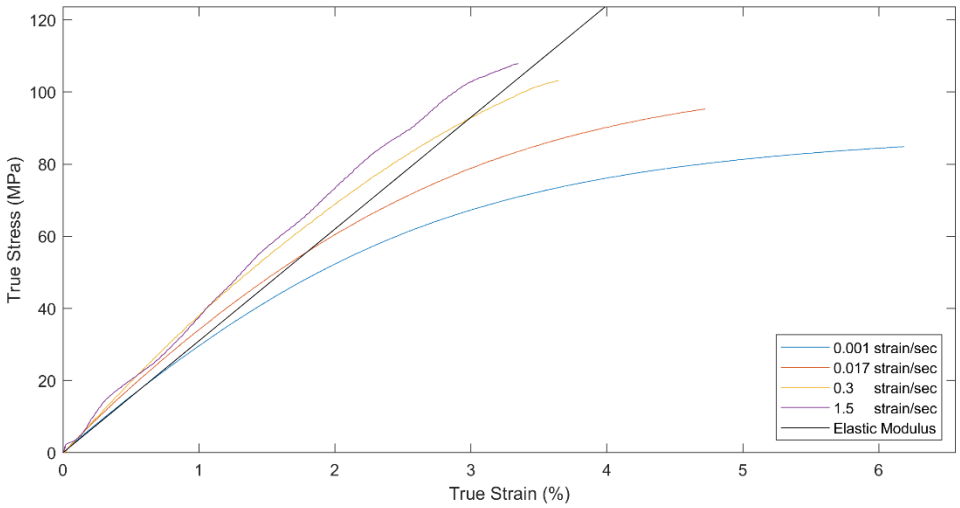

Figure 17. Interpolated stress – strain curves with an example elastic modulus of 3.1 GPa

In MAT_124, only 1 base yield curve is input for tension, and one for compression. Intersection of elastic modulus and each of the averaged tensile stress – strain curves was found. A plastic stress vs plastic strain curve could then be determined, assuming plasticity began at the intersection of elastic modulus and the averaged tensile stress – strain curve. Inputs developed from each strain rate stress – strain curve with various elastic moduli were tested with a single element at various strain rates. Plastic stress and strain were calculated using Equation 15 and Equation 16. If the plastic strain computed in the model is greater than final value in the input curve, MAT_124 computes plastic strain at the same stiffness as the final two points of the input yield curve. A perfectly plastic step was added to the end of each yield curve to keep ultimate stresses accurate for curves that fail at a plastic strain greater than the input yield curve.

$$\sigma_{plastic} = \sigma_{true} \tag{15}$$

$$\varepsilon_{plastic} = \varepsilon_{true} - \frac{\sigma_{true}}{E} \tag{16}$$

A scaling factor of yield in tension was then calculated. A scaling factor that interpolated to higher strain rate than the tensile data provided was needed. The linear fit of ultimate tensile strength to log strain rate as shown in Figure 12 was used. Ultimate tensile stress of the curve was divided by ultimate tensile stress of the input yield curve to determine the scaling factor. The scaling curve was interpolated to a strain rate of ~ 400 strain/sec. The scaling curve of yield in tension was used for compression as well since no compression data was available.

Plastic strain to failure as a function of strain rate was determined through trial and error in the single element test. Single element tests were run with much higher strain to failure than reality. Strain energy to failure was calculated for the test data as well as for single element tests, and the plastic strain at failure was selected to fit and inputs were written. The final fit is shown in Figure 18. For curves at higher strain rate than data was available, plastic strain to failure was selected to fit the ultimate tensile stress vs log strain rate curve, shown in Figure 19.

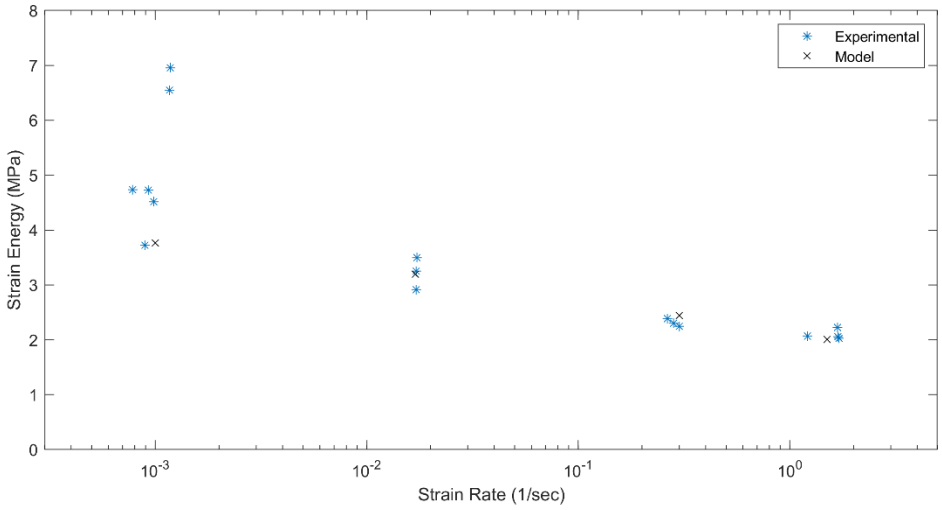

Figure 18. Strain Energy to failure vs Strain rate with single element results, MAT_124

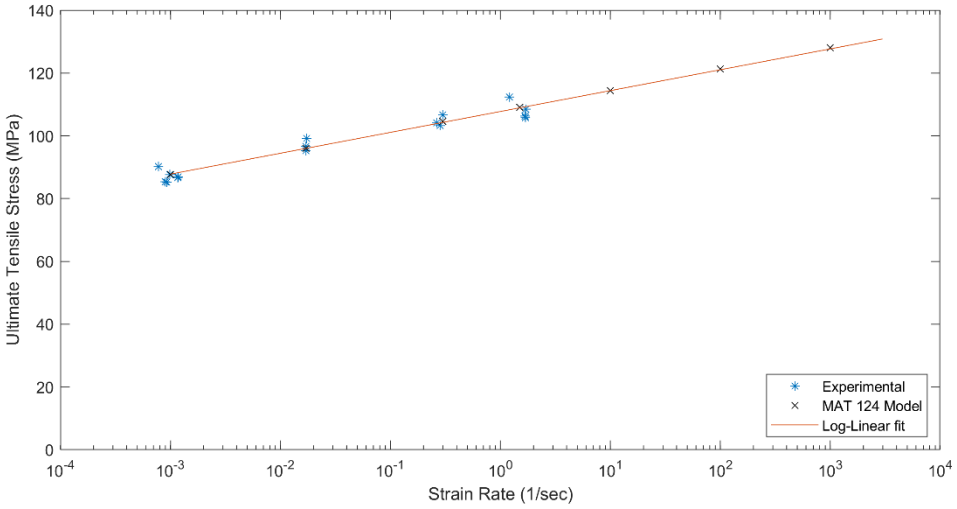

Figure 19. Ultimate Tensile Stress vs Strain Rate with single element results, MAT_124

Single element tests were run for numerous combinations of base yield curve and elastic modulus. Ultimately, the 0.3 strain/sec curve with an elastic modulus of 3.1 GPa was selected. The single element showed that the model matched the ultimate strength vs strain rate fit well, with all model values falling within 0.6% of the fit. Strain to failure produced similar results; the modeled strain to failure was within the bounds of the tensile

tests except for at quasistatic, where the model underpredicted strain to failure. At strain rates higher than 1.5 strain/sec, modeled strain to failure increased with strain rate. A visual review of the single element test overlaid with test data, as shown in Figure 20, shows that at low strain rates the model does not follow the test data. The model is initially much stiffer, and moves to perfectly plastic behavior. Since the material model was applied to an impact problem and strain rates are expected to be much higher than 0.017 strain/second, poor performance at low strain rate was not a large concern. On the other hand, increased strain to failure at high strain rates was a concern.

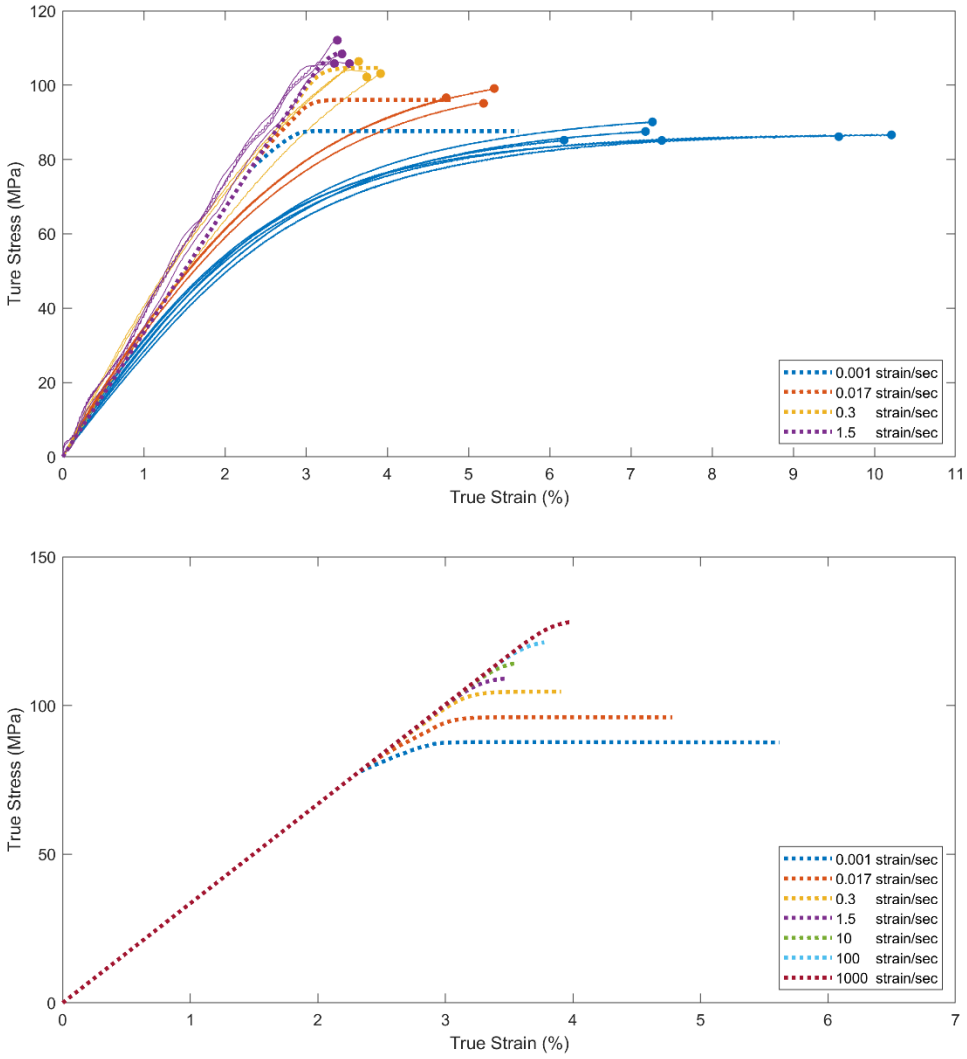

Figure 20. Single Element results for MAT_124 for strain rates with material testing (top), and with higher strain rates (bottom).

MAT_187. The material model allows for greater flexibility of inputs than MAT_124. Some assumptions had to be made about how the material would behave at higher strain rates than testing was performed. Total strain to failure and plastic strain to failure was assumed to be constant at and above 1.5 strain/sec. The ultimate tensile stress was assumed to follow the same ultimate stress vs log strain rate fit as the MAT_124 model.

The first step was to create smooth stress strain curves for strain rates up to 1500 strain/sec. The three lowest strain rate curves were run through a moving average filter and interpolated onto a lower number of points. The mean stress strain curve for 1.5 strain/sec was noisy, as can be seen in Figure 12, so the 1.5 strain/sec and higher strain rate curves were created through modification of the smoothed 0.3 strain/sec curve. The curve was scaled to have the correct strain to failure and ultimate stress for each of the remaining curves.

Elastic modulus was assigned for each stress strain curve through trial and error to retain balance between yield point and stiffness. The curve was written for input as elastic modulus vs effective strain rate. For curves of 1.5 strain/sec and above, elastic modulus was adjusted to hold plastic strain to failure constant. For each curve, plastic stress vs plastic strain was computed using Equation 15 and Equation 16. A table of natural log of plastic strain rate and the corresponding curve is then created. Plastic strain rate was initially approximated using the slope of the plastic stress vs plastic strain curve, and was updated with outputs from single element tests. The compressive plastic stress vs plastic strain curve was not used initially since no compressive test data was available.

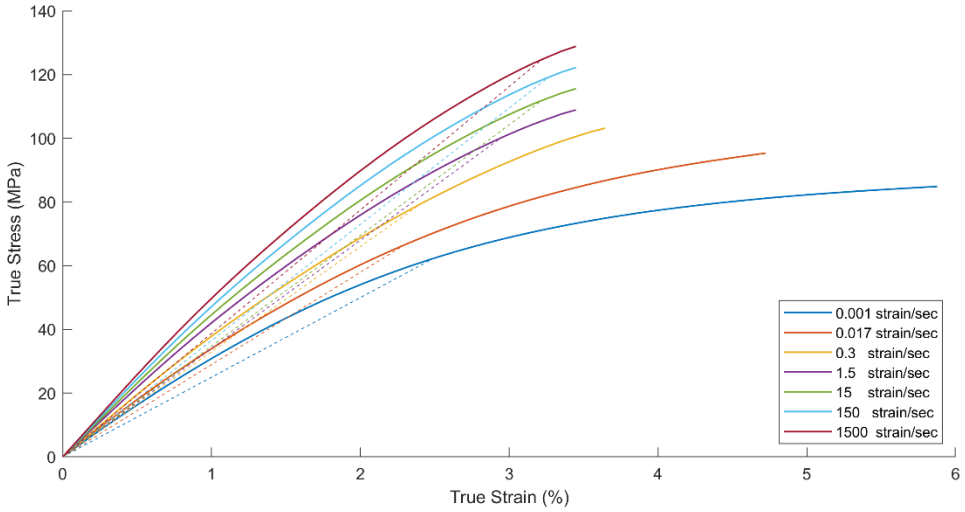

Figure 21. Smoothed stress – strain curves with elastic modulus for each strain rate

Inputs of base elastic modulus, bulk modulus, shear modulus, plastic Poisson's ratio, decay constant, and strain rate filtering factor remain. The base elastic modulus is equal to the elastic modulus used for the 0.001 strain/sec stress – strain curve. The base elastic modulus is used by the model when the strain rate is not within the range defined by the elastic modulus vs effective strain rate curve. Bulk Modulus (K) and Shear Modulus (G) were computed using Equation 17 and Equation 18 with the base elastic modulus value. Plastic Poisson's ratio was set to 0.5, the value used in MAT_124, since no experimental data was available. When using an input of elastic modulus vs strain rate, a nonzero decay constant must be used due to a bug in LS DYNA R10.0 [14]. A small value was used to get around the bug, while changing the results negligibly. Strain rate used in calculations ($\dot{\varepsilon}_{n+1}^{avg}$) are based on calculations with Equation 19 [13]. Strain rate filtering is used to improve stability of the model. Initially, the filtering factor was set to a small value increasing as needed for stability.

$$K = \frac{E}{3(1-2\nu)} \tag{17}$$

$$G = \frac{E}{2(1+\nu)} \tag{18}$$

$$\dot{\varepsilon}_{n+1}^{avg} = (1+FILT)\dot{\varepsilon}_{n+1}^{curr} + FILT\dot{\varepsilon}_{n}^{avg} \tag{19}$$

The single element test, results shown in Figure 22, provided insight into how the material model compared to tensile testing data. Ultimate tensile strength, plotted in Figure 23 with log strain rate, matched the fit with a maximum error of 2.9% for the quasistatic single element test, and less that 0.8% error at all other single element rates. Strain to failure was a similar story, at quasistatic, the modeled strain to failure was less than any of the tests. At the other three strain rates with tensile test data, the modeled strain to failure was within the bounds of the test data. Since the model will be used for impact modeling, the quasistatic strength and strain to failure not matching the test data was of little concern. At strain rates higher than tested, the strain to failure remained constant. A visual review of the single element results overlaid with test data, as shown in Figure 22, shows a good fit of model stiffness at all strain rates, with the model stress-strain response falling within the bounds of test curves at the two higher strain rates. The MAT_187 model did a better job of representing the stiffness of PMMA at all tested strain rates. Constant strain to failure at high strain rate also provided confidence that MAT_187 would outperform MAT_124 under impact loading.

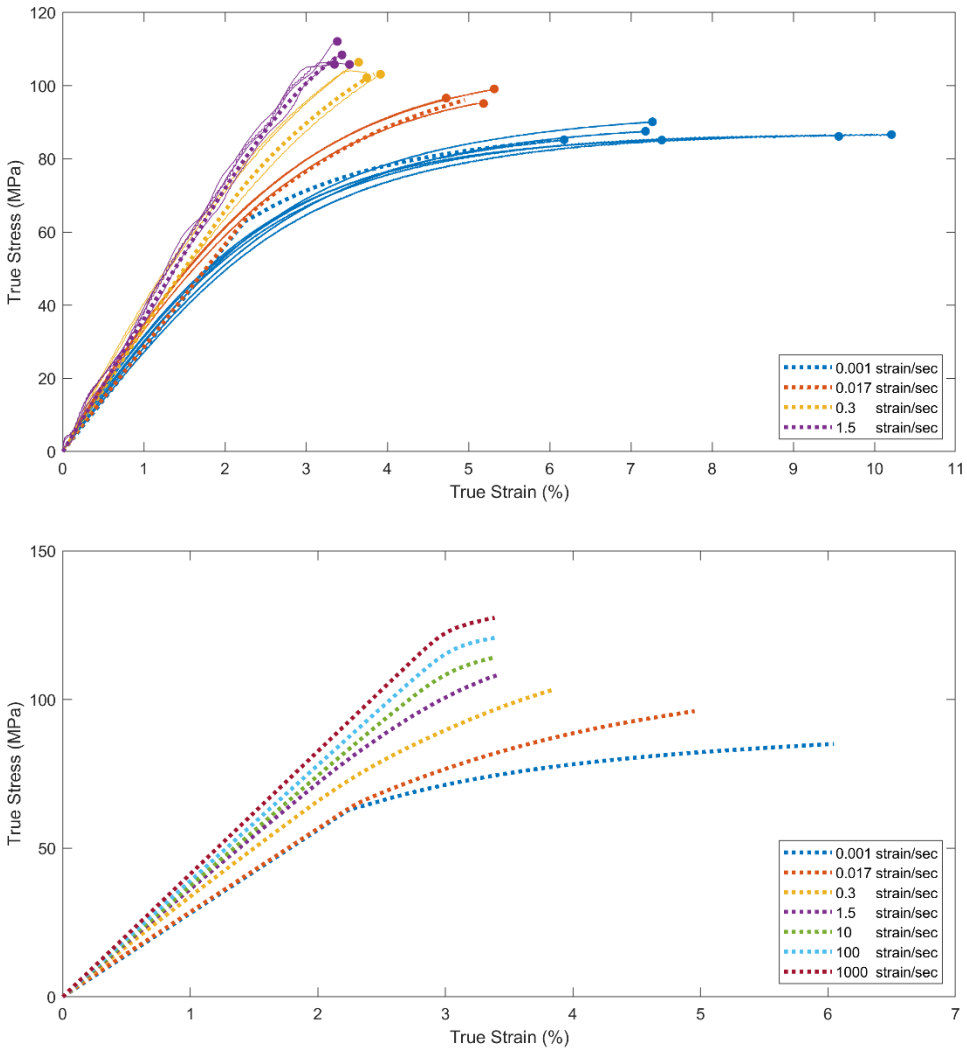

Figure 22. Single Element results for MAT_187 for strain rates with material testing (top), and with higher strain rates (bottom).

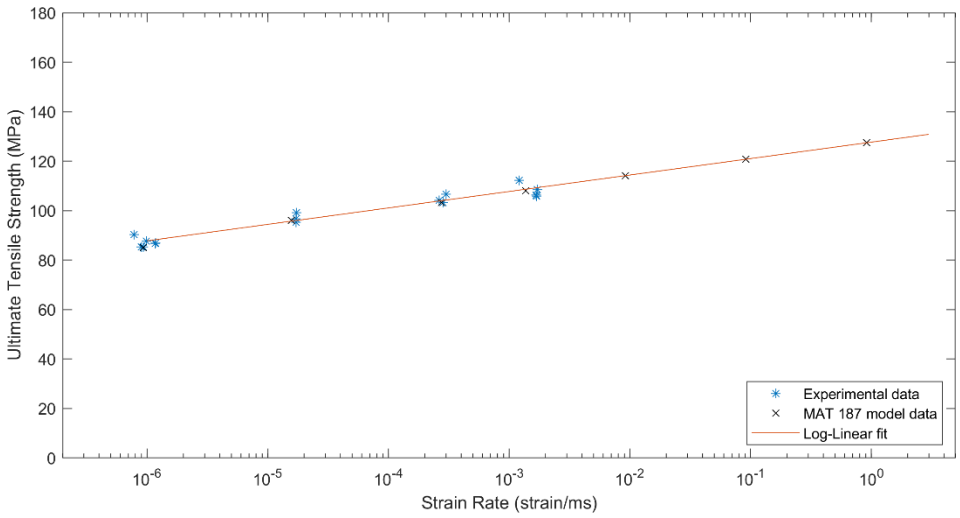

Figure 23. Ultimate Tensile Stress vs Strain Rate with single element results, MAT_187

Confirmation and Adjustment of Material Models with Impact Tower Data

Impact tower results were used to confirm and improve the performance of the material models. A comparison was made between structural response of the impact tower samples and structural response of a model of the samples. Confirming the performance of the model for a bending mode impact. Ultimately, the material model will be used to represent a windscreen impacted by a UAS. The impact can be characterized as a sheet in a bending mode impact. The limitation of this method is that the material model can only be confirmed for an impact causing a bending load. The stress-strain response of the material models is not confirmed.

The results from the impact tower discussed above as well as a data fit of impact velocity and output velocity recommended by Dr. Kyeongsik Woo were utilized. Equation 20 is used usually with p=2, and V_o representing the impact velocity at which 50% of

samples will fail. It was difficult to compare models using the fit directly, so a deviation from the velocity fit was calculated. Since the change in velocity during impact is a function of output velocity, the difference between expected output velocity and actual output velocity was multiplied by the output velocity.

$$V_{output} = \alpha\left(V_{impact}^2 - V_o^2\right)^{1/p} \tag{20}$$

$$Deviation = V_{out} * \left(\alpha\sqrt{V_{impact}^2 - V_o^2} - V_{out}\right) \tag{21}$$

Impact Tower Model. A model of the impact tower was created to compare the material models to impact tower testing data.

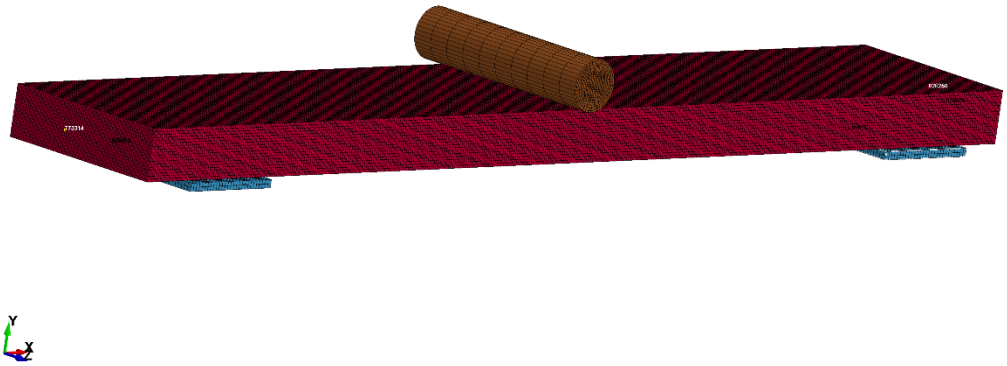

Figure 24. Impact Tower Model mesh

- Model Dimensions
  - Striker
    - Modeled with a cylinder with diameter of 6.35 mm, the same diameter as the bottom of the impactor head
    - Length was selected to contact the sample across its entire width
    - A mass element was added to the striker to bring the total mass equal to the mass of the impact tower sliding impactor
  - Impact tower base

        - Modeled with rectangular prisms with width selected to contact the sample across its entire width
        - Length was not of concern since the sample is only in contact with the inside corners following first contact
    - Sample
        - Modeled to be the average size of a left sample
            - Width of 22.78 mm
            - Thickness of 6.34 mm
            - Length of 140 mm
- Meshing
    - The sample and supports were modeled with cubic elements
        - A mesh convergence study of the sample found that elements of 0.35 mm in length, providing 18 elements through thickness, were the largest converged elements
        - The support elements were 0.5 mm in length
    - The striker was modeled with a mix of rectangular and trapezoidal elements with 40 elements circumferentially and 10 elements in length
- Constraints
    - Striker
        - Fixed in the x and z directions
        - Free in the y direction
        - Fixed in all rotations
    - Impact tower base
        - Fixed in all directions
        - Fixed in all rotations
    - Sample
        - Free in all directions
        - Free in all rotations
- Contacts

  - Automatic surface to surface contacts were used for the impact tower base to the sample
  - Eroding surface to surface contacts were used for the impactor to the sample
  - Static coefficient of friction was 0.2, Dynamic coefficient of friction was 0.15 [15]
- Hourglass control
  - Type 4, a stiffness based hourglass control was used with a coefficient of 0.03, as suggested [16]
- Gravitational Force
  - A body load was applied to the model in the y-direction with an acceleration equal to gravity, 9.81 m/s^2
- Material Model
  - MAT_020 – Rigid was applied to the striker and the impact tower base
    - Density of 7700 kg/m^3
    - Poisson's ratio of 0.3
    - Elastic Modulus of 200 GPa
  - MAT_124 and MAT_187 were both used in modeling the sample
- Section
  - Solid section of element form 1 was applied to all parts. Suggested by [16]
- Timestep control
  - Timestep was found to influence model results. A timestep of 3.96e-5 ms was automatically computed, but was not stable. A timestep of 2e-5 ms was found to be stable and no different than results with a timestep of 1e-5 ms

MAT_124. Since PMMA is stronger in compression than in tension, a model based only on tensile testing data should underpredict strength in compression and bending. The base yield curve for tension was initially used for compression. A scalar factor was then applied to the tension hardening curve and input as the compression hardening curve. Compression strength was increased incrementally, until failure mode and energy absorbed

by the sample were consistent with experimental results. The models at every impact velocity had first element failure along the top surface at one of the two locations of high plastic strain in Figure 25. The location of first failure matched the location of chip formation on tested coupons.

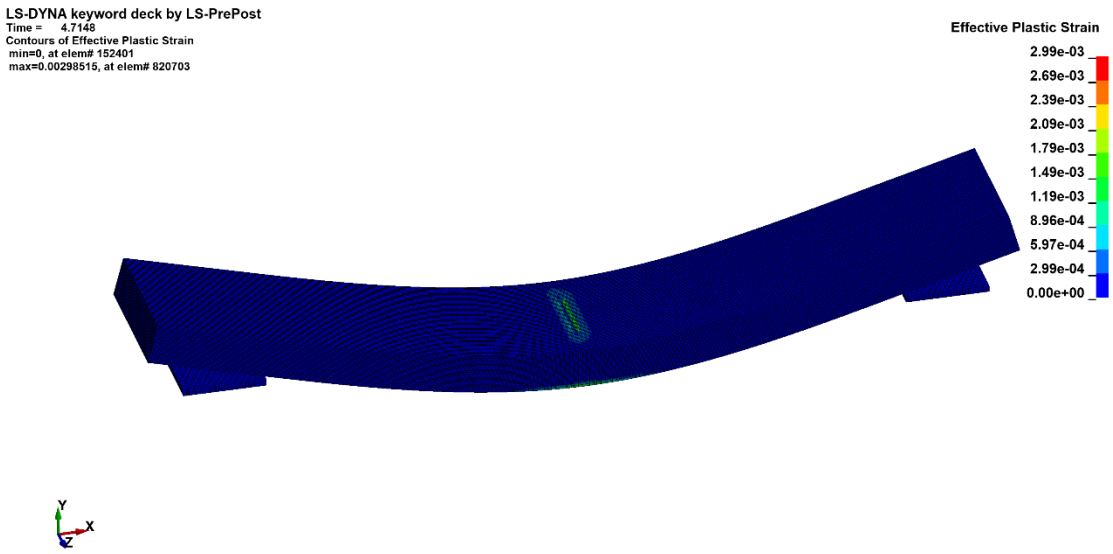

Figure 25. Effective stress of the impact tower sample model one plot stage prior to failure

The model with an adjusted compression yield curve was run at 5 impact velocities from 1 m/s to 5 m/s. The model was compared to impact data in Figure 26, Figure 27, Figure 28, and Figure 29. The energy absorbed in the model was within 1 standard deviation of the mean of the test data. Displacement at failure of the model was between 4.5% and 10% greater than one standard deviation of the test data at all impact velocities. The average acceleration of the model was 10% to 15% less than one standard deviation of the test data at all impact velocities. Compared with the velocity fit, the model was outside one standard deviation at three of the five impact velocities.

The model elastic modulus was increased from 3.1 GPa to 3.8 GPa in hopes to improve fit of average acceleration and displacement to failure of the model with test data. Stiffening of the model improved displacement to failure, with all values falling within one standard deviation of the test data, except for at 3 m/s, where it was 2.7% greater. Average acceleration of the model was nearly unchanged. Energy absorbed of the model decreased, which was expected since displacement to failure decreased with no changes to strength. Energy absorbed was still within 1 standard deviation at all impact velocities except 1 m/s, where it was 8.4% less. Compared with the velocity fit, the model was outside one standard deviation at all impact velocities. Further increasing compression strength would cause the model to fail in tension for low impact velocities. The only option would be to increase the tensile and compression strength. Doing so would have cause the model to no longer match tensile data. The original model also performed better than the stiff model when compared to the velocity fit, with the stiffer model outside one standard deviation at all impact velocities. See Appendix D for impact tower model force and velocity plots for each material model.

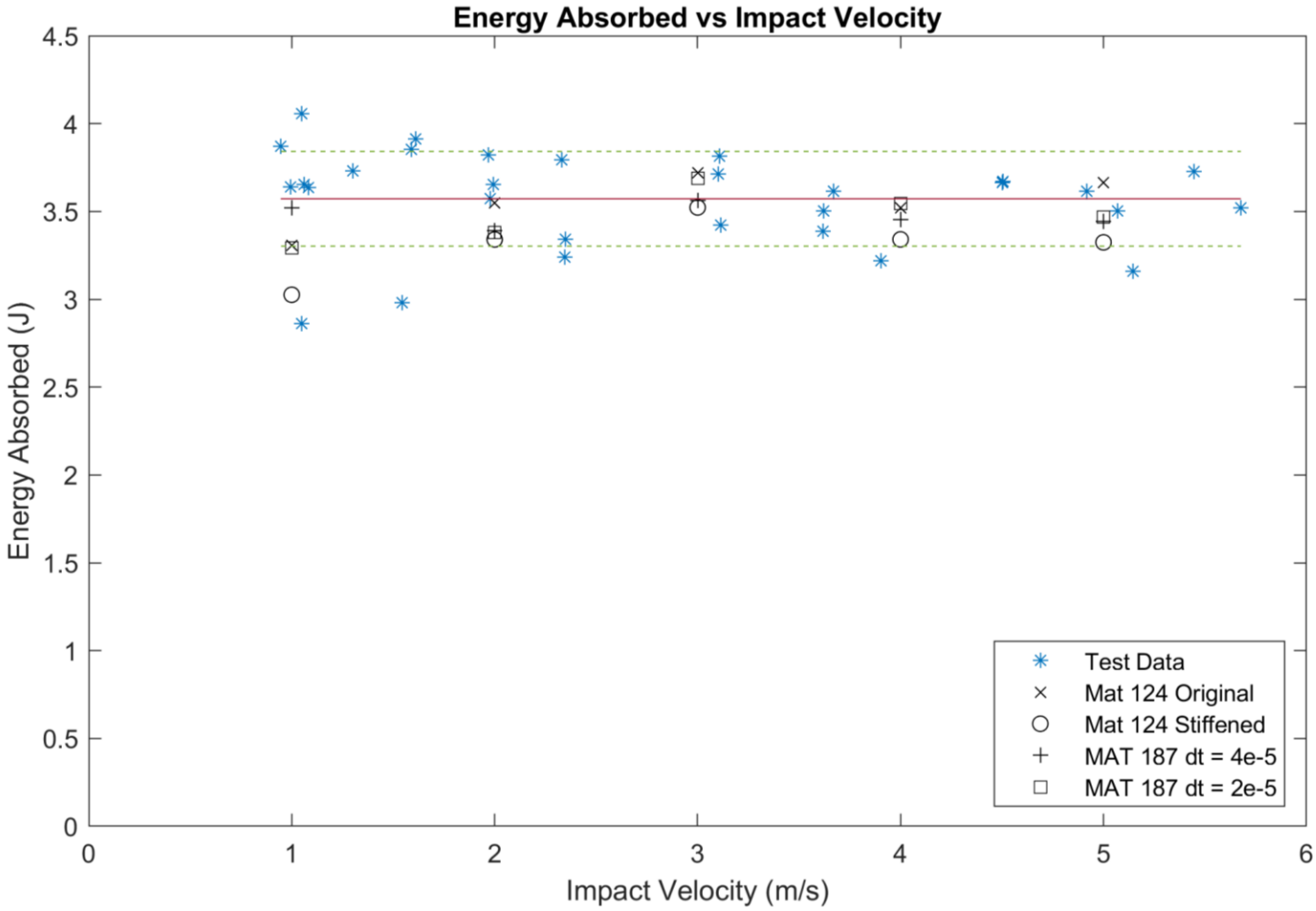

Figure 26. Comparison of models with energy absorbed by the sample during impact with the average and one standard deviation marked

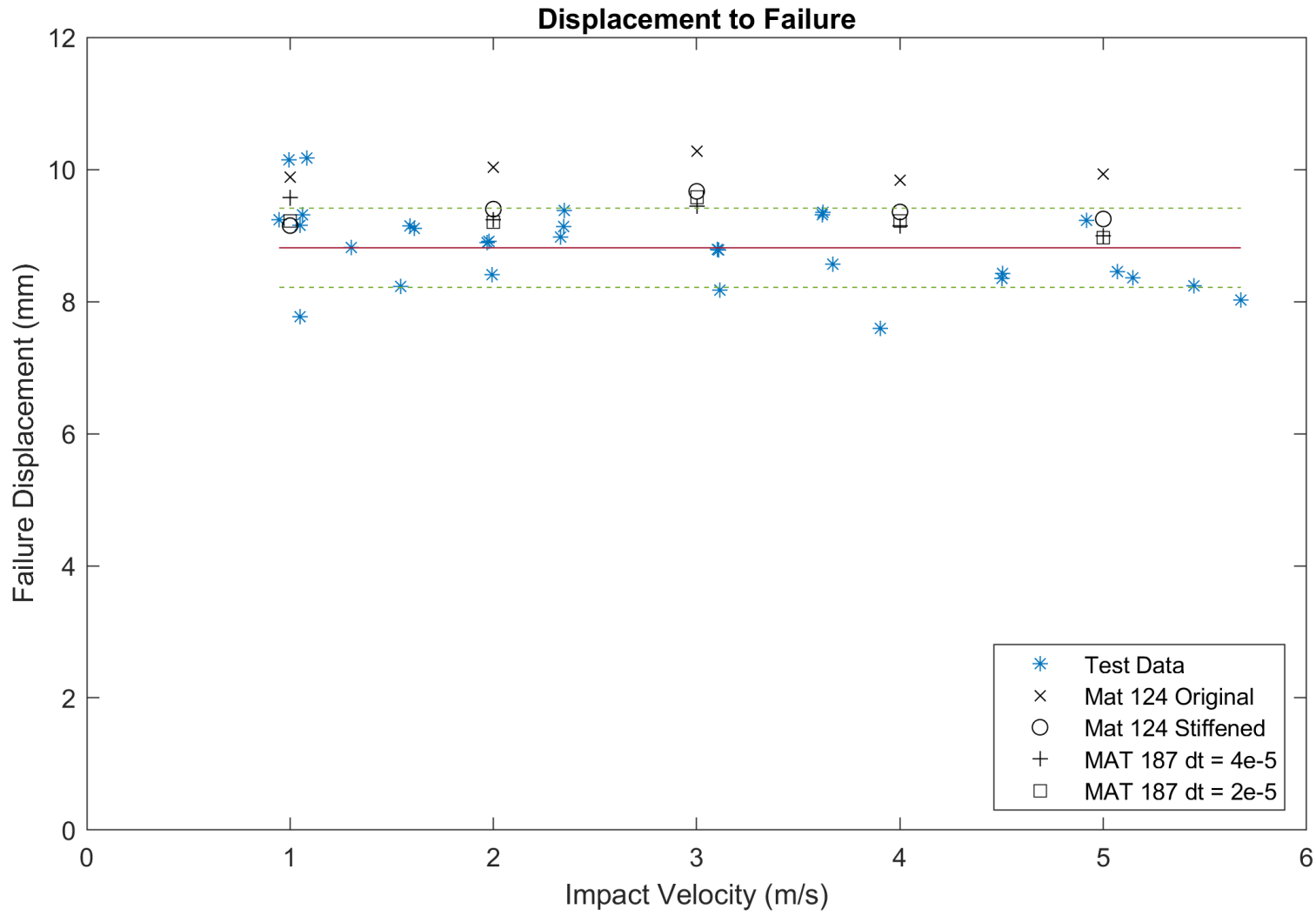

Figure 27. Comparison of models with displacement of the impactor at sample failure with the average and one standard deviation marked

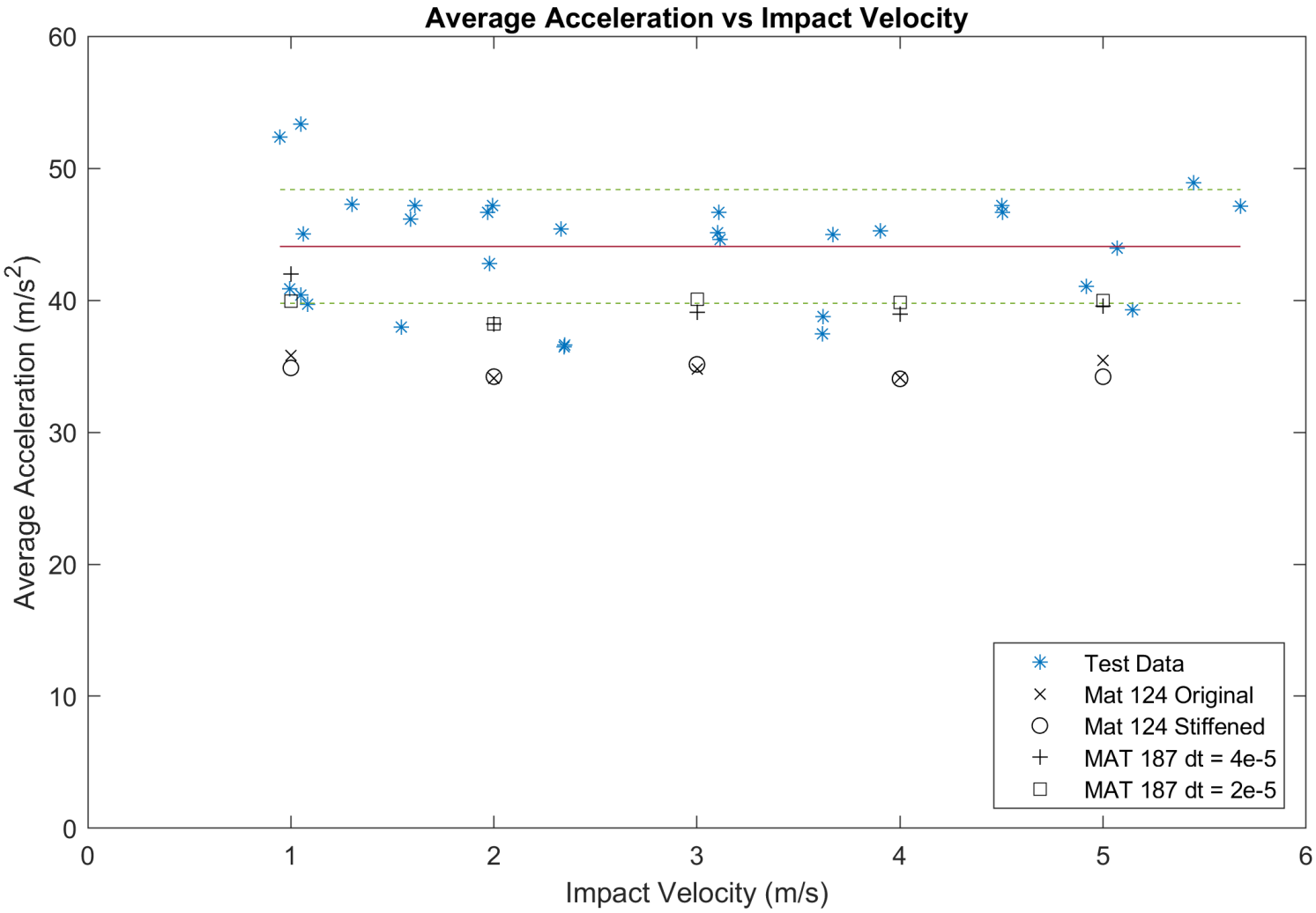

Figure 28. Comparison of models with average acceleration of the impactor through impact with the average and one standard deviation marked

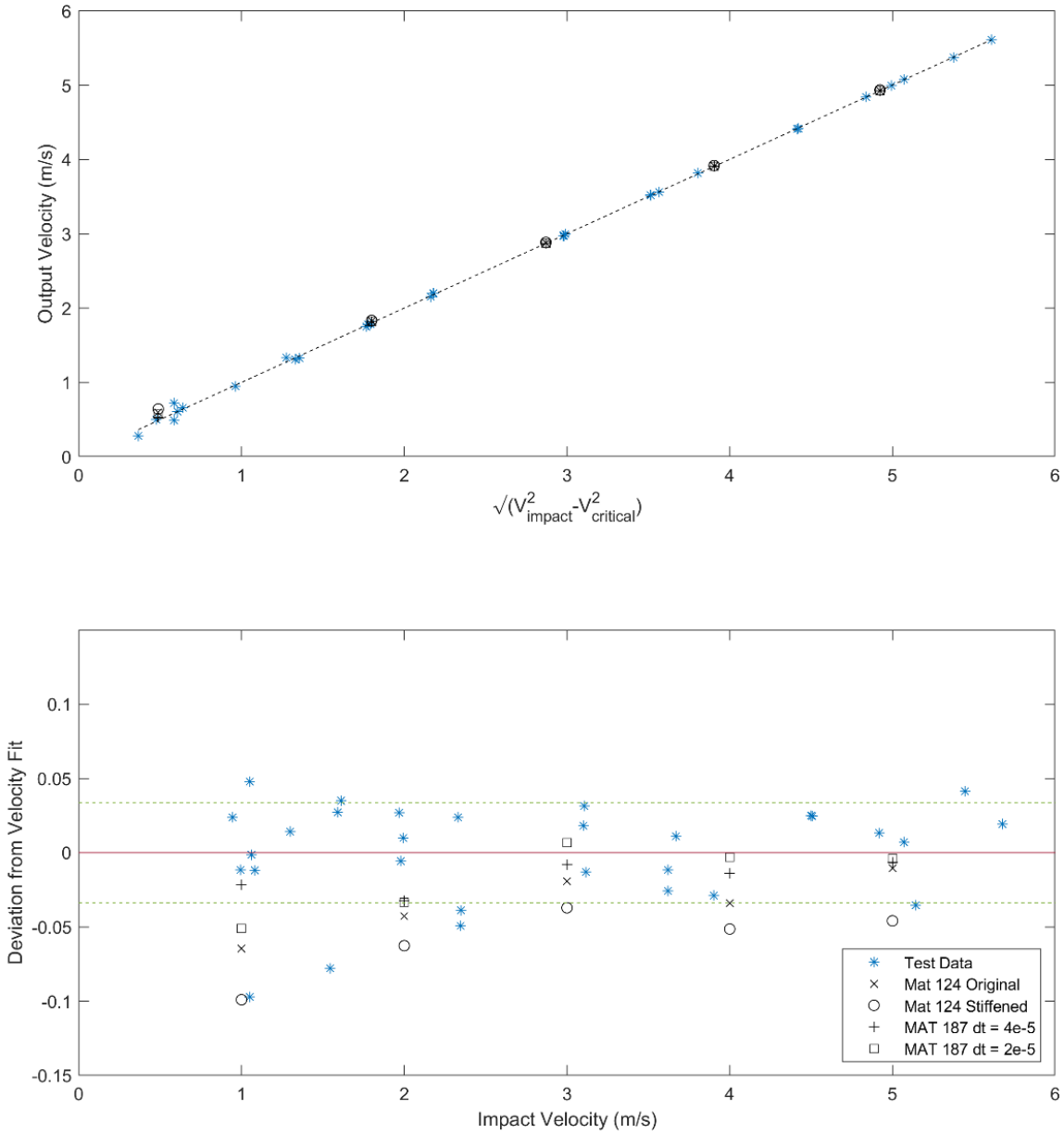

Figure 29. Model comparison with velocity fit (top) and deviation from velocity fit with the mean and one standard deviation marked (bottom)

MAT_187. The material model handles compression strength differently than MAT_124. A quasi-static yield curve is input for compression. The material model derives a hardening curve from the tensile yield curves that are input. That hardening curve is applied to the compression yield curve. The quasi-static tension yield curve was input for compression with a scaler of yield stress. The scaler was incrementally increased, until failure mode and energy absorbed by the sample were consistent with experimental results. The models at every impact velocity had first element failure along the top surface at one of the two locations of high plastic strain shown in Figure 25. Location of first failure matched the location of chip formation on tested coupons.

The model with no timestep control and adjusted compression yield curve was run at the same 5 impact velocities. In models with a high number of timesteps, instabilities were found. Elements under very little stress were suddenly failing. Timestep control was implemented and proved important for model stability. The timestep was first halved from 3.96e-5 ms to 2e-5 ms, which removed the instability. Results in models where instabilities were not observed, were still affected by the timestep change. The timestep was halved again to 1e-5 ms, which did not affect the results. A timestep of 2e-5 ms was used for further analysis.

The model was run with timestep control and compared to impact data in Figure 26, Figure 27, Figure 28, and Figure 29. The MAT_187 model energy absorbed was within 1 standard deviation for all impact velocities. The model displacement to failure was within 1 standard deviation for all impact velocities except at 3 m/s, where it was 2.7% greater. The model average acceleration was within 1 standard deviation of the mean except for at

2 m/s, where it was 4% less. The model was also within one standard deviation with the velocity fit applied except at 1 m/s, where the velocity of the impactor after sample failure was 18% higher than expected by the data fit.

Material Models Conclusions

The MAT_187 model outperformed the MAT_124 model. Two MAT_187 inputs that were unavailable in MAT_124 proved to be important for modeling PMMA: stiffness as a function of strain rate, and independent yield curves as a function of strain rate. These inputs allowed the material model to represent the ductile-brittle transition of the material between quasistatic and high strain rate. These features allowed MAT_187 to perform well in the single element test as well as with modeling the impact tower. Increased performance of MAT_187 was worth the increased computational expense over MAT_124. The MAT_187 model was confirmed to represent PMMA in impact three point bending up to a strain rate of 115 strain/sec.

The MAT_187 model was shared with NIAR for review and use in Finite Element models. NIAR will implement this material model within their Cessna 182 crash model, using it to define the stress-strain response of the windscreen. Once implemented in their model, full scale impact testing of UAS to the windscreen will be performed to confirm performance of the model. The model will then be used to virtually analyze various other crash scenarios, including a range of impact velocities, and projectiles. Providing the FAA with vital information about the danger that UAS pose to aircraft in the event of a crash.

The MAT_187 material model input file is available as a supplementary file, published on Montana State University's ScholarWorks repository alongside this

document. It is provided as a .k file which can be opened with LS-PrePost or a text editor. The model is in units of kilograms, millimeters, and milliseconds.

LAUNCH FACILITY

A full-scale test facility was needed to support windscreen model validation as well as other general aviation parts as a part of the FAA-ASSURE general aviation air to air collision study. To support model validation testing, a launcher and an instrumented test fixturing system was required. ASSURE selected the DJI Phantom 3 as the quadcopter style UAS to be studied. Due to the relatively large size of the DJI Phantom 3, no existing, cost-effective facility was available to support impact testing. A facility was developed to perform the testing.

Design of Launch Facility

Design Calculations

To simulate impact between aircraft and low-speed UAS, it was determined to be most reasonable to launch the UAS at stationary aircraft parts. An engineering design process was utilized to select a methodology and design that could launch a UAS accurately enough to impact aircraft parts at the cruising speed of a general aviation aircraft. Elastic bands were determined to be an effective means to launch UAS at relatively low cost. Some calculations were performed to determine the feasibility of this method. It would have to be shown that such a system could propel a UAS at speeds common for approaching aircraft without causing any damage to the UAS.

In order to determine launcher dimensions, some assumptions had to be made. Since the Cradle had not yet been designed, assumptions had to be made for the dimensions, mass, and aerodynamic properties. UAS release from the cradle was assumed

to be frictionless. Aerodynamic drag on the bands was neglected in this approximation. The latex bands are a non-linear elastic material with strain rate dependent behavior. For this approximation, the bands were modeled as a linear elastic material with no strain rate dependent behavior. Strength data for the Theraband gold band material was not available, so an approximation of 400% was used for allowable repeatable strain.

Iterative calculations using energy methods were used to approximate the launch velocity accounting for air resistance on the cradle. Force produced by the bands using a linear elastic model can be calculated by Equation 22.

$$F_{band} = k(L_{band} - L_{unstretched}) \tag{22}$$

Where k is the spring constant of the elastic bands. With a force curve, and approximations for mass, acceleration throughout the shot can be approximated. The bands accelerate the UAS, the cradle, and themselves. At any moment, the bands are moving on average, at half the speed of the cradle assuming constant tension of the band. Therefore, the bands will be accelerating at any moment at half the rate of cradle. The acceleration curve could be determined using Equation 23.

$$a = \frac{F_{band} - F_{drag}}{m_{UAS} + m_{cradle} + \frac{1}{2}m_{bands}} \tag{23}$$

The maximum acceleration will occur at the moment the cradle is released, where the band force is at its maximum and the drag force is zero. 100 g's was determined as an allowable acceleration without causing damage to the UAS. This was used to determine that maximum band force. At this point, the number of bands could be determined.

The launch velocity was then calculated with approximations for the band force curve and drag force curve. The work done on the system at any point was calculated using Equation 24.

$$W_{x_1 \to x_2} = \int_{x_1}^{x_2} \left(F_{band} - F_{drag}\right) dx \tag{24}$$

For the first iteration, the drag force was set to zero throughout the launch. Velocity throughout the launch was then calculated using Equation 25.

$$v_x = \sqrt{\frac{W_{0 \to x}}{\frac{1}{2} m_{cradle} + \frac{1}{2} m_{projectile} + \int_0^{\frac{w}{2}} \rho_{band} \left(\frac{2y}{w}\right)^2 dy}} \tag{25}$$

Where ρ_{band} is the mass per length of elastic band projected into the y direction. The y direction is parallel to the ground and perpendicular to the launch direction. The velocity curve was used along with Equation 26 to calculate the drag force curve.

$$F_{drag} = \frac{1}{2} C_d \rho_{air} A v^2 \tag{26}$$

Where C_d is the coefficient of drag of the cradle, ρ_{air} is the density of air, and A is the frontal area of the cradle. For the following iterations, the drag force is updated and all work, velocity, and drag force calculations were performed again. Iterations were performed until the exit velocity was within one hundredth of a meter per second of the iteration before.

Pre-existing building materials made 20 ft and 40 ft long designs easiest. Initially, launch velocity of 200 KTS was required; however, requirements were reduced to 120 KTS after initial calculations. It was apparent from these calculations that the 20 ft design would not launch a UAS at high enough speeds. The 40 ft design in calculation was capable of launching a UAS at 160 KTS with 8 band loops.

Launcher design

Preliminary design calculations lead to the design of a 40 foot long collapsible design. The launcher has two uprights that are five feet apart and five feet tall. Adjustable feet lower from the uprights, holding the wheels off the ground and stabilizing the machine during a launch. The two piece center beam allows the launcher to be collapsed and towed. The two pieces are joined using two sets of vertical stabilizers to keep the beams in line along with two clamps to hold the joint together. A 5000 lb ATV winch mounted to the rear post of the launcher allows safe draw of the slingshot.

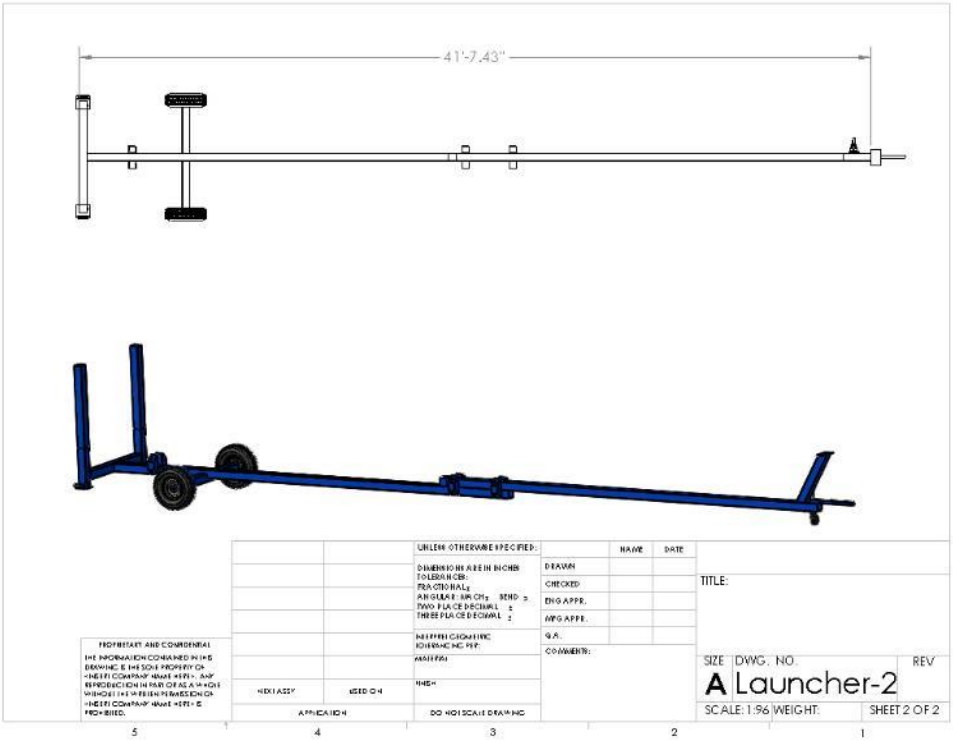

Figure 30. Launcher in shooting configuration

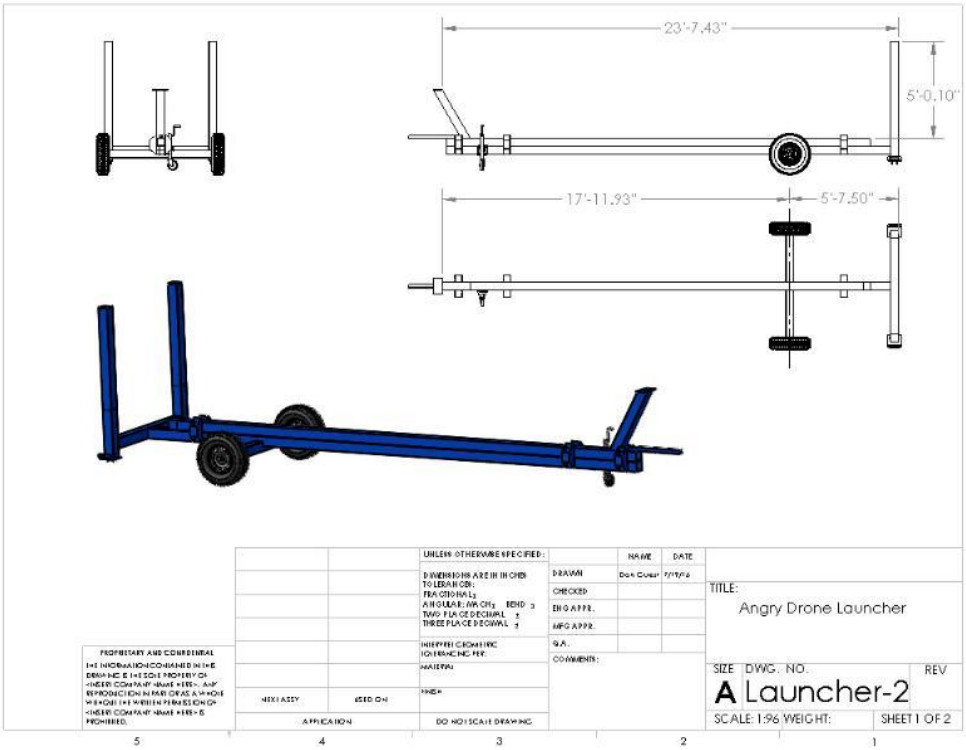

Figure 31. Launcher in towing configuration

The launch system consists of Thera-band gold, a launch cradle, and a quick release. The original cradle consisted of a strong plastic bucket with four u bolts along the top. The bucket was lined with polystyrene foam to hold the UAS and help accelerate the UAS without damage. Two sewn loops of one inch nylon webbing with bights tied on each end were run from one u bolt around the back of the bucket to the opposing u bolt. A ¼ inch shackle was placed on the webbing where the two loops cross in the back. The band system consists of sixteen loops of Thera-band gold. Four bands are run through each bight of the sewn loops and the loop is closed with an overhand knot. The band loops are placed over the uprights of the slingshot. The quick release is attached to the end of the winch cable with a ¼ inch shackle. The winch cable is then attached to the shackle on the webbing using the quick release. Light tension from the winch is used to allow placement and adjustment of the band loops on the uprights.

Figure 32. Loaded prototype launch cradle

Launcher testing

Following the build, 14 test launches were performed. Early test launches used rocks or children's toys as the projectiles. Testing began with four band loops at partial draw. Passing that testing, full draw testing was performed. These full draw tests proved the concept and showed that launcher was capable of handling higher loads. Tests with eight band loops were performed. Velocities were still lower than desired. Tests with twelve band loops were performed. Intended velocities were achieved with twelve band loops. Testing moved on to launching DJI Phantom 3 UAS's. At twelve loops, UAS launches of 150 KTS were achieved. The launcher passed testing, exceeding the required launch velocity.

Testing showed the calculations overestimated launch speed. Overestimates of allowable strain, incorrect stiffness data, not accounting for strain rate dependence of the bands, and an incomplete drag model all likely contributed to an overestimation in launch speed. An allowable strain of 400% was used in design, but was proven to cause bands to break too quickly. An allowable strain of 350% was then used.

Launcher improvement capstone

A capstone group, an undergraduate team assigned with a two semester design project, was tasked with improving the launcher velocity and accuracy. The group proposed a compound slingshot design with tracks guiding the cradle. The group also proposed an improved cradle design.

The proposed track design was based around three tensioned steel cables running the length of the launcher. The cradle was attached to the cables with small wheels and

bearings to allow the cradle to move along the track with low friction. The cables mounted to the uprights at the front of the launcher, and a second set of uprights added to the rear of the launcher. Large compression springs were mounted around the tracks to help bring the cradle to a stop. A bungee cord ran from the winch post to the cradle slowed the cradle before impacting the compression springs.

The compound sling shot design was proposed to increase the launch speeds. A compound sling shot system allows for tension in the bands for a larger portion of the draw length. In this design, the bands were routed from the cradle to rollers at each of the front uprights, then directly downward to rollers at the base of the uprights and back to the wheel axle where the bands were fixed, as shown in Figure 33.

Figure 33. Compound slingshot design

The cradle was redesigned to improve durability and reduce drag. The redesigned cradle was manufactured from aluminum to improve impact toughness. The update was designed to fit a DJI Phantom 3 without any extra space. This reduced the weight of the cradle as well as the frontal area of the cradle. The cradle utilized sewn webbing loops. The webbing loop design reduces axial loading on the bucket, but causes a crushing load. [17]

After review of the design, the track system was rejected. The design would cause a large increase in loading of the center joint of the launcher. The elastic response of the launcher frame at the beginning of launch was also of concern. A vibration from the frame was expected, which would have caused a variable tension of the tracks during launch. Additionally, band tension causes a bow in the launcher frame which may have been enough to remove tension from the tracks at full draw.

The compound sling shot system was approved and built. In testing some issues arose. In the build phase, the design was changed from two separate brackets holding the lower rollers to a single bracket with a long shaft. The shaft displaced enough under loading for rollers to contact the launcher frame and stop rotating. The upper set of rollers also displaced significantly. This displacement causes the bands to walk off the rollers. The brackets were produced from a material selected in the build phase for formability, not stiffness. Due to these issues, the compound sling shot designed is not used.

The cradle redesign was approved and built. The new design passed testing. The cradle was used for all launches in 2018 and 2019. The cradle has been yielded in places from the crushing load while winching as well as impact with the ground and launch frame

post launch. The cradle redesign has proven more durable than previous version; however, with repeated impact weakening the structure, it will not last the lifetime of the launcher.

Impact tower capstone

A capstone group was tasked with designing and building a structure to hold square plates and aircraft wings for impact. The impact tower needed to be able to withstand impact from a 10 lb projectile traveling at 250 KTS. The impact area needed to be at least 38” by 38”. The impact tower needed to allow for load cells to be added measure impact loads. The impact tower also needed to be portable, and have a setup time under 30 minutes with three people. The project budget was $5000.

The capstone group decided on a design based around Unistrut, predrilled square steel structural members. Unistrut structural members allowed for easy assembly and allowed the design to be modular, breaking down into 4 pieces for transport. Shelf like structures were intended to support a wing from above and below with a ratchet strap holding the wing against the frame. The wing holders could be removed for tests on metal plates. The design included a 0.25” thick ASTM A514 steel plate. The steel plate was selected to withstand repeated impacts without permanent deformation. [18]

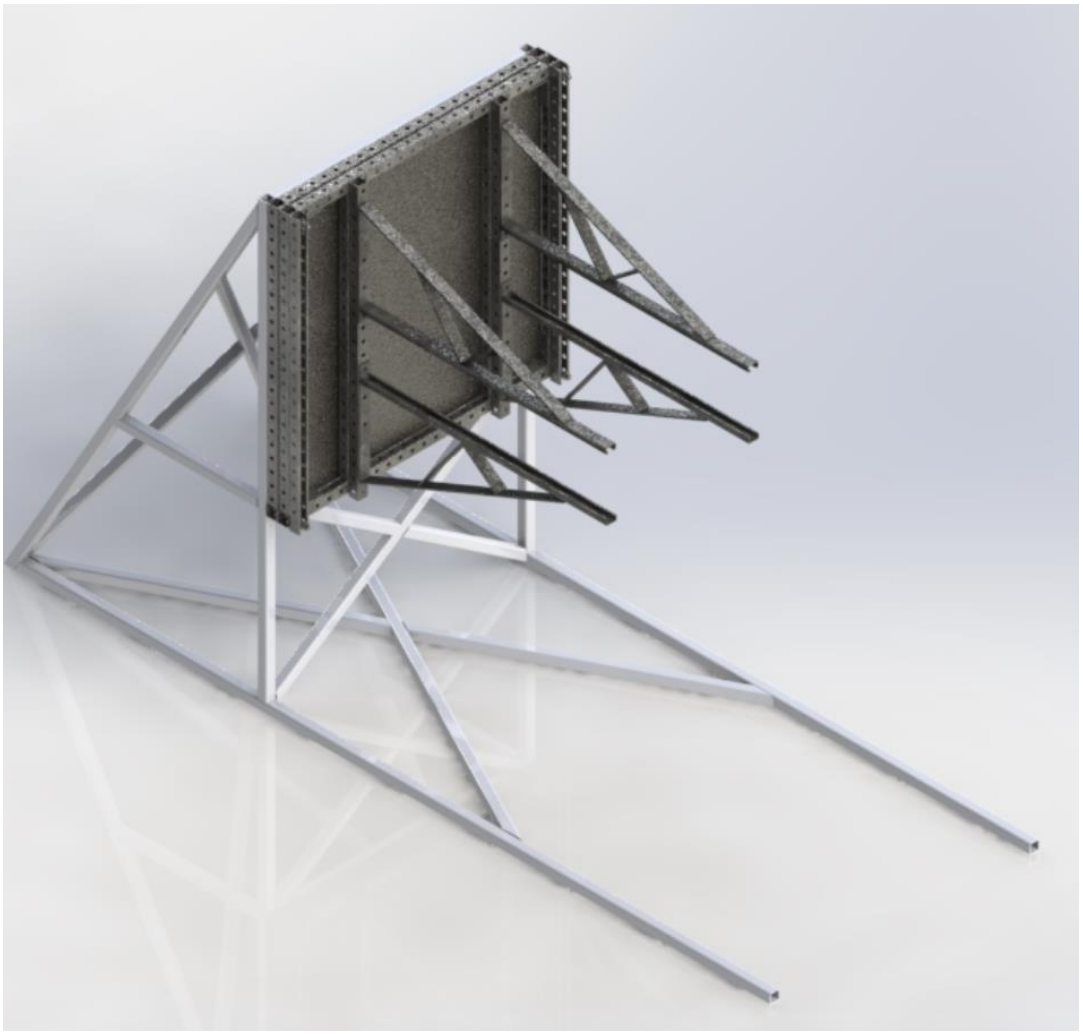

Figure 34. Impact tower design with wing holders mounted

The capstone group made some necessary design modifications in the building process. Crossing structural members were redesigned such that they would pass by each other to reduce manufacturing difficulty. Structural members intended to hold an aircraft wing were unavailable from the manufacturer. Ultimately, the wing holder was not completed.

The impact tower passed all its requirements in testing except for wing holding capability. The tower could be assembled in 30 minutes by two people. The steel plate has

proven to withstand repeated impact. The tower was more compliant than desired. Due to requirements for ease of transport and assembly, the tower was designed with lightweight materials. The frame was prone to flexing and the front of the base lifted from the ground on impact.

Since delivery from the capstone group, efforts have been made to reduce movement and compliance of the impact tower. To reduce movement, 80 sandbags were filled and placed on the frame. The sandbags reduced front end lift, but the frame compliance was still higher than desired. Additional structural members were added, improving the overall stiffness. Still, a higher stiffness impact tower was needed, and the impact tower was retired in favor of a design utilizing a shipping container in the summer of 2019.

Shipping Container Impact Tower

A new impact tower was designed to address the compliance issues of the existing design. A shipping container was utilized as a heavy and stiff base. Two 6” I-beams were utilized for the mounting surface, attached to a long face of the shipping container. The shipping container has structural beams that run the length of the face at the top and bottom. The structural member along the top sits proud of the face, allowing for direct mating of the I-beam. The structural member along the bottom sits shy of the face, requiring a short section of square tube to fill the gap. The I-beams were welded to the shipping container 34” apart, centered with the center of the shipping container, as shown in Figure 35. The shipping container was adjusted to ensure that the mounting face was vertical. Testing was then performed with the 0.25” steel plate mounted. Deflection of the I-beams can be seen

in high speed video footage, but is much lower than the previous design. Further testing of the shipping container impact tower will be performed in summer of 2020

Figure 35. Shipping container impact tower with the 0.25” thick steel plate mounted

Instrumentation of Test Facility

Instrumentation was an important consideration at the launch facility to be used to confirm numeric impact models. High speed cameras are used to record impacts as well as measure the launch velocities. A National Instruments cDAQ 9174 chassis with an NI 9205 general purpose 16 bit, 32 channel voltage measurement module has been acquired for additional instrumentation capacity. An NI 9205 allows voltage measurement of up to 32 channels at a total of 250 kHz [10]. The high speed DAQ allows for the future inclusion of load cells to record loading throughout impact.

High Speed Camera Analysis. Measurement of speed is necessary to use testing to confirm numeric impact models. A high speed camera filming at 1000 frames per second or faster is used along with a speed board of fixed dimension to measure speed. The speed board is placed near the target, parallel to the flight path of the UAS, with space such that the UAS passes the speed board before impacting the target. The speed board is placed as close to the path of the UAS as possible without interfering with the UAS or the launcher cradle. The camera is set to maximum zoom to allow the maximum distance from the camera to the speed board. The camera is positioned with the speed board in view. The camera is then focused. As shown in Figure 36, the speed board length, speed board to UAS path distance, and camera to speed board length are measured. The UAS path length is then calculated.

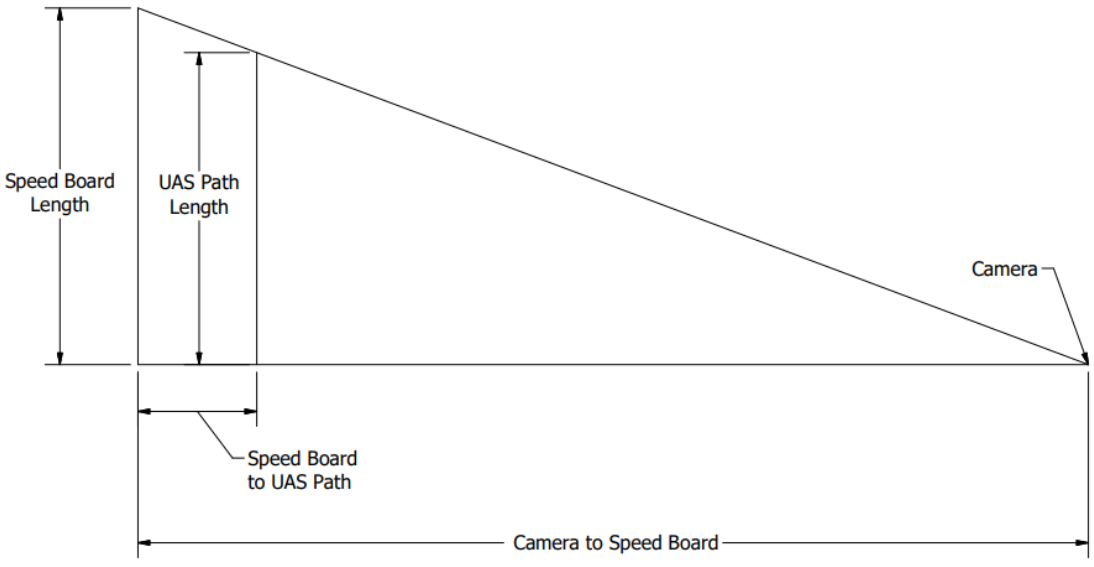

Figure 36. Speed measurement setup

With the camera set up, the system is ready for a test. The high speed cameras record in a circular buffer, allowing the recording to be started well before launch, and stopped just after impact. For a test, the camera starts recording while the launcher is winching. The camera is then triggered a few seconds after impact, saving footage of the launch. The video files are then cropped and saved. The footage is viewed frame by frame, finding the frame that the UAS center of mass is in front of the start of the speed board, as shown in Figure 37, and the frame number is recorded. The same process is repeated to find when the UAS center of mass is in front of the end of the speed board, as shown in Figure 38. Since the frame rate and the number of frames between positions are known, the time between positions can be calculated. Using the UAS path length and the time to travel that distance, the speed is calculated.

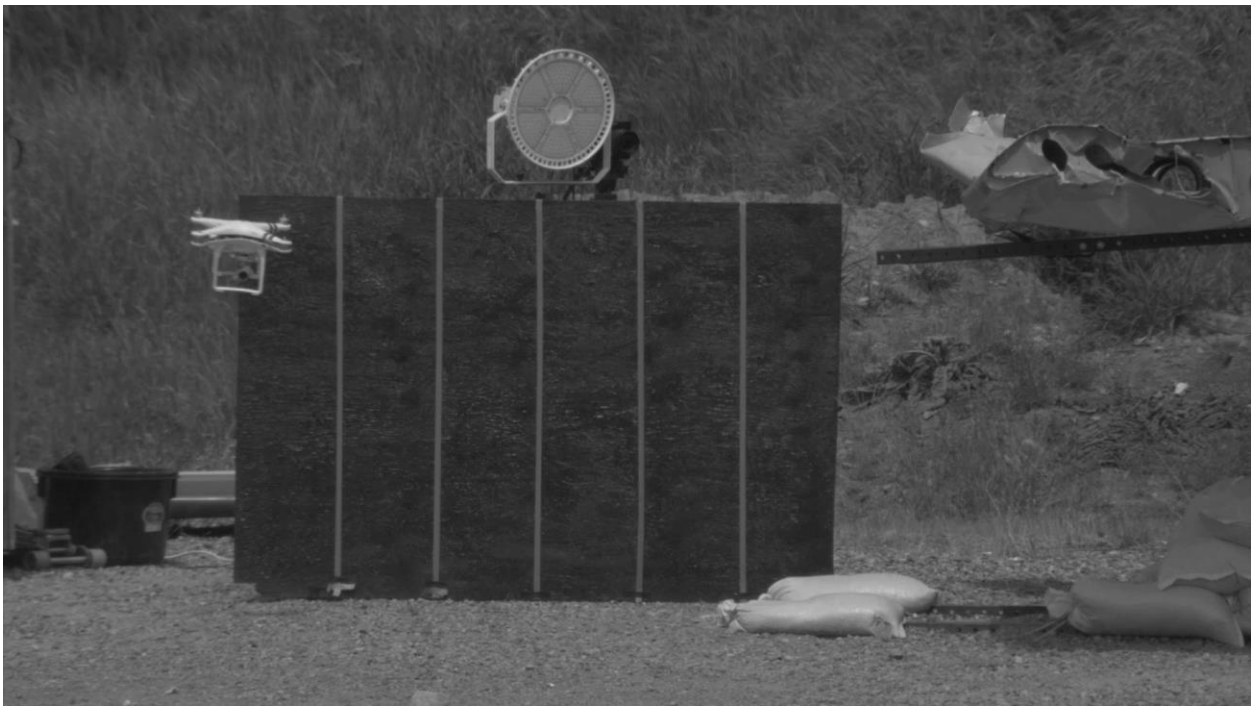

Figure 37. Frame at start of speed board

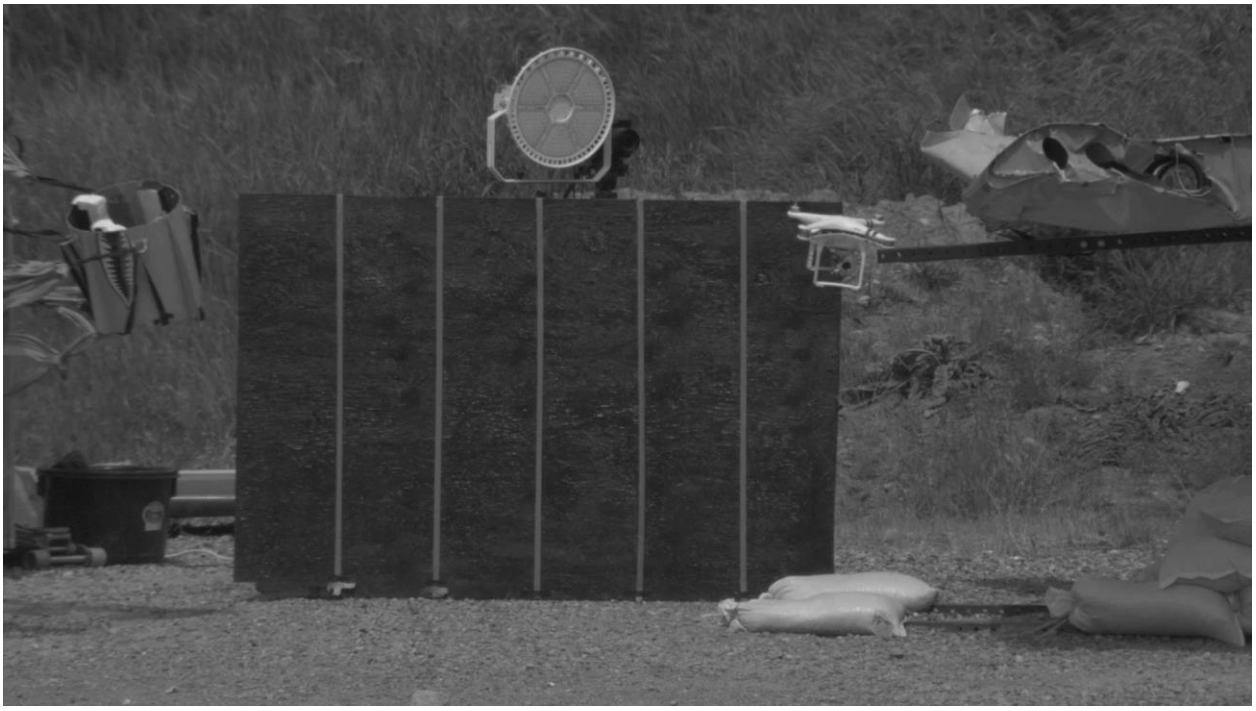

Figure 38. Frame at end of speed board

As previously discussed, numeric impact model confirmation is a primary purpose of the launch facility. To confirm a model, it is imperative that the impact conditions in the model and in testing are identical. In order to fully understand the impact orientation, a high speed camera is setup to record the impact. The camera is framed to show the front surface of the target as well as the UAS immediately before impact.

Figure 39. Impact orientation recorded with high speed video

In some situations, only one high speed camera is available, and both speed measurement and impact must be recorded with a single camera. Compromises must be made to record both shots at the same time. In order to view the front surface of target as well as the speed board, the camera must be placed closer to the speed board and the zoom adjusted to include both the speed board and target in frame. In this setup, the UAS path length is shorter, causing a greater error in speed calculation. The setup also does not allow for the desired camera angle to record the impact.

Capabilities of the Launcher

The launcher was designed with the intent to maximize launch speed, accuracy, and repeatability of the launcher. For each launch that was conducted, the speed, accuracy, and approximate rotation of the drone before impact was recorded, see Appendix A for this record. Though many shots have taken place with incomplete or reconstructed DJI Phantom 3's, in discussion of capability, only launches with complete systems will be considered.

Launch speed is highly dependent on the band setup. The number of band loops and the length of each band loop are important factors. Prior to 2018, 12 total band loops were used. The median launch velocity was 115 knots. Starting in 2018, 16 total band loops were used. The median launch velocity increased to 117 knots. The band loops were lengthened in 2018 to decrease the number of band failures. Band failure decreased significantly, but at the cost of launch velocity. Early in 2018, the launcher was setup with 16 band loops of a short length. The launcher proved capable of launching at ~135 knots. If launch speeds of 135 knots are required, bands may be shortened, but increase in band failure would be expected. Along with the additional cost, band failure impacts launch accuracy.

Launch accuracy is very important, especially for tests on smaller aircraft parts such as wing leading edges and struts. The launcher had better accuracy in the vertical direction than horizontal. This difference is largely due to crosswinds and the winch. The winch pulls to the same location vertically, but varies horizontally along the winch drum. The variation along the drum introduces about 2" of variability in aim in either direction. Variations in band tension from corner to corner will add to inaccuracy. Variation increases when bands

break during launch, causing inaccuracies of as much as 2’. Flight of the projectile will also add to inaccuracy. Crosswinds increased inaccuracies of launch. Horizontally, the launcher varies about ±5”. Vertically, the launcher varies about ±2”. When possible, test articles should be oriented with the short dimension in the vertical direction. The accuracy has proven to be capable enough for wing leading edge tests, hitting the leading edge in each test.

Projectile orientation at impact varied greatly. In testing, the Phantom 3 has rotated in flight as much as 130º in any direction. Large rotations were most likely to occur in the nose down direction. Rotations were likely due to interactions with the cradle as the projectile is released. Improvements to the cradle may decrease rotation.

Weather was restrictive to launcher use. Precipitation, snowpack, cold weather, and wind all posed problems for the launcher. Expensive electronics such as the high speed camera made use in rain and snow impossible. Snowpack has impeded access to the launcher. Cold weather proved to impact band strength. The coldest day of launching was about 40ºF, at which time band failure was more common than usual. Increasing band loop length may allow for launches in cold weather. Wind on axis with the launcher caused variation in launch speed, but was not a large problem. Crosswind proved to be a problem. Crosswinds under ~10 mph were acceptable, but decreased accuracy. Launches in strong crosswinds are unsafe. During one launch in 2016, a heavy crosswind caused the cradle to crash into an upright.

Repeatability of launches is very important. All factors that decrease accuracy also decrease repeatability. Wind was a large factor in repeatability. Small crosswinds can be

adjusted for in aim, but inconsistencies in wind speed and direction cause problems. Launcher movement during a launch also impacted repeatability. Forces during launch cause a vibration that can move the launcher. Before each shot, the launcher aim is checked, but the new aim may not be the same.

Impact Testing

Impact testing with DJI Phantom 3 UAS's was performed to determine likely damage to General Aviation aircraft in an air to air collision and prove the machine capability. Tests were performed on a Piper PA-28 140 wing, and a Cessna 182 wing.

Piper PA-28 140 Wing Testing

A Piper Cherokee wing was donated for research. The wing was damaged near the wing root and an undamaged section near the wing tip. The wing had a 0.032" short takeoff and landing (STOL) cuff on the leading edge. The wing structure with a STOL cuff is shown in Figure 40. Five tests were performed with the wing set on sawhorses.

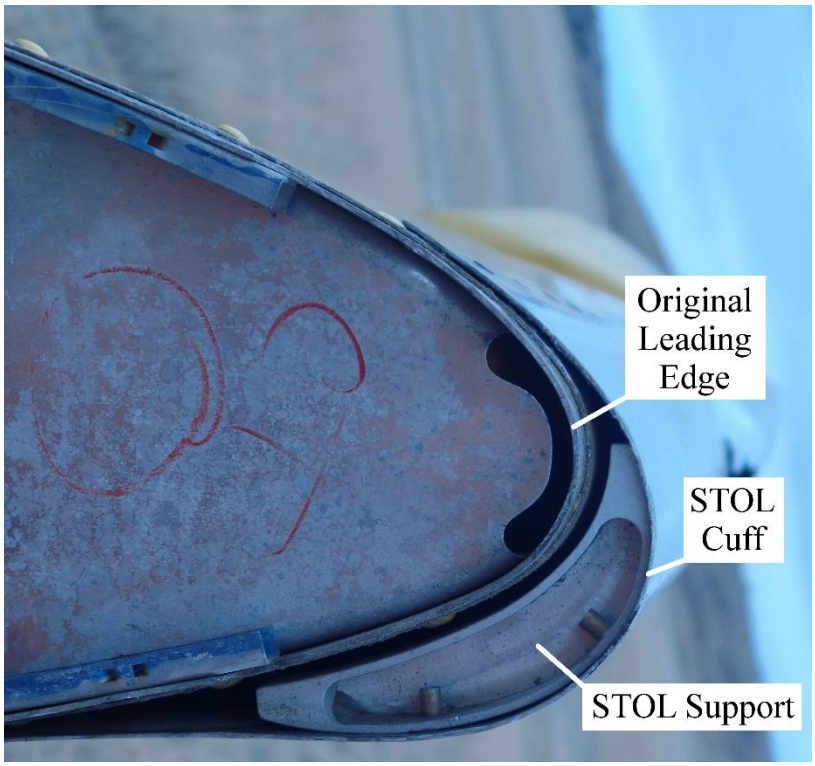

Figure 40. Piper Cherokee wing profile

The instrumentation for testing consisted solely of a Fastec TS3 camera. The camera was set to capture both speed measurement and impact. Following the test, the impact area was measured, and photos were taken.

Wing Test 1. In the first test, a DJI Phantom 3 without a camera was used. The UAS impacted the wing at 151 KTS. The UAS impacted while pitched nose up at around 10 degrees, right up at 5 degrees as shown in Figure 41.

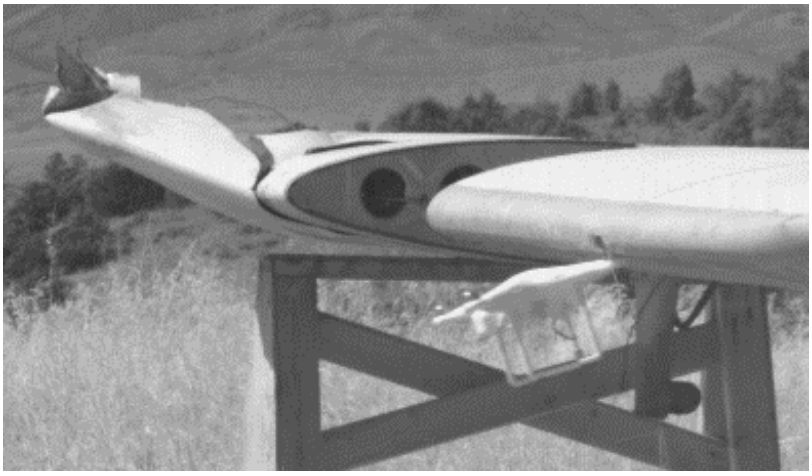

Figure 41. Test 1 impact orientation

A motor of the UAS impacted the lower left corner of a rectangular hole that was original to the wing, as shown in Figure 41. The rest of the UAS passed below the wing. The impact caused fracture starting at the low left edge of the rectangular whole, moving through a 1/8” hole. The material on both sides of the fracture was deformed. The left side met the original leading edge of the wing.

Figure 42. Damage from test 1

Wing Test 2. In the second test, a DJI Phantom 3 without a camera was used. The UAS impacted the wing at 157 KTS. The UAS impacted while pitched nose up at around 15 degrees, left up at 10 degrees, and rotated left forward at 5 degrees as shown in Figure 43.

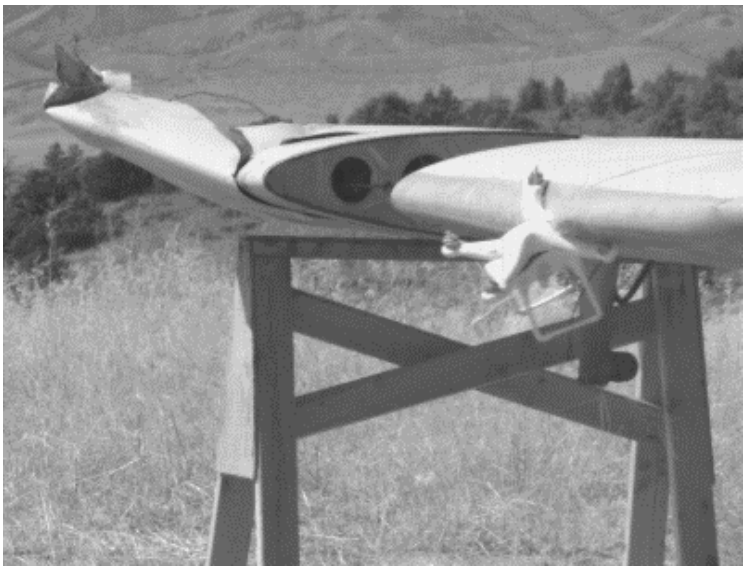

Figure 43. Test 2 impact orientation

The UAS impacted with wing with the leading left motor above the center of the leading edge and the leading right motor below the center of the leading edge. The trailing left arm made contact below and to the left of the leading left arm. The trailing right arm passed underneath the wing without making impact. The damage, shown in Figure 44, shows areas of damage from the leading left arm, the trailing left arm, the leading right arm, and the body of the UAS. The leading right arm produced a 2.2” by 2.3” dent with a depth of 0.4”. A 0.5” bulge occurred at the back edge of the damage. The leading left arm produced a 2.5” by 4” dent with a depth of 0.6”. The trailing left arm produced a 1” by 2.2” dent with a depth of 0.25”. A 0.7” high bulge occurred at the back edge of the damage. The

body caused a 4” by 3” dent as well as a crack at the top left corner of the rectangular hole. The preexisting crack at the bottom left of the rectangular hole propagated.

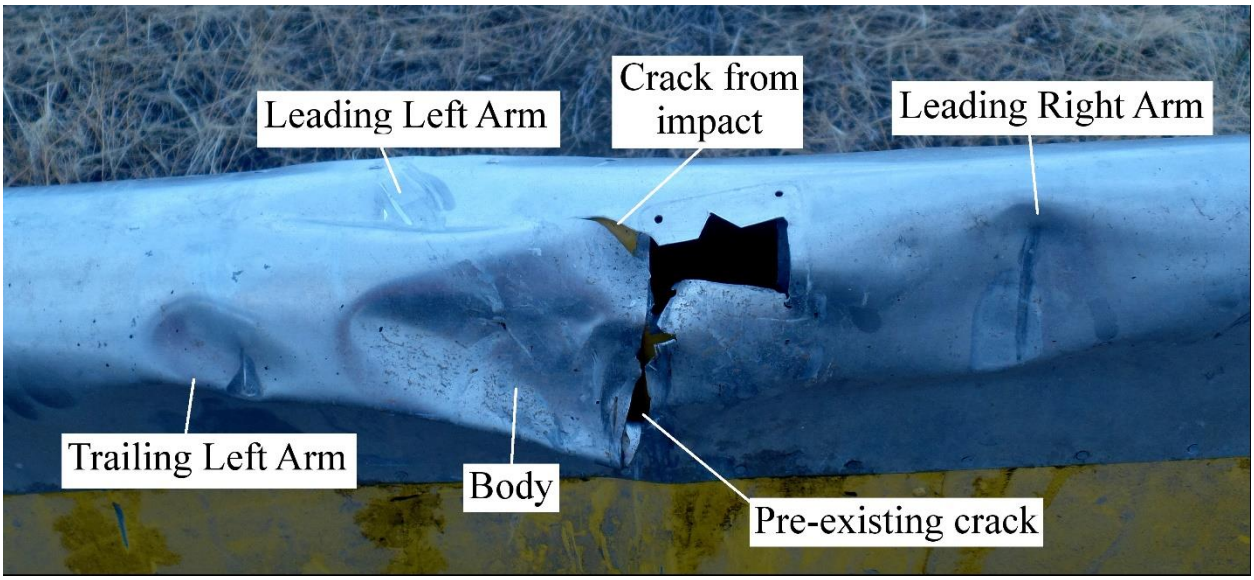

Figure 44. Damage from test 2

Wing Test 3. In the third test, a DJI Phantom 3 with a camera was used. The UAS impacted the wing at 115 KTS. The UAS impacted while pitched nose down at around 85 degrees as shown in Figure 45.

Figure 45. Test 3 impact orientation

The trailing left motor made impact with the leading edge of the wing. The motor shaft penetrated the leading edge, causing a fracture of 3.6” from tip to tip, shown in Figure 46. The secondary leading edge sustained minimal damage from impact with the motor shaft. The rest of the UAS passed underneath the wing without making impact.

Figure 46. Damage from Test 3

Wing Test 4. In the fourth test, a DJI Phantom 3 with a camera was used. The UAS impacted the wing at 115 KTS. The UAS impacted while pitched nose down at around 10 degrees, left up at 20 degrees, and rotated left forward at 135 degrees as shown in Figure 47.

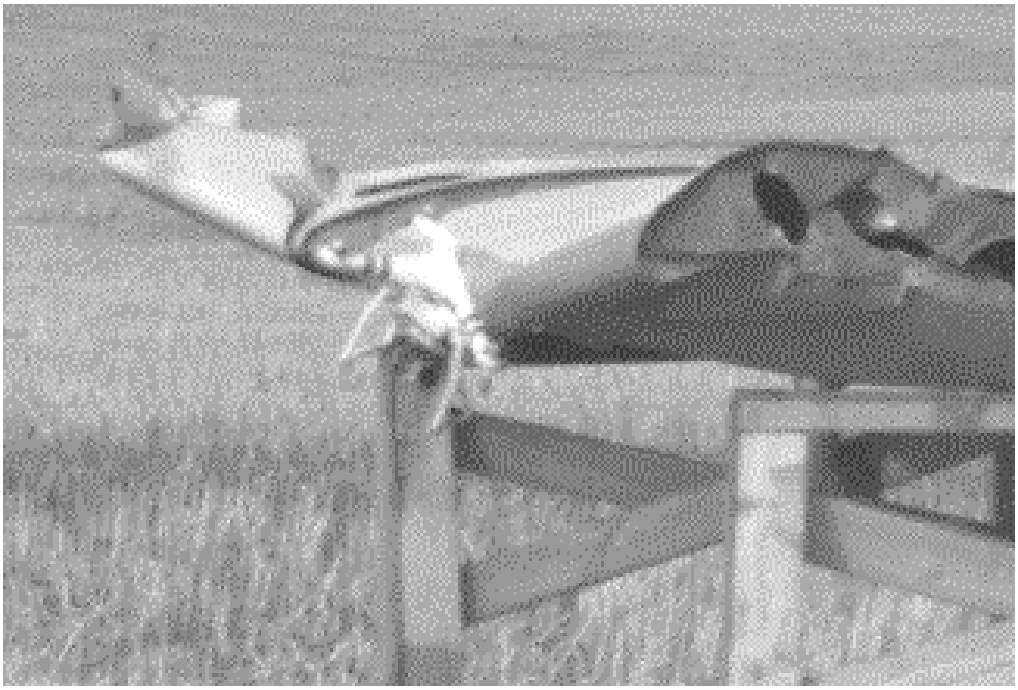

Figure 47. Test 4 impact orientation

The leading left arm impacted the leading edge of the wing. The trailing left arm impacted the top surface of the wing. The leading right arm impacted the bottom of the wing. The UAS impacted and accelerated downward with the trailing right arm not impacting the wing. The impact caused a 12” by 6” dent with a maximum depth of 1.6” as shown in Figure 48. The damage caused the STOL cuff to part with the wing on the top surface with rivet failure. The damage extended into the secondary leading edge. Damage occurred to the skin of the wing as well as a rib as shown in Figure 48 and Figure 49.

Figure 48. Damage from Test 4

Figure 49. Interior Damage from Test 4

Wing Test 5. In the fifth test, A DJI Phantom 3 with a camera was used. The UAS impacted the wing at 115 KTS. The UAS impacted while pitched nose up at around 10 degrees, and left up at 5 degrees as shown in Figure 50.

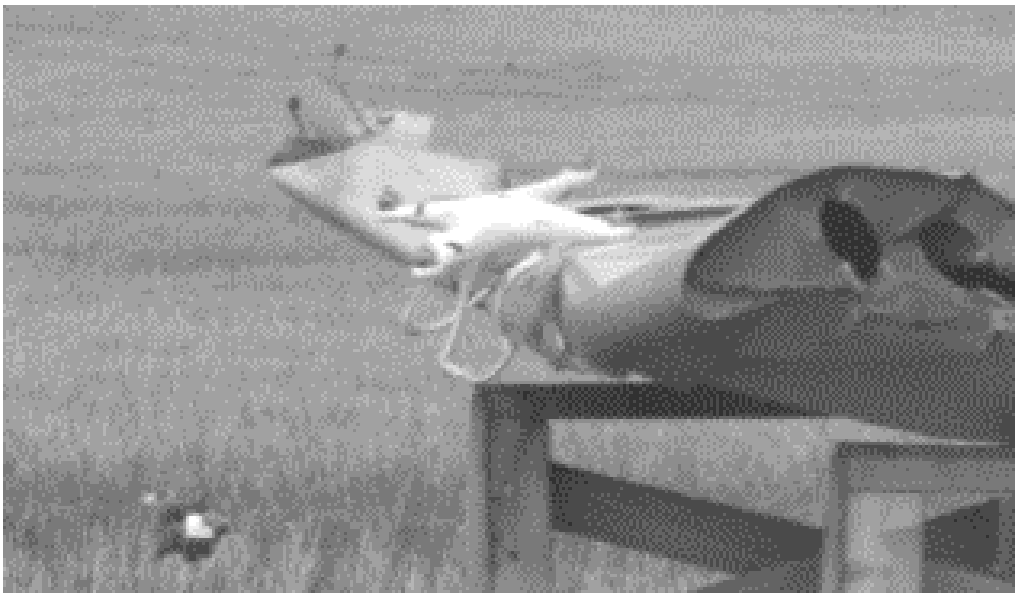

Figure 50. Test 5 impact orientation

The UAS body impacted the top surface of the wing near the leading edge. The UAS legs impacted the leading edge. The UAS camera separated from the UAS impact and passed below the wing. The body of the UAS caused an 18” by 10” dent with a depth of 0.5”. The right legs caused a 3.5” by 4” dent with a depth of 0.3”. The left legs of the UAS caused a 1.5” by 1.5” dent with a depth of 0.2” to the STOL cuff.

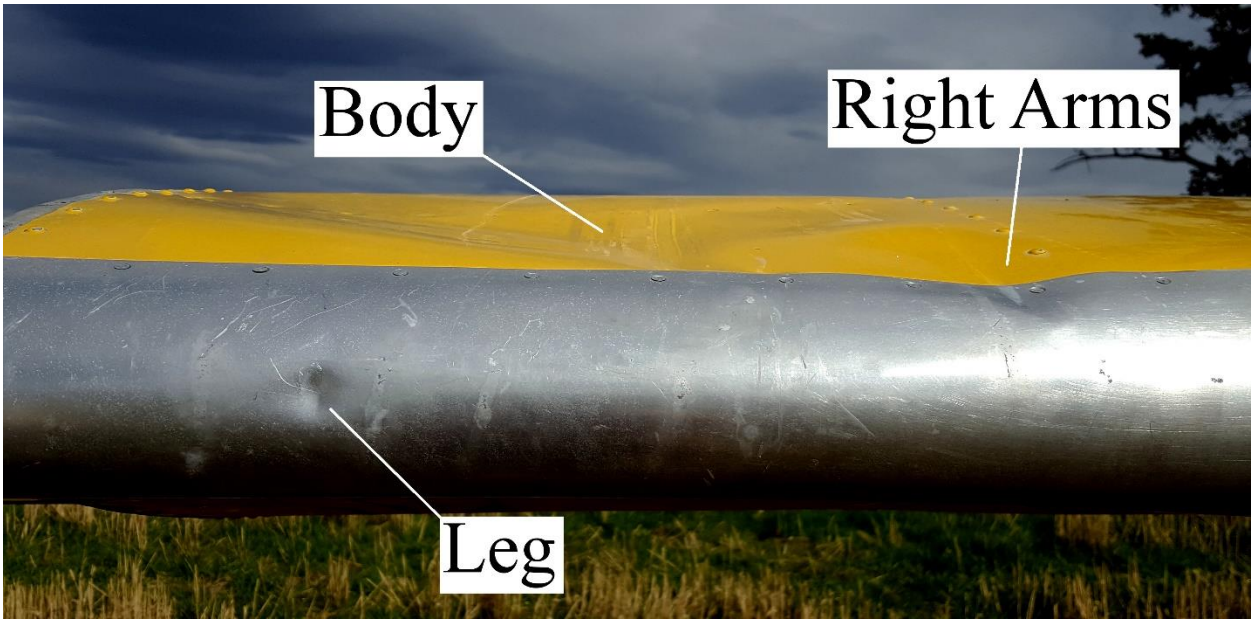

Figure 51. Damage from Test 5

Cessna 182 Wing Testing

A Cessna 182 Wing was donated for research. The wing had a 0.032” aluminum short takeoff and landing (STOL) cuff on the leading edge. The wing was fixed to the capstone impact tower with two rachet straps, one on either side of the impact zone.

The testing instrumentation consisted of two high speed cameras and a set of strain gauges. A Photron FASTCAM Mini UX100 setup to capture impact and a Chronos 1.4 setup to measure speed. Four biaxial strain gauges were setup on the leading edge on either side of the target impact area. The target impact area was halfway between strain gauges two and three.

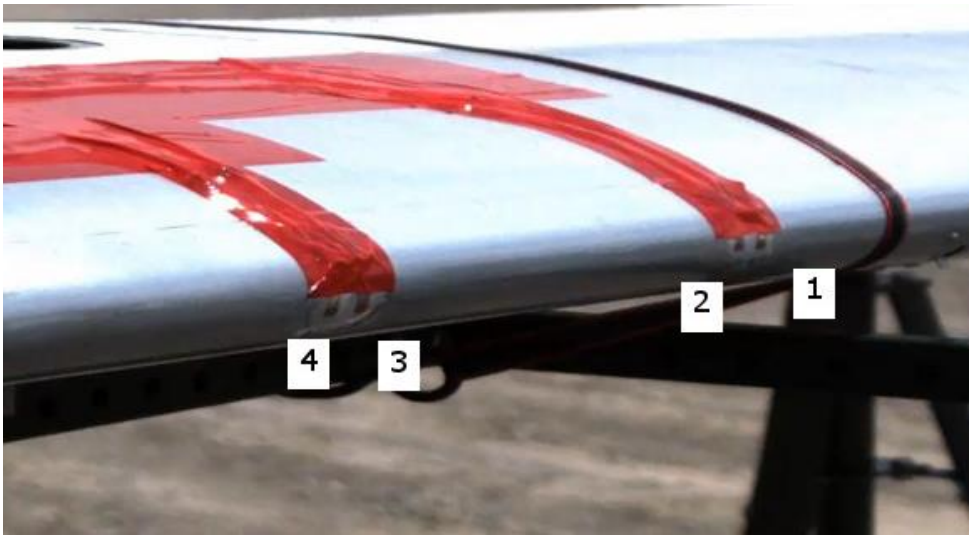

Figure 52. Strain gauge layout

Wing Test 1. Test 1 had instrumentation failure. The DAQ associated with the strain gauges did not record during the test and video file from the Chronos 1.4 was corrupted. With those failures, only the impact was captured. The impact location missed the target area. Upon further inspection, it was found that the launcher was out of alignment with the target.

Figure 53. Cessna 182 test 1 impact

Wing Test 2. Test 2 was run with the intent of further testing the instrumentation set up. The impact location had to overlap with that in test 1 in order to use the strain gauges. Since the impact location is previously damaged, the test cannot be used to determine damage from UAS impact. All instrumentation performed as intended in this test.

In the second test, a complete DJI Phantom 3 was used. The UAS impacted the wing at 117 KTS. The UAS impacted the wing pitched nose down at around 45 degrees. Cumulative damage from the two impacts was substantial. A large crack formed in STOL cuff and original leading edge in the impact zone.

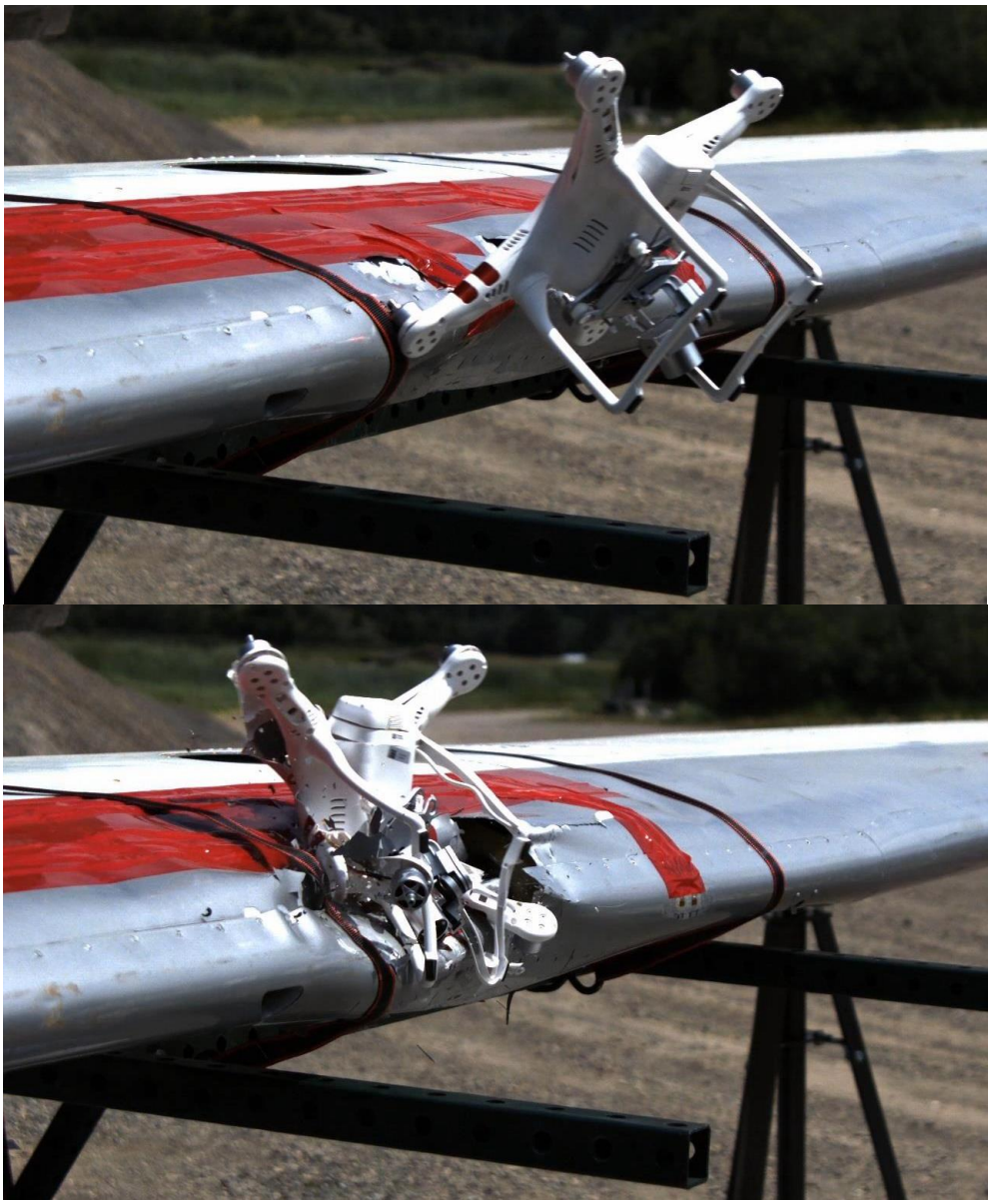

Figure 54. Cessna 182 test 2 impact

Test Facility Conclusions

The launch facility has been thoroughly tested and was successfully used for crash testing of quadcopter UAS to aircraft wings. The launcher has been proven to be capable of launching UAS at high enough velocity and accurately enough for testing. While the launcher has proven capable and ready for testing, some further testing of the test fixturing needs to be performed.

The launcher has proven to be capable of launching the DJI Phantom 3 at 120 KTS while being accurate enough to hit the leading edge of a wing. The launcher has proven to have accuracy of about ±2" vertically and about ±5" horizontally. The orientation at impact on the other hand, varies by a large margin. The UAS rarely flies flat and level, usually rotating significantly prior to impact.

Test fixturing has been developed to meet the needs of FE model validation. The sawhorses used with the Piper Cherokee wings provided no horizontal support to the wing and were not suitable for instrumentation integration. A capstone group designed an impact tower to provide support and allow instrumentation integration. When used with the Cessna 182 wing, the capstone impact tower provided some horizontal support, but was more compliant than desired. The capstone impact tower also did not have the flexibility to integrate the wide range of test fixtures that are desired. The shipping container impact tower was developed to solve these issues. Testing of the shipping container impact tower will be completed in summer of 2020.

Once testing on the shipping container impact tower is completed, the facility will be ready for finite element confirmation testing of aircraft parts. NIAR is developing an

FE model of a Cessna 182, including a windscreen model which utilizes the material model developed in the following chapter. Instrumented impact testing of Cessna 182 parts will provide vital information for confirmation of these models.

SUMMARY AND CONCLUSIONS

Understanding the risks to aircraft in the event of a crash with UAS is important for the FAA to make informed decisions on regulation of UAS. The FAA created ASSURE to carryout research of crash between UAS and aircraft. As a part of an ASSURE study, Montana State University has worked to understand general aviation crash with development of a Cessna 182 windscreen material model and formation of a full scale crash test facility.

A material model has been developed for the PMMA used in Cessna 182 windscreens. Two material models were developed, utilizing MAT_124 and MAT_187. In order to develop the models, a windscreen was cut into coupons for tensile and impact testing. The tensile data was utilized to create the model inputs. A model of the impact tower was then created to compare and adjust the material models with impact testing data. Ultimately, inputs for stiffness as a function of strain rate and independent yield curves as a function of strain rate were determined to be important for accurately modeling PMMA. Due to these inputs, the MAT_187 model performed better in both the single element test and the impact tower model.

The MAT_187 material model was shared with NIAR for implementation in their Cessna 182 model. In previous years, NIAR developed and confirmed a model of a DJI Phantom 3, shown in Figure 55. The Phantom 3 model was used along with impact models of a commercial transport and a business jet to virtually analyze impact at critical locations, such a wing leading edge, vertical stabilizer, horizontal stabilizer, and windscreen. The windscreen impact is shown here in Figure 56 and Figure 57. To prepare for Cessna 182

windscreen model confirmation, a similar model of impact between the Phantom 3 model and the windscreen test setup will be prepared. Using 3D reverse engineering tools, they have been able to generate a 3D model of the windscreen and the windscreen test fixture. The two models will be virtually assembled and defined for confirmation testing of the windscreen model.

Code	Material Model	LS-DYNA Model
	Johnson Cook	*MAT_015
	Piecewise Linear Plasticity	*MAT_024
	Enhanced Composite with Damage	*MAT_054
	Crushable Foam	*MAT_063

Figure 55. Exploded view of the DJI Phantom 3 model developed for LS-DYNA at NIAR [19]

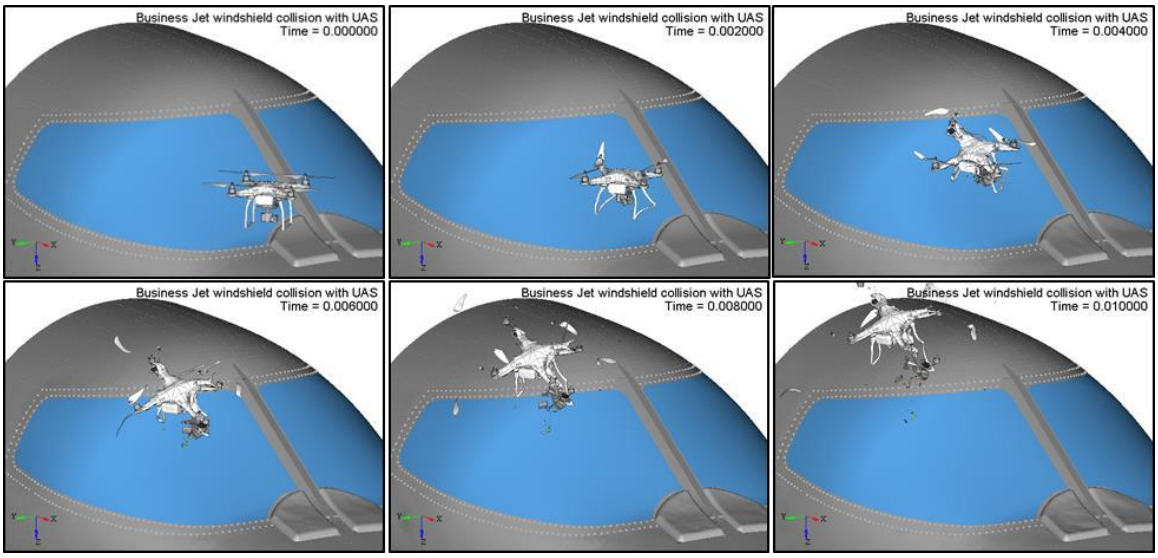

Figure 56. Business jet windscreen model of impact at 250 KTS, from NIAR [19]

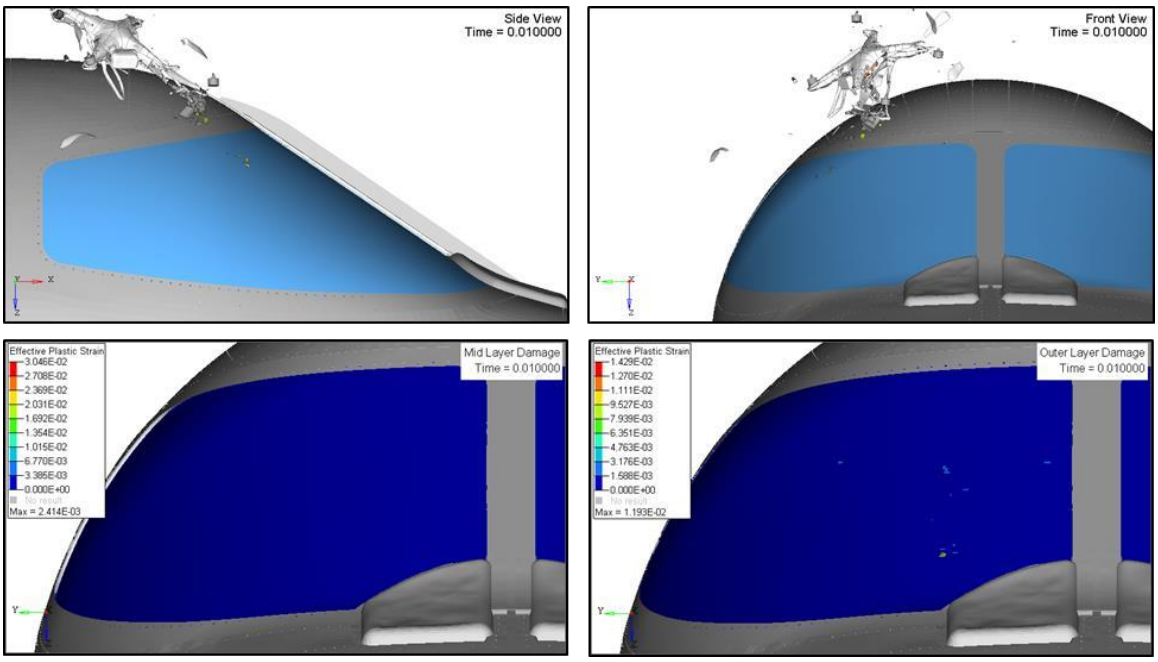

Figure 57. Modeled damage of the business jet windscreen from 250 KTS impact, from NIAR [19]

The crash test facility was developed in order to confirm FE models being developed of aircraft parts. The facility was built to test crash of DJI Phantom 3's at 120 knots into aircraft parts. The launcher proved its capabilities with testing on Piper Cherokee and Cessna 182 wings. In addition to launching, a test fixture system with flexible instrumentation has been developed. In addition to impact velocity measurement, the facility is capable of high speed voltage based measurement, including load cells and strain gauges. With final testing of the test fixture system in summer of 2020, the facility will be ready for FE model validation testing.

The crash test facility will be utilized for the full scale testing required to confirm the windscreen model. For comparison with the FE model, instrumentation is needed. High speed cameras will be used to determine impact velocity, orientation, and location. Load cells will be utilized to determine reactionary forces between the test fixture and the

ground, and between the test fixture and the shipping container impact tower. High speed digital image correlation will be utilized to determine displacement of a section of the windscreen. Additionally, any damage to the windscreen will be recorded. Four windscreens are to be impacted by DJI Phantom 3's. Two at a common approach speed of a Cessna 182, around 75 KTS. Two at the maximum launcher speed, around 120 KTS.

The impact velocity, orientation, and location from testing will be used to create an impact case for the fixtured windscreen FE model. The model results will then be compared to the test damage, load cell data and displacement data. If the results of the model and from the four tests match closely, the model performance is confirmed, and can be applied for further analysis. Otherwise, adjustments to the material model will be required before it can be used in the Cessna 182 model.

A confirmed model will be used to analyze new crash scenarios including a variety of crash velocities, orientations, and UAS. The confirmed aircraft model will also available for future analysis with newly developed UAS models,providing the FAA with key information about the risk UAS pose to aircraft even as the UAS market changes, and. allowing them to make informed regulatory decisions as they continue to integrate UAS into the airspace.

FUTURE WORK

Future and Ongoing work include the following:

- Work to fully confirm the windscreen material model is in progress.
- Instrumented full scale testing of windscreens will be performed and compared to the FE model being developed at NIAR.
- In addition, full scale testing is planned to confirm Cessna 182 wing and strut models being developed at NIAR.
- PMMA material model improvement
  - Material Testing
    - Compression testing – Quasistatic
    - Shear testing – Quasistatic
    - Samples from multiple windscreens
  - Impact Tower Testing
    - Improve velocity measurement system
    - Strain gauged impact tower samples
    - Test with a range of impact tower masses
- Windscreen material model implementation
  - The windscreen material model has been shared with NIAR for implementation in their Cessna 182 model. They are taking the following steps to implement the model
    - Reverse Engineering windscreen geometry into a CAD model
    - Mesh the windscreen, including a mesh sensitivity study
    - Input the windscreen material model
    - NIAR is also developing an FE crash model of the test fixture that will hold the windscreen for confirmation testing. At this point, the windscreen model is ready to be input to the test fixture model.
      - The meshed windscreen and fixture models will be virtually assembled, and a previously developed and confirmed DJI Phantom 3 crash model will be imported

        - Contact relationships between all components will be defined
        - Boundary and initial conditions for the model will be defined
    - Windscreen model confirmation – Scheduled for summer of 2020
        - Prior to windscreen model confirmation, some work needs to be done to the full scale test facility, see the next 1st level bullet for details
        - Impact test four windscreens
            - Two at approach speed of ~75 KTS
            - Two at maximum launch speed of ~120 KTS
        - Run the fixtured windscreen model with testing impact conditions – To be performed at NIAR
        - Compare results of the model and testing – To be performed at NIAR
    - Once confirmation testing is completed, the windscreen can be virtually assembled into the Cessna 182 model
        - Each component is meshed and has a material model defined
        - Contact relationships between components are defined
- Full scale test facility
    - Finalize wing and strut fixtures
        - A capstone group designed and was in the process of building the fixtures when they lost access to campus resources due to COVID-19
    - Finalize windscreen fixture
    - Instrumentation testing
        - Flat and angled panel tests will be performed to confirm instrumentation
        - Load cells need to be tested in this setup to confirm loads are within range
        - The following DIC test setup needs to be determined
            - Measurement view size
            - Calibration article size
            - Frame Rate
            - Shutter Speed
        - This testing will also serve as testing of the shipping container impact tower

- Wing and strut model confirmation – Scheduled for summer of 2020
  - This process is very similar to windscreen confirmation
  - Finalize wing, strut, and fixture models – In progress at NIAR
  - Impact test four wings and four struts
    - Two at approach speed of ~75 KTS
    - Two at maximum launch speed of ~120 KTS
  - Run the FE models with testing impact conditions – To be performed at NIAR
  - Compare results of the model and testing – To be performed at NIAR

REFERENCES CITED

[1] D. S. Cairns and G. Johnson, "Volume I - UAS Airborne Collision Severity - Projectile and Target Definitions," 16 December 2016. [Online]. Available: http://www.assureuas.org/projects/deliverables/a3/Volume%20I%20UAS%20Airborne%20Collision%20Severity%20Projectile%20and%20Target%20Definition.pdf.

[2] "Unmanned Aircreaft Systems," 18 February 2020. [Online]. Available: https://www.faa.gov/uas/.

[3] C. Shalby, M. Puente and H. Fry, "Illegal drones ground water-dropping helicopters at critical moment in Maria fire battle," 2 November 2019. [Online]. Available: https://www.latimes.com/california/story/2019-11-01/maria-fire-drone-hinders-firefighting-efforts-as-blaze-doubles-in-size-overnight.

[4] "ASSURE About Us," [Online]. Available: http://www.assureuas.org/about.php.

[5] R. D. Cook, D. S. Malkus, M. E. Plesha and R. J. Witt, "Finite Elements in Structural Dynamics and Vibrations," in *Concepts and applications of Finite Element Analysis,* New York, John Wiley & Sons,Inc., 2002, pp. 373-376,616-619.

[6] "What are the differences between implicit and explicit?," [Online]. Available: https://www.dynasupport.com/faq/general/what-are-the-differences-between-implicit-and-explicit.

[7] J. O. Hallquist, "LS-DYNA Theory Manual," Livermore, 2006.

[8] L. &. C. Chen, "Tension and compression tests of two polymers under quasi-static and dynamic loading," *Polymer Testing,* vol. 21(2), pp. 113-121, 2002.

[9] H. Lobo, "Methodology for Selection of Material Models for Plastics Impact Simulation," in *6th European LS-DYNA Users' Conference*, Gothenburg, 2007.

[10] "DataSheet NI 9205," 4 July 2017. [Online]. Available: https://www.ni.com/pdf/manuals/378020a_02.pdf.

[11] K. Woo, "Three-Point bending," 2019.

[12] N. Mavrodontis, "Converting Engineering Stress-Strain to True Stress-Strain in Abaqus," Simuleon, 9 October 2017. [Online]. Available:

https://info.simuleon.com/blog/converting-engineering-stress-strain-to-true-stress-strain-in-abaqus.

[13] "LS-DYNA Keyword User's manual," Livermore, 2018.

[14] "Release Notes for LS-DYNA version R11.1.0," [Online]. Available: http://ftp.lstc.com/anonymous/outgoing/support/FAQ/ReleaseNotes/Release_Notes_LS-DYNA_R11_1_0_rev0.txt.

[15] "Material Contact Properties Table," 2008. [Online]. Available: http://atc.sjf.stuba.sk/files/mechanika_vms_ADAMS/Contact_Table.pdf.

[16] S. Bala and J. Day, "General Guideliness for Crash Analysis in LS-DYNA," 2013. [Online]. Available: http://ftp.lstc.com/anonymous/outgoing/jday/faq/guidelines.pdf.

[17] K. Abrahamson, W. Bullock, D. Murphy and C. Schaeffer, *UAV Drone Launcher Capstone Final Report*, Montana State University, 2017.

[18] C. Gardner, A. Hartke, I. Maret and A. Murray, *Instrumented Impact Panel for Drone Impact Studies Capstone Final Report*, Montana State University, 2016.

[19] G. Olivares, L. Gomez, J. Espinosa de los Monteros, R. Baldridge, C. Zinzuwadia and T. Aldag, "Volume II - UAS Airborne Collision Severity Evaluation - Quadcopter," July 2017. [Online]. Available: http://www.assureuas.org/projects/deliverables/a3/Volume%20II%20-%20UAS%20Airborne%20Collision%20Severity%20Evaluation%20-%20Quadcopter.pdf.

APPENDICES

APPENDIX A

DJI PHANTOM 3 LAUNCH DATA

Table 4. DJI Phantom 3 launch setup and velocity

Date	Shot Number	Battery	Camera	Landing Gear	Velocity High Speed Camera	Impact High Speed Camera	Speed (knots)	Number of Bands
8/8/2016	29	Yes	No	Yes	Fastec	-	151	12
	30	Yes	No	Yes	Fastec	-	157	12
8/18/2016	31	Yes	Yes	Yes	Fastec	-	107	12
10/9/2016	32	Yes	Yes	Yes	Fastec	-	115	12
	33	Yes	Yes	Yes	Fastec	-	115	12
	34	Yes	Yes	Yes	Fastec	-	118	12
	35	Yes	Yes	Yes	Fastec	-	115	12
4/22/2017	36	Yes	Yes	Yes	Fastec	-	123	12
6/15/2017	38	Yes	Yes	No	Fastec	-	118	12
	39	Yes	Yes	No	-	Fastec	-	12
6/21/2017	40	Yes	Yes	No	Fastec	-	110	12
	41	Yes	No	No	Fastec	-	115	12
7/20/2017	44	Yes	Yes	Yes	Fastec	-	133	16
7/2/2018	46	No	No	Yes	Fastec	-	114	12
7/6/2018	47	No	No	Yes	Fastec	-	122	16
	48	No	No	Yes	-	Fastec	-	16
	49	No	No	Yes	Nikon	Fastec	135	16
7/9/2018	50	No	No	Yes	Nikon	Fastec	131	16
7/13/2018	51	Yes	Yes	Yes	Nikon	Chronos	123	16
	52	Yes	Yes	Yes	Nikon	Chronos	124	16
	53	Yes	Yes	Yes	Nikon	Chronos	127	16
7/15/2018	54	Yes	Yes	Yes	Nikon	Chronos*	107	16
	55	Yes	Yes	Yes	Nikon	Chronos	113	16
	56	Yes	Yes	Yes	Nikon	Chronos	107	16
7/16/2018	57	Yes	Yes	Yes	-	Chronos	-	16
	58	Yes	Yes	Yes	-	Chronos	-	16
7/17/2018	59	Yes	Yes	Yes	Chronos	Photron	120	16
	60	Yes	Yes	Yes	Chronos	Photron	115	16
	61	Yes	Yes	Yes	Chronos*	Photron	-	16
	62	Yes	Yes	Yes	Chronos	Photron	117	16

* File corrupted

Table 5. DJI Phantom 3 test targets and impact orientation

Date	Shot #	Target	Flight Orientation At Impact		
			Nose up positive	Right up positive	CCW positive (from above)
8/8/2016	29	Piper Wing	10°	5°	0°
	30	Piper Wing	15°	-10°	-5°
8/18/2016	31	Piper Wing	-90°	-20°	90°
10/9/2016	32	Piper Wing	-85°	0°	0°
	33	Piper Wing	-10°	-20°	-135°
	34	Piper Wing	-10°	0°	0°
	35	Piper Wing	10°	-5°	0°
4/22/2017	36	Steel Plate	-90°	-5°	-10°
6/15/2017	38	Steel Plate	-70°	-30°	-45°
	39	Steel Plate	-80	45°	0°
6/21/2017	40	Steel Plate	-100°	-70°	20°
	41	Steel Plate	-110°	15°	-35°
7/20/2017	44	Steel Plate	-110°	5°	0°
7/2/2018	46	Steel Plate	-170°	10°	-5°
7/6/2018	47	Steel Plate	-110°	-15°	20°
	48	Steel Plate	-140°	10°	10°
	49	Steel Plate	-120°	45°	10°
7/9/2018	50	Steel Plate	-80°	-90°	-10°
7/13/2018	51	Piper Wing	-	-	-
	52	Piper Wing	-	-	-
	53	Piper Wing	-130°	0°	0°
7/15/2018	54	Piper Wing	-	-	-
	55	Piper Wing	-90°	0°	-20°
	56	Piper Wing	15°	90°	0°
7/16/2018	57	Piper Wing	-130°	10°	0°
	58	Piper Wing	-5°	-5°	0°
7/17/2018	59	Piper Wing	-5°	-10°	0°
	60	Steel Plate	-85°	-10°	40°
	61	Cessna Wing	-60°	-10°	30°
	62	Cessna Wing	-45°	0°	0°

Table 6. Specifications of high speed cameras used in testing

Camera	Frame Rate (Frames/Second)	Resolution at Test Frame Rate (px)	Speed Measurement Resolution (knots)
Fastec TS3	1000	1024x600	~4
Photon FASTCAM Mini UX100	4000	1280x1024	~1
Nikon Point and Shoot	1200	400x144	~4
Chronos 1.4	1500	1280x720	~3

APPENDIX B

MATERIAL MODEL INPUT DETERMINATION CODE

MATLAB R2018b was used to calculate the material model inputs as well as process tensile and impact tower outputs. The following code was written to determine these inputs.

MAT_124inputs

Used to determine MAT_124 material model inputs.

```
% MAT_124inputs
% Creates input data for the MAT_124 material modle

close all
```

Initialize

```
f1 = figure; %('units','normalized','outerposition', [0 0 1 1])
% Samples grouped by strain rate
High_Rate    = {'L2A',  'L5B',   'R5', 'R7'             };
MidH_Rate    = {'L3A',  'L3B', 'R14B'                   };
MidL_Rate    = {'L6A',  'L6B',  'L13'                   };
Low_Rate     = {'L2B',  'L5A',  'L12', 'R4', 'R8', 'R10'};

E_Mod = 3100;   % MPa

% Define variable array sizes
tlength = length(High_Rate) + length(MidH_Rate) + length(MidL_Rate) + length(Low_Rate);
long = 1e5;
Tstress = zeros(long, tlength);
Tstrain = zeros(long, tlength);
str = 0:0.00001:0.15;
strint = zeros(length(str),tlength);
MS = zeros(1,tlength);
SE = zeros(1,tlength);
BS = MS; SR = MS; MR = MS;
MAS = zeros(1,4);
SRA = zeros(1,4);
% Control Plot colors
choosecolor = true;
color = [     0 0.4470 0.7410;...
         0.8500 0.3250 0.0980;...
         0.9290 0.6940 0.1250;...
         0.4940 0.1840 0.5560;...
         0.4660 0.6740 0.1880;...
         0.3010 0.7450 0.9330;...
```

```
          0.6350 0.0780 0.1840;
          1      1      0     ];
```

Calculate Stress and Strain

```
hold on
% Evaluate quasistatic tensile tests
colori = color(1,:);
for i = 1:length(Low_Rate)
    % Call LowRate to return stress-strain data
    [MS(i), BS(i), SR(i), MR(i),p1, Tstressin,Tstrainin,time] =
LowRate(char(Low_Rate(i)),colori);
    % Interpolate stress onto a strain array of constant step size
    [Tstr,index] = unique(Tstrainin);
    strint(:,i) = interp1(Tstr,Tstressin(index),str);
end
% Interpolate a single stress strain curve for the strain rate group
MeanStress(:,1) = mean(strint(:,1:i),2);
MSA(1) = mean(MS(1:i)); % mean ultimate tensile strength
SRA(1) = mean(SR(1:i)); % mean strain rate


% Evaluate second slowest tensile tests
colori = color(2,:);
for j = 1:length(MidL_Rate)
    r = i + j;
    [MS(r), BS(r), SR(r), MR(r),p2,Tstressin,Tstrainin] =
HighRateTrim(char(MidL_Rate(j)),colori);
    [Tstr,index] = unique(Tstrainin);
    strint(:,r) = interp1(Tstr,Tstressin(index),str);
end
MeanStress(:,2) = mean(strint(:,(i+1):r),2);
MSA(2) = mean(MS((i+1):r));
SRA(2) = mean(SR((i+1):r));

% Evaluate second fastest tensile tests
colori = color(3,:);
for j = 1:length(MidH_Rate)
    g = j + r;
    % Call HighRateTrim to return stress-strain data
    [MS(g), BS(g), SR(g), MR(g),p3,Tstressin,Tstrainin] =
HighRateTrim(char(MidH_Rate(j)),colori);
    [Tstr,index] = unique(Tstrainin);
    strint(:,g) = interp1(Tstr,Tstressin(index),str);
end
MeanStress(:,3) = mean(strint(:,(r+1):g),2);
MSA(3) = mean(MS((r+1):g));
SRA(3) = mean(SR((r+1):g));

% Evaluate fastest tensile tests
```

```
colori = color(4,:);
for k = 1:length(High_Rate)
    s = g + k;
    [MS(s), BS(s), SR(s), MR(s),p4,Tstressin,Tstrainin] =
HighRateTrim(char(High_Rate(k)),colori);
    [Tstr,index] = unique(Tstrainin);
    strint(:,s) = interp1(Tstr,Tstressin(index),str);
end
MeanStress(:,4) = mean(strint(:,(g+1):s),2);
MSA(4) = mean(MS((g+1):s));
SRA(4) = mean(SR((g+1):s));

xlim([0,inf])
ylim([0,inf])
```

Plot Stress and Strain

```
f2 = figure('Name','Interpolated Curves and approximate model Curves');
plot(str*100,MeanStress,'-')
hold on
plot([0,4],[0,E_Mod*0.04],'k')
axis([0 .065*101 0 max((MS))*1.1])
title('True Stress vs True Strain at varied strain rate')
xlabel('True Strain (%)')
ylabel('True Stress (MPa)')
legend({'0.001 strain/sec', '0.017 strain/sec', '0.3     strain/sec',...
        '1.5     strain/sec','Elastic Modulus'},'location','southeast')
```

Interpolate to find a smooth plastic stress strain curve

This curve is used to develop the base yield curve input

```
Curv = 3;   % Base Stress Strain Curve Low = 1, MidL = 2, MidH = 3, High = 4

% Interpolate Curv stress-strain to a new strain array
numb = 4;
str2 = 0:(10^(-numb)):0.07;     % strain array of even distribution
Mstrint = interp1(str,MeanStress(:,Curv),str2);


% Find the intersection point of the stress-strain curve and elastic
% modulus. Use that as the yield point, and create a plastic stress-strain
% cuve
[StrainInt,StressInt] = intersections(str2,Mstrint,[0,.04],[0,E_Mod*0.04],1);
iout = find(str2 > (round(StrainInt(end),numb)-5*10^(-numb-1)) & str2 <
(round(StrainInt(end),numb)+5*10^(-numb-1))) ;
pStress = Mstrint(iout(end):end);
pStrain  = str2(iout(end):end) - pStress/E_Mod;
pStrain = pStrain - pStrain(1);
```

```
% Create an evely spaced plastic strain array and interpolate plastic
% stress for the curve
[pStrMax,imp] = max(pStrain);
pstr = linspace(0,pStrMax,10);
Pstrint = interp1(pStrain(1:imp),pStress(1:imp),pstr);
```

Calculate LCSR curve

A curve relating ultimate tensile strength to strain rate linear fit of ultimate tensile strenght and log strain rate

```
StRfail = [0.001,0.017,0.3,1.5]; % Strain rates of tensile data
% plastic strain rates, determined from single element tests
pStRfail = [0.00095, 0.0162, 0.28 ,   1.111];

% Linear fit of utlimate tensile strength and log strain rate
SvSRfit = polyfit(log(SRA),MSA,1);
fitMS = polyval(SvSRfit,log(SR));
PeakFits = polyval(SvSRfit,log(pStRfail));

fprintf('Max Tensile stress fit is S = %g*ln(e_rate) + %g \n', SvSRfit(1),SvSRfit(2))

f3 = figure('Name','LCSR fit');
semilogx(SR,MS,'*')

% Calculate strain energy to failure for each tensile test
idFail = sum(~isnan(strint));
for i = 1:tlength
    SE(i) = trapz(str(1:idFail(i)),strint(1:idFail(i),i));
end
% Average strain energy to failure for each strain rate group
SEm = zeros(1,4);
SEm(1) = mean(SE(1:6));
SEm(2) = mean(SE(7:9));
SEm(3) = mean(SE(end-8:end-5));
SEm(4) = mean(SE(end-4:end));

% Evenly spaced log strain rate for LCSR curve creation
Nsteps = 40;
SRcln = linspace(log(0.001),6,Nsteps);
SRc   = exp(SRcln);
LCSRT = polyval(SvSRfit,SRcln)/max(Pstrint);

figure(f2)
for i = 1:4

plot(EpsZ{i}(1:indout(i))*100,PCurveZ{i}(1:indout(i)),'Color',color(i,:),'HandleVisibilit
```

```
y','off','LineWidth',1)
end
```

Single Element Comparison

```
rates = {'0p001','0p017','0p3','1p5'};
rateN = [ 0.001 , 0.017 , 0.3 , 1.5];
fps = figure('Name','Plastic Stress Strain Curves');
workingDir = 'C:\Users\Forrest\Dropbox\Thesis\LSWorking\Impact
Tower\5inby1inSample\PostTensileModel\SingleElement Stress Strain Plots\';
[SEmodel, MSmodel, Prate] =
SingleElementStressvsStrain('LCSRCurve3v3',workingDir,rates,f1,fps,color);

figure(f1)
xlabel('True Strain (%)')
ylabel('Ture Stress (MPa)')
```

Plotting

```
pStRfail = [0.00095, 0.015, 0.28 ,   1.5];
pStrFail = [0.03 , 0.019, 0.005, 0.0015];

figure(f3)
hold on
semilogx(SRc,LCSRT*max(Pstrint),'HandleVisibility','off')
semilogx(rateN,MSmodel,'kx')
title('Ultimate Tensile Stress vs Strain Rate')
xlabel('Strain Rate (1/sec)')
ylabel('Ultimate Tensile Stress (MPa)')
ylim([0,140])
legend('Experimental', 'Model','Location','southeast')

figure(fps)
title('Plastic Stress vs Plastic Strain')

figure('Name','Plastic Strain to Failure')
semilogx(pStRfail/1000,pStrFail,'x')
hold on
Nsteps = 20;
Dln = .1;

SRcln2 = linspace(log(pStRfail(1)),log(pStRfail(2)),Nsteps);
LCFail = linspace(pStrFail(1),pStrFail(2),Nsteps);
for i = 2:(length(pStrFail)-1)
    SRcln2 = [SRcln2(1:end-1),linspace(log(pStRfail(i)),log(pStRfail(i+1)),Nsteps)];
    LCFail = [LCFail(1:end-1),linspace(pStrFail(i),pStrFail(i+1),Nsteps)];
end

LCFail = linspace(pStrFail(1),pStrFail(end),Nsteps);
```

```
SRcln2 = linspace(log(pStRfail(1)),log(pStRfail(end)),Nsteps);
LCFail = [LCFail,LCFail(end)];


LRcln2 = horzcat(SRcln2,SRcln2(end)+Dln);
LRc2 = horzcat(exp(LRcln2));
semilogx(LRc2/1000, LCFail)
xlabel('Strain rate (1/ms)')
ylabel('Plastic Strain to Failure')
```

Write output curves to file

```
% Plastic Strain to failure vs plastic strain rate
fid = fopen('FailPStrain3.csv', 'w');
out = vertcat(LRc2/1000,LCFail);
fprintf(fid,'%.9e %.9e \n',out);
fclose(fid);
disp('FailPStrain3.csv written')

% LCSR tension curve
fid = fopen('LCSRT.csv', 'w');
out = vertcat(SRc/1000,LCSRT);
fprintf(fid,'%.9e %.9e \n',out);
fclose(fid);
disp('LCSRT.csv written')

% Base yield curve
fid = fopen('BaseLoadCurve3.csv', 'w');
pstr = [pstr,pstr(end)+(pstr(end)-pstr(end-1))];
Pstrint = [Pstrint,Pstrint(end)];
out = vertcat(pstr,Pstrint);
fprintf(fid,'%.6f %.6f \n',out);
fclose(fid);
disp('BaseLoadCurve.csv written')

crv = {'Low Rate', 'Mid Low Rate', 'Mid High Rate', 'High Rate'};
fprintf(horzcat(crv{Curv},' curve used as the base with Elastic modulus of %g MPa
\n'),E_Mod)
```

MAT_187inputs

Used to determine MAT_187 material model inputs.

```
% MAT_187inputs
% Creates input data for the MAT_187 material model

close all
```

Initialize

```
f1 = figure;

% Samples grouped by strain rate
High_Rate    = {'L2A',  'L5B',   'R5', 'R7'             };
MidH_Rate    = {'L3A',  'L3B', 'R14B'                  };
MidL_Rate    = {'L6A',  'L6B',  'L13'                  };
Low_Rate     = {'L2B',  'L5A',  'L12', 'R4', 'R8', 'R10'};


E_Mod = 2897;   % MPa, Base elastic modulus
nu    = 0.39;   % Poissons ratio

% Define variable array sizes
tlength = length(High_Rate) + length(MidH_Rate) + length(MidL_Rate) + length(Low_Rate);
long = 1e5;     % length of interpolation strain array
Tstress = zeros(long, tlength);
Tstrain = zeros(long, tlength);
str = 0:0.00001:0.15;   % strain array of constant step size
strint = zeros(length(str),tlength);
MS = zeros(1,tlength);
SE = zeros(1,tlength);
BS = MS; SR = MS; MR = MS;
MSA = zeros(1,4);
SRA = zeros(1,4);
BSA = zeros(1,4);
% Control Plot colors
choosecolor = true;
color = [     0 0.4470 0.7410;...
         0.8500 0.3250 0.0980;...
         0.9290 0.6940 0.1250;...
         0.4940 0.1840 0.5560;...
         0.4660 0.6740 0.1880;...
         0.3010 0.7450 0.9330;...
         0.6350 0.0780 0.1840;
         1      0      0     ];
```

Calculate Stress and Strain

```
hold on

% Evaluate quasistatic tensile tests
colori = color(1,:);
for i = 1:length(Low_Rate)
    % Call LowRate to return stress-strain data
    [MS(i), BS(i), SR(i), MR(i),p1, Tstressin,Tstrainin] =
LowRate(char(Low_Rate(i)),colori);
    [Tstr,index] = unique(Tstrainin*.95); % Remove duplicate strain values
    % Interpolate stress onto a strain array of constant step size
    strint(:,i) = interp1(Tstr,Tstressin(index),str);
end
% Interpolate a single stress strain curve for the strain rate group
MeanStress(:,1) = mean(strint(:,1:i),2);
MSA(1) = mean(MS(1:i));     % mean ultimate tensile strength
SRA(1) = mean(SR(1:i));     % mean strain rate
BSA(1) = mean(BS(1:i));     % mean breaking strain

% Evaluate second lowest strain rate tensile tests
colori = color(2,:);
for j = 1:length(MidL_Rate)
    r = i + j;
    % Call HighRateTrim to return stress-strain data
    [MS(r), BS(r), SR(r), MR(r),p2,Tstressin,Tstrainin] =
HighRateTrim(char(MidL_Rate(j)),colori);
    [Tstr,index] = unique(Tstrainin);
    strint(:,r) = interp1(Tstr,Tstressin(index),str);
end
MeanStress(:,2) = mean(strint(:,(i+1):r),2);
MSA(2) = mean(MS((i+1):r));
SRA(2) = mean(SR((i+1):r));
BSA(2) = mean(BS((i+1):r));

% Evaluate second highest strain rate tensile tests
colori = color(3,:);
for j = 1:length(MidH_Rate)
    g = j + r;
    [MS(g), BS(g), SR(g), MR(g),p3,Tstressin,Tstrainin] =
HighRateTrim(char(MidH_Rate(j)),colori);
    [Tstr,index] = unique(Tstrainin);
    strint(:,g) = interp1(Tstr,Tstressin(index),str);
end
MeanStress(:,3) = mean(strint(:,(r+1):g),2);
MSA(3) = mean(MS((r+1):g));
SRA(3) = mean(SR((r+1):g));
BSA(3) = mean(BS((r+1):g));

% Evaluate highest strain rate tensile tests
colori = color(4,:);
```

```
for k = 1:length(High_Rate)
    s = g + k;
    [MS(s), BS(s), SR(s), MR(s),p4,Tstressin,Tstrainin] =
HighRateTrim(char(High_Rate(k)),colori);
    [Tstr,index] = unique(Tstrainin);
    strint(:,s) = interp1(Tstr,Tstressin(index),str);
end
MeanStress(:,4) = mean(strint(:,(g+1):s),2);
MSA(4) = mean(MS((g+1):s));
SRA(4) = mean(SR((g+1):s));
BSA(4) = mean(BS((g+1):s));

% Initialize Stress-Strain plot
f2 = figure;
hold on
axis([0 .065*101 0 140])
title('True Stress vs True Strain at varied strain rate')
xlabel('True Strain (%)')
ylabel('True Stress (MPa)')

FigPl = figure('Name','Plastic Stress Strain');
hold on
```

LCSR calculation

A curve relating ultimate tensile strength to strain rate linear fit of ultimate tensile strength and log strain rate

```
SvSRfit = polyfit(log(SRA),MSA,1);
fitMS   = polyval(SvSRfit,log(SR));

% Create an interpolated curve for LCSR fit
Nsteps = 8;
SRcln = linspace(log(0.001),6,Nsteps);
SRc   = exp(SRcln);
LCSRT = polyval(SvSRfit,SRcln)/max(MeanStress(:,3));

f3 = figure('Name','LCSR fit');
semilogx(SR/1000,MS,'*')
axis([2e-7 5 0 180])
title('Ultimate Tensile Strength vs Strain Rate')
xlabel('Strain Rate (strain/ms)')
ylabel('Ultimate Tensile Strength (MPa)')
hold on
```

Interpolate to find a smooth effective stress vs strain curve

```
rates = [0.001,0.017,0.3,1.5,15,150,1500];  % Strain rates for the LCSS curves
ratesleg = {'0.001 strain/sec','0.017 strain/sec','0.3   strain/sec',...
            '1.5   strain/sec','15    strain/sec','150   strain/sec','1500  strain/sec'};
efail = [7 , 5, 3.7, 3.5, 3.5,3.5,3.5]/100; % breaking strain for LCSS curve creation
pStrToFail = [0.04 , 0.02, 0.01, 0.008, 0.008, 0.008,0.008]; % Plastic strain to failure

numb = 3;
LL = length(rates);
sStress = cell(1,LL);
sStrain = cell(1,LL);
StrainY = zeros(1,LL);


% Create a smooth stress-strain curve for each of "rates"
for i = 1:length(rates)
    if i <= 3   % The test data can be used
        indstr = sum(~isnan(MeanStress(:,i)));
        n = ceil(str(indstr)/10^(-numb));
        str2 = linspace(0,str(indstr),n);
        Mstrint = interp1(str,MeanStress(:,i),str2);
        idFail = sum(~isnan(Mstrint));
        Mstrint = smooth(Mstrint(1:idFail));
        escale = 1;
    else    % Smoothing is required
            % The 3rd curve developed is scaled by ultimate strength and
            % breaking strain to create a smooth curve
        indstr = sum(~isnan(MeanStress(:,3)));
        n = ceil(str(indstr)/10^(-numb));
        str2 = linspace(0,str(indstr),n);
        Mstrint = interp1(str,MeanStress(:,3),str2);
        idFail = sum(~isnan(Mstrint));
        Mstrint = smooth(Mstrint(1:idFail));
        Mstrint = Mstrint*polyval(SvSRfit,log(rates(i)))/max(MeanStress(:,3));
        escale  = efail(i)/efail(3);
    end
    % Stress and strain array for strain rate: rates(i)
    sStress{i}  = smooth(Mstrint,5)';   % 5 point moving average filter for further
smoothing
    sStrain{i}  = str2(1:idFail)*escale;
    figure(f2)
    plot(100*sStrain{i},sStress{i},'Color',color(i,:),'LineWidth',1);

    % check slope, to ensure the curve intersects the elastic modulus
    Slope  = (sStress{i}(2:end) - sStress{i}(1:end-1))./(sStrain{i}(2:end) -
sStrain{i}(1:end-1));
    islope = find(Slope < E_Mod, 1, 'first');
end

%
% figure(fSlope)
```

```
% plot([0,0.05],[E_Mod,E_Mod])
% xlabel('Strain')
% ylabel('Stiffness (MPa)')
```

Single Element Comparison

this section is used to compare a set of single element tests against the test data

```
fSA = figure('Name','Model Stress Strain');

ratesM = {'0p001','0p017','0p3','1p5'};%,'10','100','1000'};%,,'150','1500'};
%{'0p001','0p017','0p017s','0p3','1p5','15','150'};%, '0p3','1p5'};
workingDir = 'C:\Users\Forrest\Dropbox\Thesis\LSWorking\Impact
Tower\5inby1inSample\PostTensileModel\SingleElement Stress Strain Plots\';
[SEmodel, MSmodel, Prate, Pfail, Mrate,Sfail] =
SingleElementStressvsStrain('MAT187v2',workingDir,ratesM,f1,FigPl,color);

figure(f1)
axis([0 11 0 150])
xlabel('True Strain (%)')
ylabel('True Stress (MPa)')
legf1 = {'0.001 strain/sec', '0.017 strain/sec', '0.3     strain/sec', '1.5
strain/sec', '10      strain/sec','100    strain/sec', '1000  strain/sec'};
legend(legf1,'location','southeast')
box on

figure(f3)
semilogx(Mrate, MSmodel,'kx')
semilogx(SRc/1000,LCSRT*max(MeanStress(:,3)))
legend('Experimental data', 'MAT 187 model data', 'Log-Linear
fit','Location','southeast')
```

Calculate LCSS curves

```
fBS = figure('Name', 'Strain to Failure');
semilogx(SR,BS*100,'*')
hold on
semilogx(Mrate*1000,Sfail*100,'kx')
title('Failure Strain vs Strain Rate')
xlabel('Strain Rate (1/s)')
ylabel('Breaking Strain (%)')
legend('Experimental data', 'MAT 187 model data','Location','northeast')

% Calculate strain energy to failure for each tensile test
idFail = sum(~isnan(strint));
for i = 1:tlength
    SE(i) = trapz(str(1:idFail(i)),strint(1:idFail(i),i));
end
% Average strain energy to failure for each strain rate group
```

```
SEm = zeros(1,4);
SEm(1) = mean(SE(1:6));
SEm(2) = mean(SE(7:9));
SEm(3) = mean(SE(end-8:end-5));
SEm(4) = mean(SE(end-4:end));

Strfail = pStrToFail;
StRfail = [0.001,0.017,0.3,1.5];
SRsteps = -7:0;
SRsteps = exp(SRsteps);
pStress = cell(1,LL);
pStrain = cell(1,LL);
pstr    = cell(1,LL);
pstrint = cell(1,LL);
pstrRate = zeros(1,LL);
Yield    = zeros(1,LL);
Legf2 = {};

% Elastic modulus input curve, developed through trial and error
LCEMOD = [2500, 2897, 3300, 3400, 3475, 3650,3875];
% Plastic strain rate for each strain rate group, used by LS-DYNA to
% determine yield behavior and strain. Found through performing single
% element tests
pStrToFail = [0.03, 0.0143, 0.0052, 0.0035, 0.003, 0.003, 0.003];
for i = 1:length(rates)
    % Find intersection between stress-strain curve and elastic modulus,
    % the point that yield will begin
    [StrainInt,~] = intersections(sStrain{i},sStress{i},[0,.04],[0,LCEMOD(i)*0.04],1);
    iout = find(sStrain{i} > StrainInt,1,'first') ;
    pStress{i} = [LCEMOD(i)*StrainInt(end), sStress{i}(iout(end):end)];
    pStrain{i} = [0, sStrain{i}(iout(end):end)] - pStress{i}/LCEMOD(i);
    [pStrMax,imp] = max(pStrain{i});

    % interpolation of plastic strain for each group
    n = ceil(pStrMax/7.5e-4);
    if n<4
        n = 4;
    end
    pstr{i} = linspace(0,pStrMax,n);
    pstrint{i} = interp1(pStrain{i}(1:imp),pStress{i}(1:imp),pstr{i});
    pstr{i} = pstr{i}/pstr{i}(end)*pStrToFail(i);
    % Create an approximate stress strain curve
    EStress = [0,pstrint{i}];
    EStrain = [0,pstr{i} + pstrint{i}/LCEMOD(i)];

    % approximate plastic strain rate, used in the first round of single
    % element tests, replaced by outputs from the single element test
    pstrRate(i) = rates(i) - (EStress(end) - EStress(end-1))/...
                             (EStrain(end) - EStrain(end-1))*rates(i)/LCEMOD(i);

    Yield(i) = pStress{i}(1);
```

```
    Legf2 = horzcat(Legf2,horzcat(num2str(rates(i)),' strain/sec'));
    figure(FigPl)
    plot(pstr{i},pstrint{i},'Color',color(i,:))
    figure(f2)
    plot(EStrain(1:2)*100,EStress(1:2),'--','Color',color(i,:),'HandleVisibility','off')
end

figure(f2)
legend(ratesleg,'Location','southeast')

% plastic strain rates evaluated from single element tests
pstrRate(1:4) = [8.4e-7, 1.24e-5, 1.6e-4, 9e-4]*1000;

fpstrF = figure('Name','Plastic Strain to Failue');
semilogx(pstrRate,pStrToFail,'*')
hold on
semilogx(Prate*1000,Pfail,'kx')
xlabel('Plastic Strain Rate (1/sec)')
ylabel('Plastic Strain to Failure')

% Create plastic strain to failure vs plastic strain rate curve with equal
% strain rate spacing. LS-DYNA interpolates to a curve with equal spacing.
% This curves ensures that the interpolation is doing what we want.
pstrRateOut = linspace(pstrRate(1),pstrRate(end-2),999);
pstrFailOut =
interp1(log(pstrRate([1,2,3,4,5])),pStrToFail([1,2,3,4,5]),log(pstrRateOut));
pstrFailOut = [pstrFailOut,pstrFailOut(end)];
pstrRateOut = [pstrRateOut,pstrRateOut(end) + pstrRateOut(2) - pstrRateOut(1)];

hold on
semilogx(pstrRateOut,pstrFailOut)

% Create an elastic modulus vs effective strain rate with equal strain rate
% spacing
EstrRateOut = linspace(rates(2),rates(end-1),5000);
EMODRates = interp1(log(rates(2:end)),LCEMOD(2:end),log(EstrRateOut));

fEMOD = figure('Name','Elastic Modulus vs Strain Rate');
semilogx(rates,LCEMOD,'*')
hold on
semilogx(EstrRateOut,EMODRates)
```

Write Output Tables to file

```
% Yield curve for each plastic strain rate
for i = 1:length(sStress)
```

```
    file = horzcat('LCSS',num2str(i),'.csv');

    fid = fopen(file,'w');
    out = vertcat(pstr{i},pstrint{i}/1000);
    fprintf(fid,'%.6f,%.6f \n',out);
    fclose(fid);
    disp([file, ' written'])
end

% Strain rate vs the curve number
fid = fopen('LCSS.csv', 'w');
out = vertcat(log(pstrRate/1000), 1:length(rates));
fprintf(fid,'%.6f,%.6f \n',out);
fclose(fid);
disp('LCSS.csv written')

% Elastic modulus vs effective strain rate
fid = fopen('LCEMOD.csv', 'w');
out = vertcat((EstrRateOut/1000), EMODRates/1000);
fprintf(fid,'%.6f,%.6f \n',out);
fclose(fid);
disp('LCEMOD.csv written')

% Plastic strain to failure vs plastic strain rate
fid = fopen('FailStrain.csv', 'w');
out = vertcat((pstrRateOut/1000), pstrFailOut);
fprintf(fid,'%.6f,%.6f \n',out);
fclose(fid);
disp('FailStrain.csv written')


fclose('all');

% Calculate bulk modulus and shear modulus based on elastic modulus and
% poissons ratio, used in LS-DYNA for time step calculation
E_Mod = 2600;
fprintf('Calculated with Elastic modulus of %g MPa \n',E_Mod)
G_Mod = E_Mod/2/(1+nu);
K_Mod = E_Mod/3/(1-2*nu);

fprintf('Shear Modulus is %g MPa \n',G_Mod)
fprintf('Bulk  Modulus is %g MPa \n',K_Mod)
```

LowRate

Used to processes quasistatic tensile data.

```
% LowRate
% Evaluates voltage outputs from quasistatic tensile testing and outputs
% maximum stress, breaking strain, averate strain rate, average crosshead
% speed, the plot handle, true stress, true strain, and a time array. True
% stress vs true strain is also plotted

function [MaxStress,BreakingStrain,StrainRate,MachineRate,p,Tstress,Tstrain,Time] =
LowRate(Sample,colori)

clear IN strain stress Tstrain Tstress t

filename = horzcat(Sample,'wdim.txt');

samplerate = 1;         % kHz

IN = importdata(filename);
% % % F = IN(:,1); % Load Cell
% % % E = IN(:,2); % Extensometer
% % % D = IN(:,3); % Crosshead Displacement

area    = IN(1,4);      % Sample crossectional area
Oshift  = IN(4,4);      % Sample specific data point shift for filtering end
Dfilt   = IN(5,4)/10^4; % Displacement filter condition
Ishift  = IN(7,4)*100;  % Smaple specific data point shift for filtering start
Ffilt   = 2500;         % Force filter condition

% Filter out the first 0.5 seconds of data
droptime = 0.5;
dropsamples = droptime*samplerate*1000;
IN = IN(dropsamples:end,:);

% Define a time array
dt = 1/samplerate/1000;
t = ((1:length(IN(:,1)))-1)*dt;  % sec

% Voltage to mechanical unit conversions
F_calib = 22480*4.448/10;       % N/V,
E_calib = 40/10/100;            % strain/V
D_calib = 2/10;                 % in/V

Dzero1 = mean(IN(2:250,3));             % average dispacement at the start
IN(:,3) = (IN(:,3) - Dzero1)*D_calib;   % Displacement from Dzero1

% Find the start of loading
for i = 1:length(IN(:,3))
    check = IN(i,3);
```

```
    if check > Dfilt
        indexDropIN = i;    % Array index that satisfies the filter
        break
    end
end
indexin = indexDropIN - Ishift; % Adding extra data points before the filter
if indexin < 1
    indexin = 1;                % Incase the shift goes below 1
end

% Zero force, strain, and displacement at the start of loading
Fzero = mean(IN((indexin-100):indexin,1));
Ezero = mean(IN((indexin-100):indexin,2));
Dzero = mean(IN((indexin-100):indexin,3));

IN(:,1) = (IN(:,1) - Fzero)*F_calib;    % N,        Load
IN(:,2) = (IN(:,2) - Ezero)*E_calib;    % mm/mm,    Strain
IN(:,3) = (IN(:,3) - Dzero)*25.4;       % mm,       Displacement

% Find Failure
for i = length(IN(:,1)):-1:1
    check = IN(i,1);
    if check > Ffilt
        indexDropOUT = i;   % Array index that satisfies the filter
        break
    end
end

indexout = indexDropOUT + Oshift;   % Add data points after the filter

% % titlecell = {'Load vs Time','Strain vs Time', 'Displacement vs Time'};
% % xlabelstr = 'Time (sec)';
% % ylabelcell = {'Load (N)', 'Strain (mm/mm)', 'Displacement (mm)'};
% %
% % for i = 1:3
% %     subplot(3,1,i)
% %     plot(t,IN(:,i))
% %     hold on
% %     plot(t(indexin:indexout),IN(indexin:indexout,i))
% %     title(titlecell{i})
% %
% %     xlabel(xlabelstr)
% %     ylabel(ylabelcell{i})
% %     legend('Before and After Testing', 'Testing Event','Location','northwest')
% % end
% %
% %
% % figure
% % hold on

% Average crosshead speed and strain rate
```

```
DR_mean = (IN(indexout,3) - IN(indexin,3))/(t(indexout)-t(indexin));
SR_mean = (IN(indexout,2) - IN(indexin,2))/(t(indexout)-t(indexin));

stress = IN(indexin:indexout,1)/area;   % MPa, Engineering Stress
strain = IN(indexin:indexout,2);        % mm/mm, Engineering Strain
Tstrain = log(1 + strain);              % mm/mm, True strain
Tstress = stress.*(1 + strain);         % MPa  , True stress

% Plotting
if colori == 0
    p = plot(Tstrain*100,Tstress);
    c = get(p, 'Color');
    plot(Tstrain(end)*100,Tstress(end),'o',...
        'Color',c,...
        'MarkerFaceColor',c,...
        'MarkerSize',5,...
        'HandleVisibility','off')
elseif colori == 1
    if Sample(1) == 'L'
        colori = [0 0.4470 0.7410];
    else
        colori = [0.8500 0.3250 0.0980];
    end
    p = plot(Tstrain*100,Tstress,'Color',colori,'HandleVisibility','off');
    c = get(p, 'Color');
    plot(Tstrain(end)*100,Tstress(end),'o',...
        'Color',c,...
        'MarkerFaceColor',c,...
        'MarkerSize',5,...
        'HandleVisibility','off')
else
    p = plot(Tstrain*100,Tstress,'Color',colori,'HandleVisibility','off');
    plot(Tstrain(end)*100,Tstress(end),'o',...
        'Color',colori,...
        'MarkerFaceColor',colori,...
        'MarkerSize',5,...
        'HandleVisibility','off')
end

% Outputs with better names
Time = t(indexin:indexout);
MaxStress      = max(Tstress);
BreakingStrain = max(Tstrain);
StrainRate     = SR_mean;
MachineRate    = DR_mean;
```

HighRateTrim

Used to process all other strain rate tensile data

```
% HighRateTrim
% Evaluates voltage outputs from quasistatic tensile testing and outputs
% maximum stress, breaking strain, averate strain rate, average crosshead
% speed, the plot handle, true stress, true strain, and a time array. True
% stress vs true strain is also plotted

function [MaxStress,BreakingStrain,StrainRate,MachineRate,p,Tstress,Tstrain,Time] =
HighRateTrim(Sample,colori)

clear IN strain stress Tstrain Tstress t

filename = horzcat(Sample,'wdim.txt');

IN = importdata(filename);
% % % F = IN(:,1); % Load Cell
% % % E = IN(:,2); % Extensometer
% % % D = IN(:,3); % Crosshead Displacement

area        = IN(1,4);        % Sample cross-sectional area
speed       = IN(2,4);        % Expected crosshead speed
samplerate  = IN(3,4);        % Data sample rate in testing, kHz
Oshift      = IN(4,4);        % Sample specific data point shift for filtering end
Dfilt       = IN(5,4)/10^4;   % Displacement filter
FiltT       = IN(6,4);        % Force filter condition

% Filter out the first 0.5 seconds
droptime = 0.5;
dropsamples = droptime*samplerate*1000;
IN = IN(dropsamples:end,:);

% Define a time array
dt = 1/samplerate/1000;
t = ((1:length(IN(:,1)))-1)*dt;  % sec

% Voltage to mechanical unit conversions
F_calib = 22480*4.448/10;       % N/V,
E_calib = 40/10/100;            % strain/V
D_calib = 2/10;                 % in/V

Dzero1 = mean(IN(2:250,3));             % average displacement before testing
IN(:,3) = (IN(:,3) - Dzero1)*D_calib;   % Displacement zeroed at Dzero1

% Find the start of loading
for i = 2:length(IN(:,1))
    check = IN(i,3);
    if check > Dfilt
```

```
        indexDropIN = i;    % Array index that satisfies the filter
        break
    end
end

% Adding extra data points before the filter based on sample rate and
% crosshead speed
num = ceil(15*samplerate/speed); % Number of samples expected for 15mm displacement
inrate = (IN(indexDropIN,3) - IN(indexDropIN-num,3))/(t(indexDropIN)-t(indexDropIN-num));
Ishift = ceil(Dfilt/inrate*samplerate*1000);
indexin = min(indexDropIN) - Ishift;

% Zero force, strain, and displacement at the start of loading and convert
% to mechanical units
Fzero = mean(IN((indexin-100):indexin,1));
Ezero = mean(IN((indexin-100):indexin,2));
Dzero = mean(IN((indexin-100):indexin,3));
IN(:,1) = (IN(:,1) - Fzero)*F_calib;    % N,     Load
IN(:,2) = (IN(:,2) - Ezero)*E_calib;    % mm/mm, Strain
IN(:,3) = (IN(:,3) - Dzero);            % mm,    Displacement

% Find Failure
if FiltT == 1
[~,indexTmax] = max(IN(:,1));   % index of max load
elseif FiltT == 2
[~,indexTmax] = max(IN(:,2));   % index of max strain
end

indexout = indexTmax + Oshift; % shift failure index by sample


% for i = 1:3
%     subplot(3,1,i)
%     plot(t,IN(:,i))
%     hold on
%     plot(t(indexin:indexout),IN(indexin:indexout,i))
% end
% figure; hold on

% Average crosshead speed and strain rate
DR_mean = (IN(indexout,3) - IN(indexin,3))/(t(indexout)-t(indexin));
SR_mean = (IN(indexout,2) - IN(indexin,2))/(t(indexout)-t(indexin));

stress = IN(indexin:indexout,1)/area;       % MPa,   Engineering Stress
strain = IN(indexin:indexout,2);            % mm/mm, Engineering Strain
strainZero = find(strain <0,1,'last');      % index of strain = 0
strain = strain(strainZero:end) - strain(strainZero);   % filtered eng strain
stress = stress(strainZero:end) - stress(strainZero);   % filtered eng stress

Tstrain = log(1 + strain);      % mm/mm, True strain
Tstress = stress.*(1 + strain); % MPa  , True stress
```

```
% Plotting
if colori == 0
    p = plot(Tstrain*100,Tstress);
    c = get(p, 'Color');
    plot(Tstrain(end)*100,Tstress(end),'o',...
        'Color',c,...
        'MarkerFaceColor',c,...
        'MarkerSize',5,...
        'HandleVisibility','off')
elseif colori == 1
    if Sample(1) == 'L'
        colori = [0 0.4470 0.7410];
    else
        colori = [0.8500 0.3250 0.0980];
    end
    p = plot(Tstrain*100,Tstress,'Color',colori,'HandleVisibility','off');
    c = get(p, 'Color');
    plot(Tstrain(end)*100,Tstress(end),'o',...
        'Color',c,...
        'MarkerFaceColor',c,...
        'MarkerSize',5,...
        'HandleVisibility','off')
else
    p = plot(Tstrain*100,Tstress,'Color',colori,'HandleVisibility','off');
    plot(Tstrain(end)*100,Tstress(end),'o',...
        'Color',colori,...
        'MarkerFaceColor',colori,...
        'MarkerSize',5,...
        'HandleVisibility','off')
end

% Outputs with better names
Time = t(indexin:indexout);
MaxStress      = max(Tstress);
BreakingStrain = max(Tstrain);
StrainRate     = SR_mean;
MachineRate    = DR_mean;
```

SingleElementStressvsStrain

Used to process results from a single element test

```
function [SELS,MaxStress,Prate,Pfail,Mrate,Sfail] =
SingleElementStressvsStrain(folder,workingDir,rates,figurehandleSS,figurehandlePS,color)

workingDir = horzcat(workingDir,folder,'\');

Stress = cell (1,length(rates));
Strain = cell (1,length(rates));
SELS   = zeros(1,length(rates));
Prate  = zeros(1,length(rates));
Mrate  = zeros(1,length(rates));
Pfail  = zeros(1,length(rates));
MaxStress = zeros(1,length(rates));
pStrainR = figure('Name','Plastic Strain Rate');
subpleg = ceil(length(rates)/2);

% Run the calculations for each rate input
for i = 1:length(rates)
    % import stress-strain data from LS-DYNA output
    stress     = importdata(horzcat(workingDir,'~Stress'       ,rates{i},'.csv'));
    strain     = importdata(horzcat(workingDir,'~Strain'       ,rates{i},'.csv'));
    pstrain    = importdata(horzcat(workingDir,'~PlasticStrain',rates{i},'.csv'));
    Stress{i}  =  stress.data(:,2)*1000;
    Strain{i}  =  strain.data(:,2);
    PStrain{i} = pstrain.data(:,2);
    t{i}       = pstrain.data(:,1);
    [Sfail(i),index]  = max(Strain{i});     % Failure Strain
    [Pfail(i),indexp] = max(PStrain{i});    % Failure Plastic Strain
    % Plastic and total strain rates
    PSR{i}     = (PStrain{i}(2:indexp) - PStrain{i}(1:indexp-1))./(t{i}(2:indexp) -
t{i}(1:indexp-1));
    SR {i}     = (Strain {i}(2:indexp) - Strain {i}(1:indexp-1))./(t{i}(2:indexp) -
t{i}(1:indexp-1));
    % plot
    figure(figurehandleSS)
    hold on
    plot(Strain{i}(1:index)*100,Stress{i}(1:index),':','Color',color(i,:),'LineWidth',
2.5)  % ,'HandleVisibility','off'
    figure(figurehandlePS)
    hold on

plot(PStrain{i}(1:index),Stress{i}(1:index),':','Color',color(i,:),'HandleVisibility','of
f','LineWidth', 1.5)
    figure(pStrainR)
    subplot(subpleg,2,i)
    ppsr = plot(Strain{i}(1:indexp-1),PSR{i},'--','Color',color(i,:));
    yyaxis right
```

```
    plnr = plot(PStrain{i}(1:indexp-1),log(PSR{i}),':','Color',color(i,:));
    ylabel('Natural log of Strain Rate (1/ln(ms))')
    legend('Log Plastic Strain Rate')
    yyaxis left
    hold on
    psr  = plot(Strain{i}(1:indexp-1),SR{i},'Color',color(i,:));
    title({['Strain Rate at Total Strain rate of ', rates{i}, ' (1/s)'],['Failure at ',
num2str(t{i}(index)/1000), ' seconds']})
    xlabel('Strain')
    ylabel('Strain Rate (1/ms)')
    legend([psr,ppsr,plnr],{'Effective Strain Rate','Plastic Strain Rate','Log Plastic
Strain Rate'},'Location','southwest')
    ylim([0,max(SR{i})*1.1]);
    xlim([0,max(Strain{i})*1.05]);
    SELS(i) = trapz(Strain{i}(1:index),Stress{i}(1:index));
    MaxStress(i) = max(Stress{i});
    Prate(i) = PSR{i}(end);
    tfail(i) = t{i}(index);
    Mrate(i) = mean(SR{i});
end
```

APPENDIX C

IMPACT TOWER FORCE AND VELOCITY PLOTS

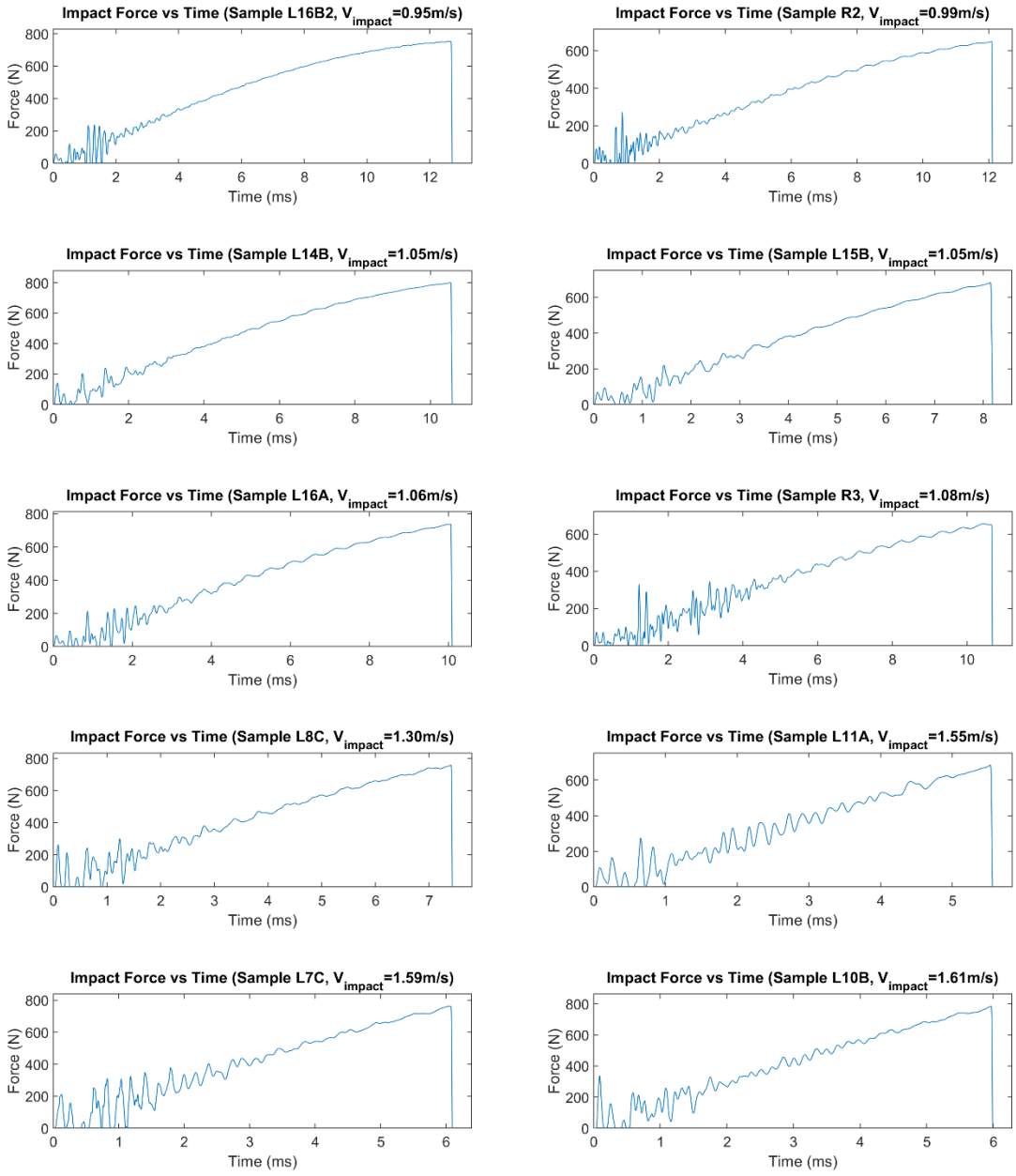

Figure 58. Impact Force vs time for samples with impact velocities of 1.61 m/s or less

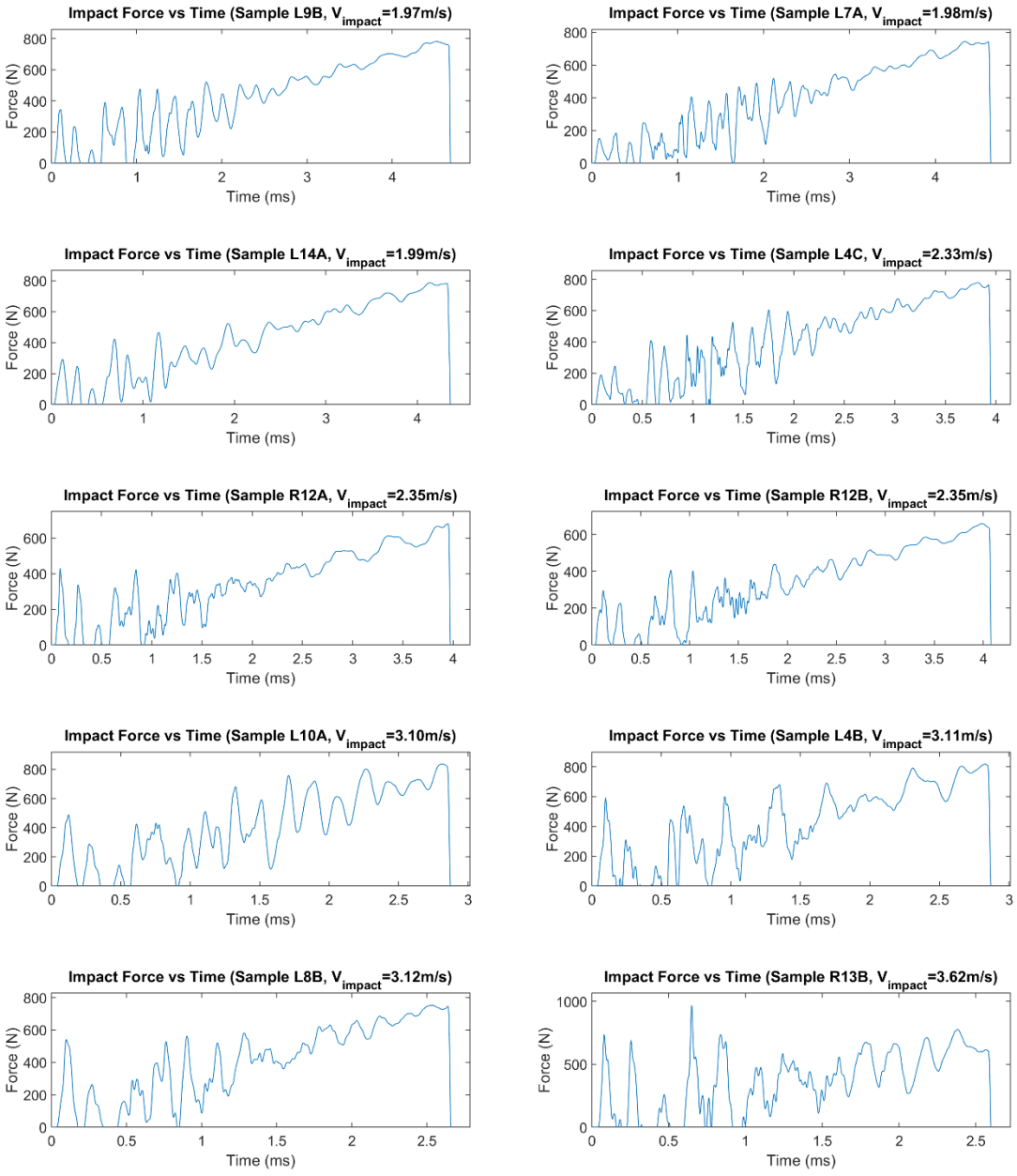

Figure 59. Impact Force vs time for samples with impact velocities between 1.97 m/s and 3.62

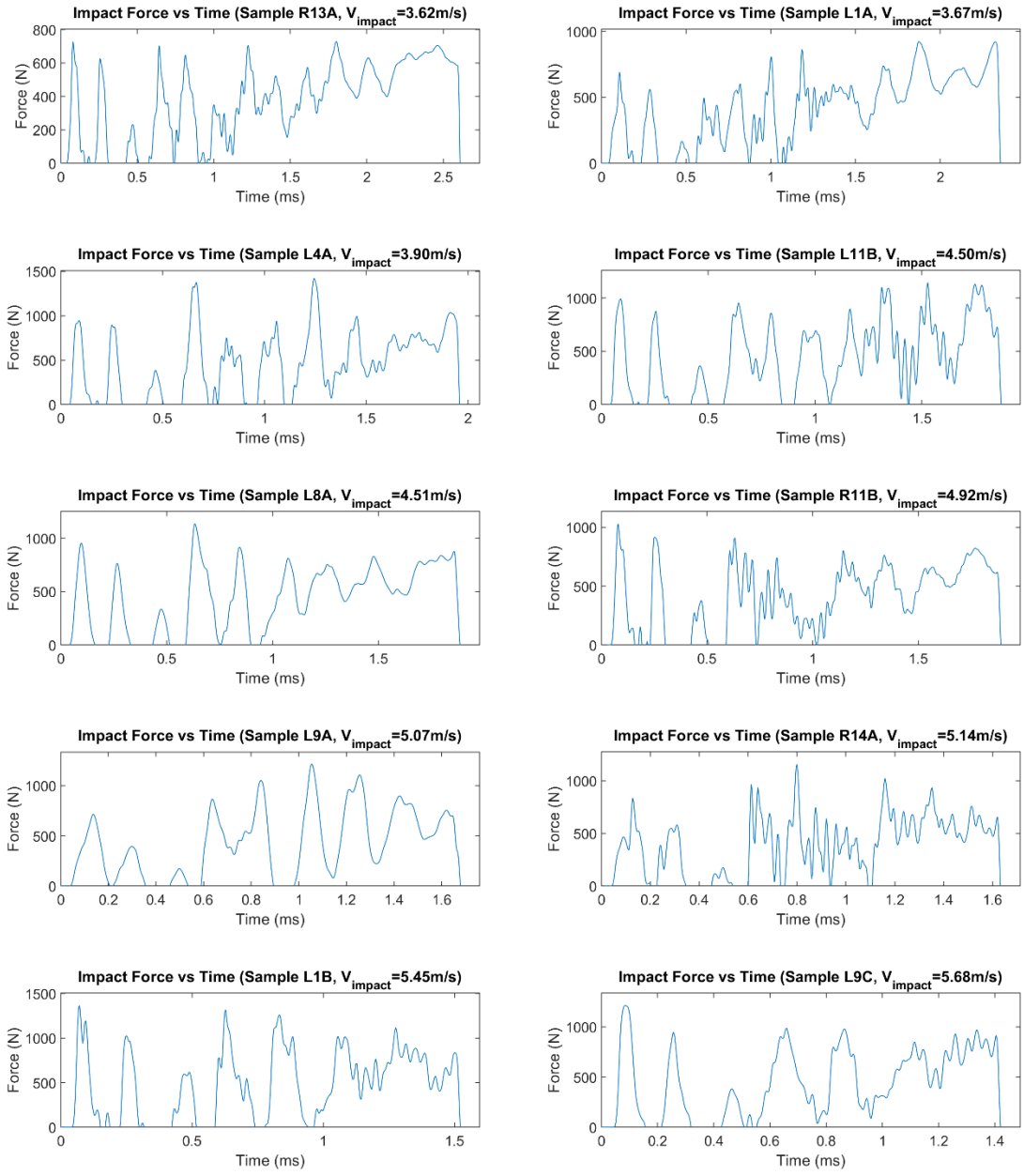

Figure 60. Impact Force vs time for samples with impact velocities of 3.62 m/s or greater

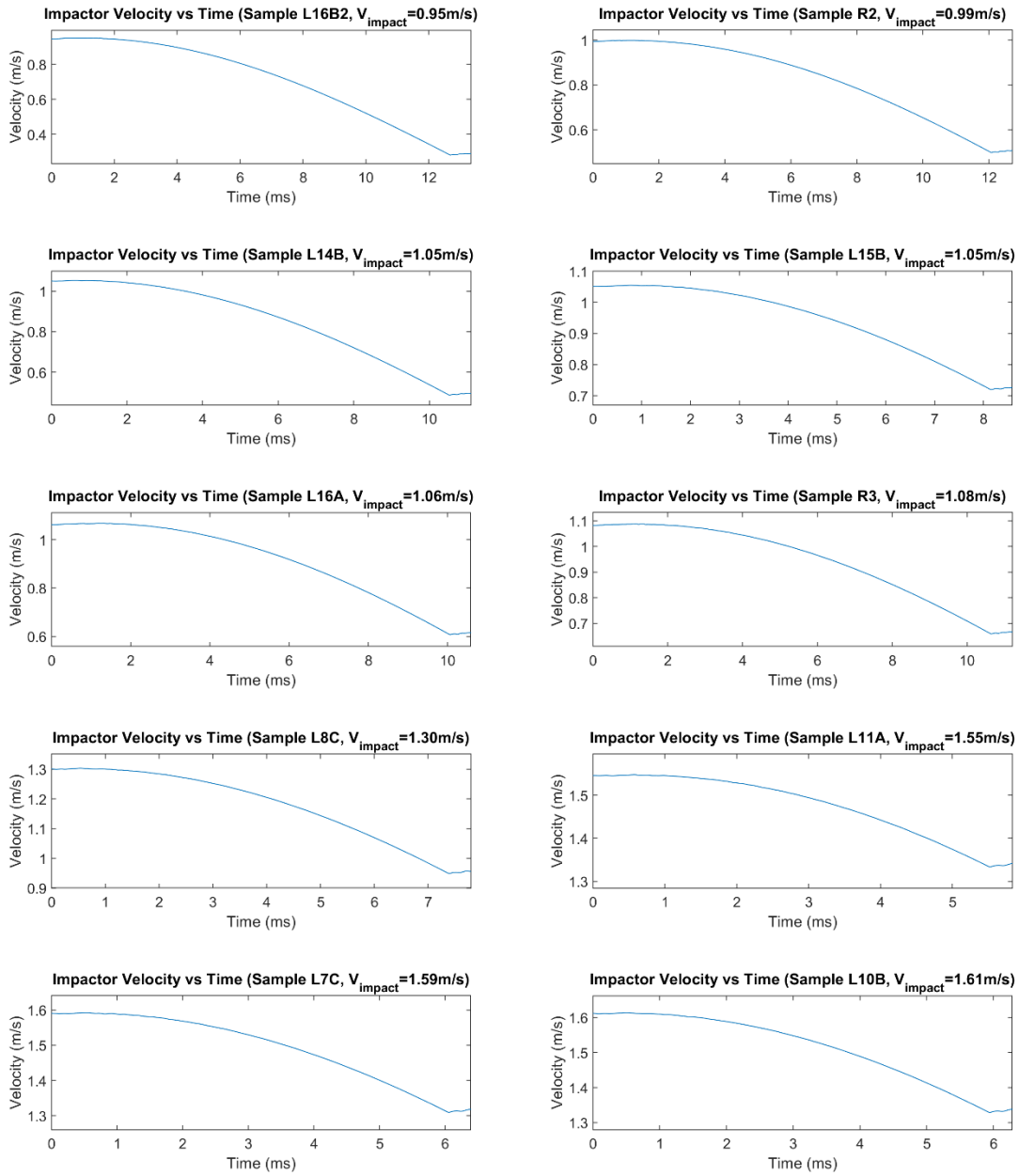

Figure 61. Impactor velocity vs time for samples with impact velocities of 1.61 m/s or less

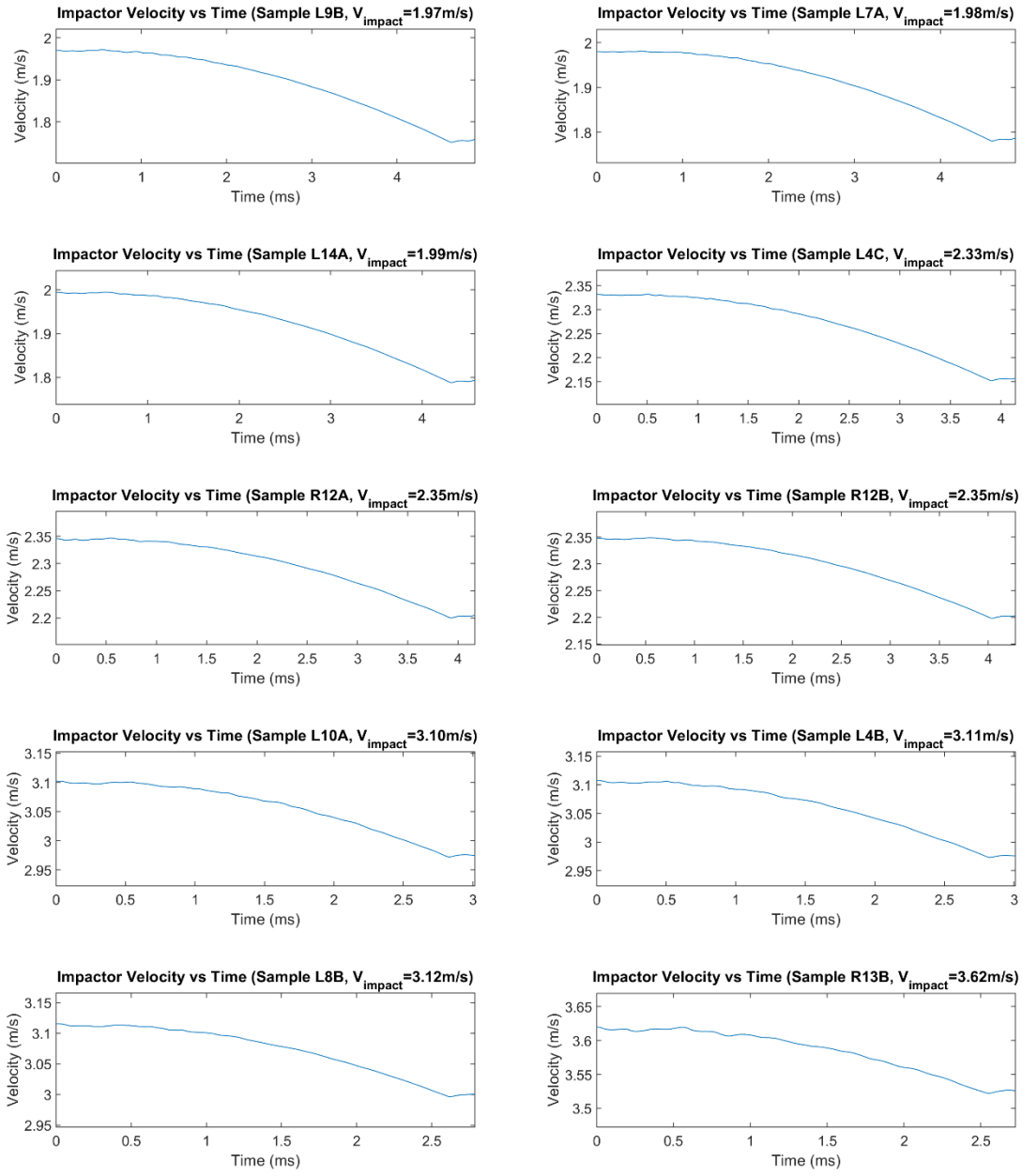

Figure 62. Impactor velocity vs time for samples with impact velocities between 1.97 m/s and 3.62 m/s

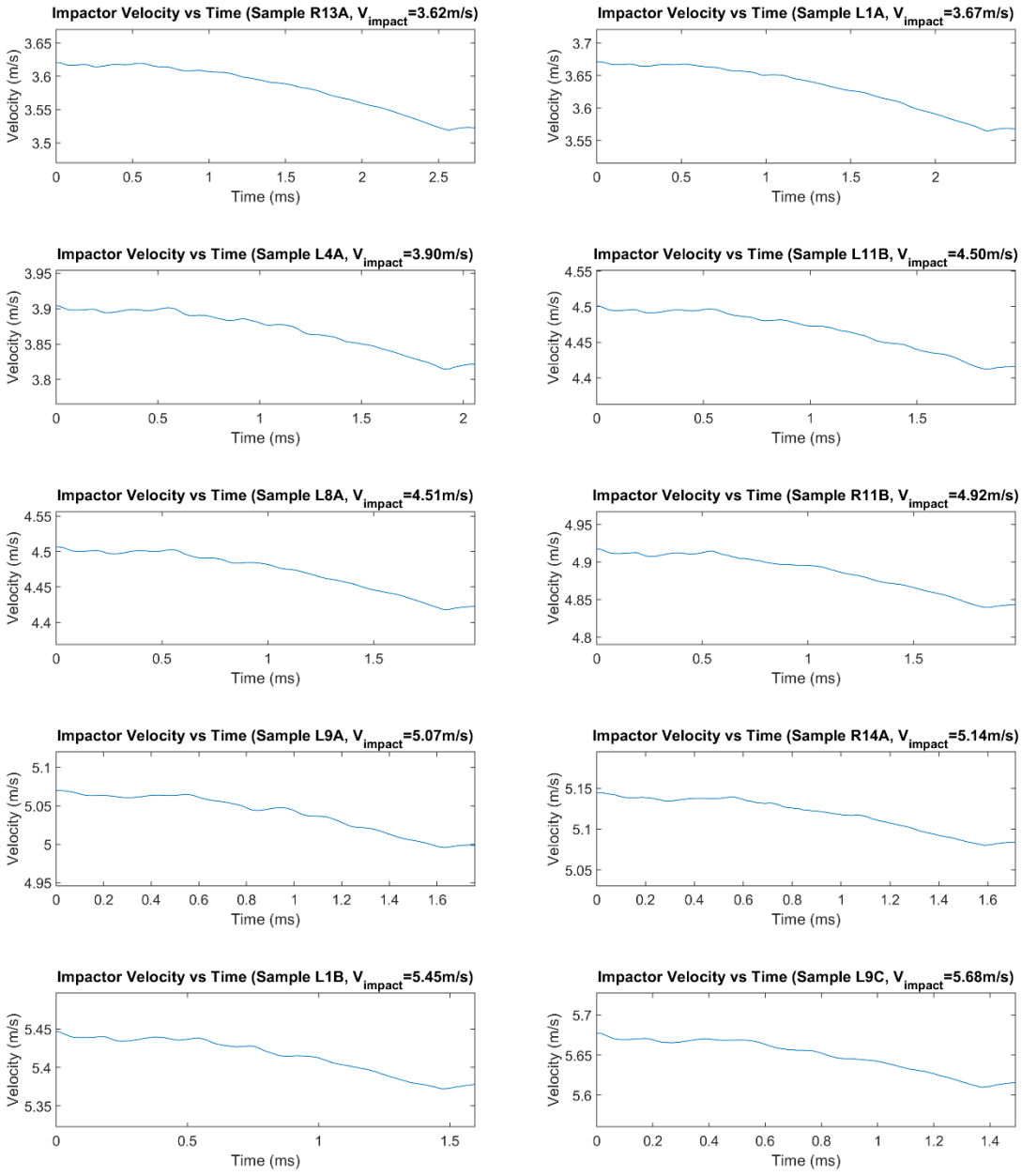

Figure 63. Impactor velocity vs time for samples with impact velocities of 3.62 m/s or greater

APPENDIX D

IMPACT TOWER MODEL FORCE AND VELOCITY PLOTS

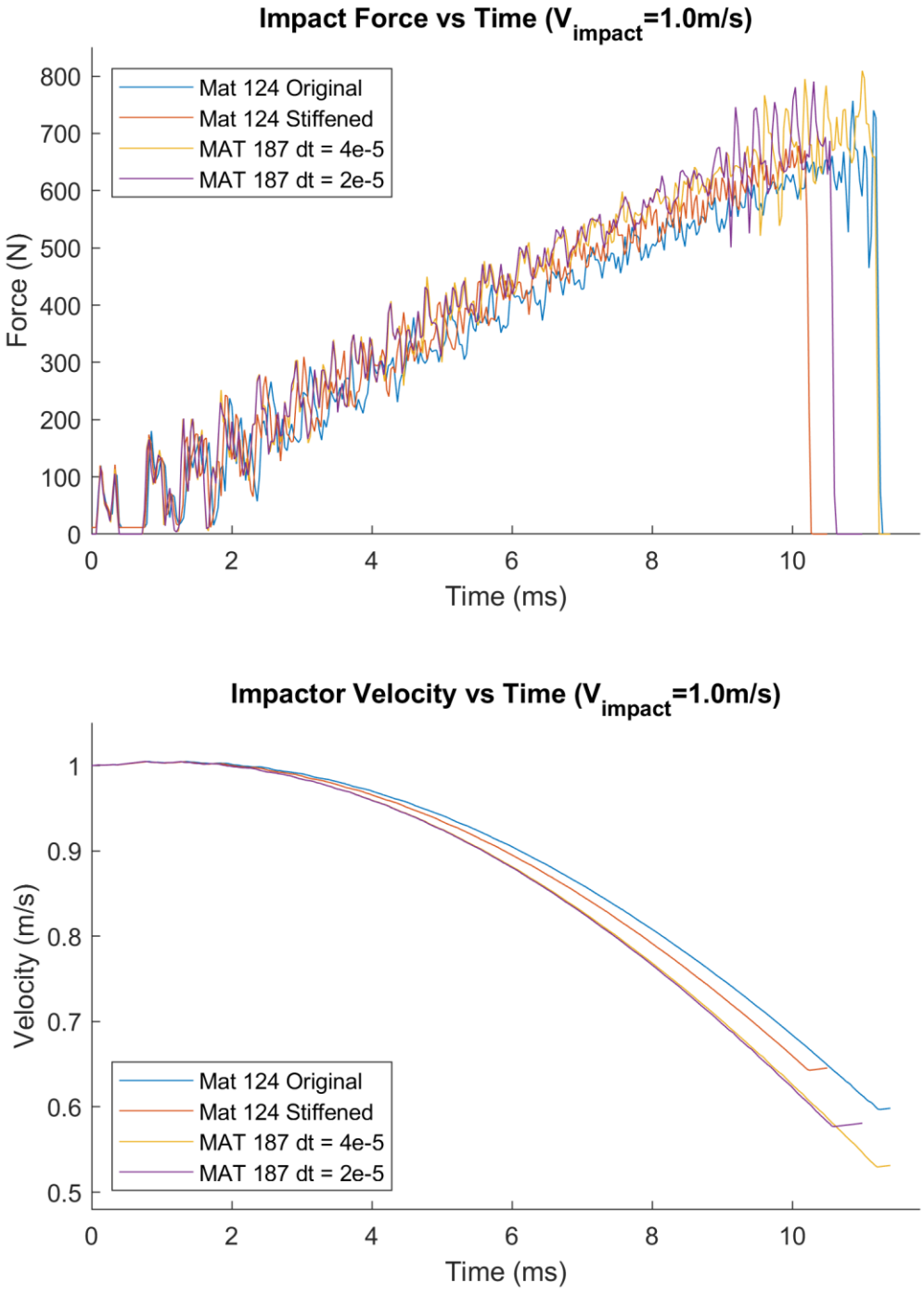

Figure 64. Impact Force vs Time and Impactor Velocity vs time for each material model in the impact tower model with an impact velocity of 1m/s

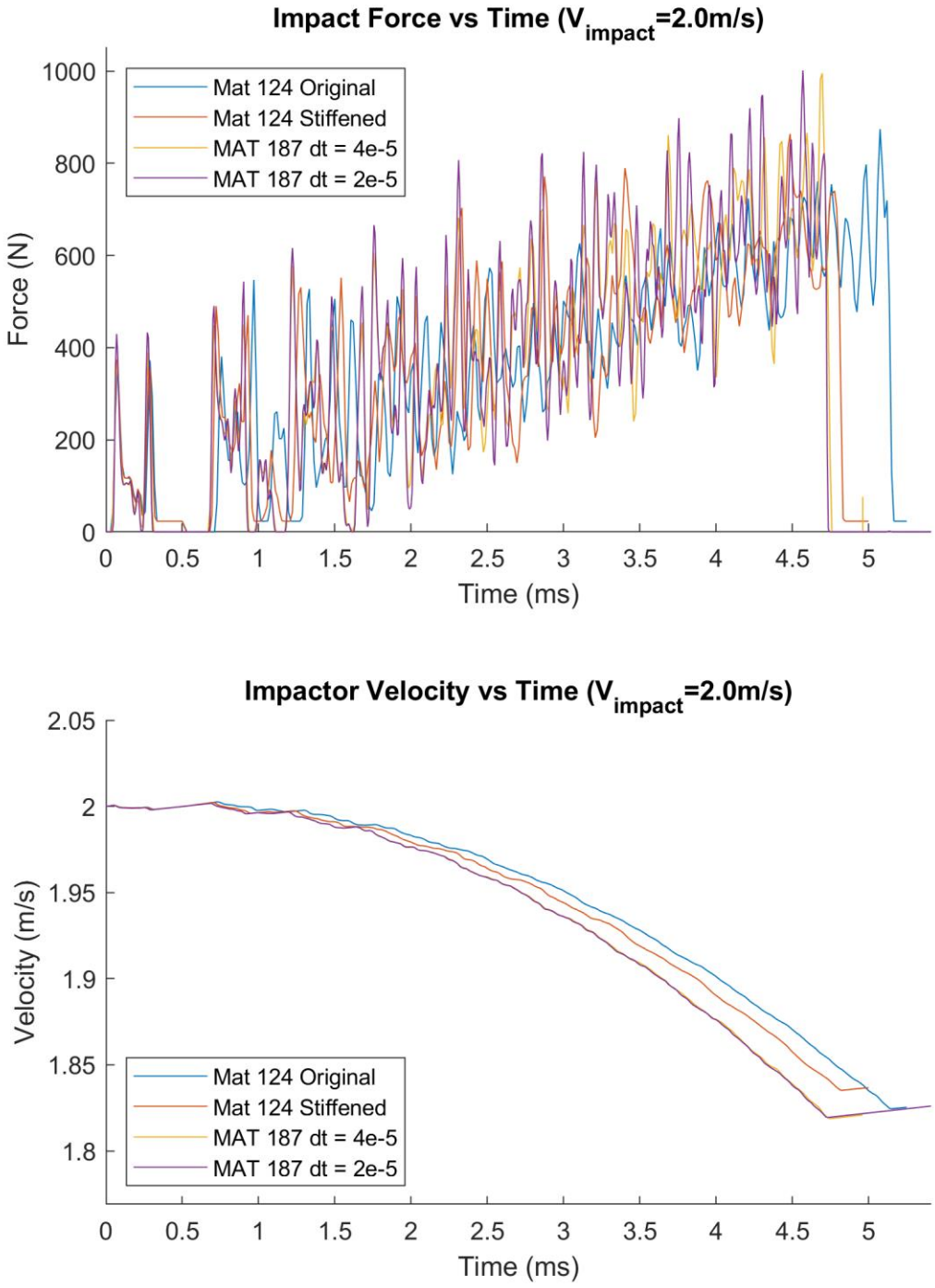

Figure 65. Impact Force vs Time and Impactor Velocity vs time for each material model in the impact tower model with an impact velocity of 2m/s

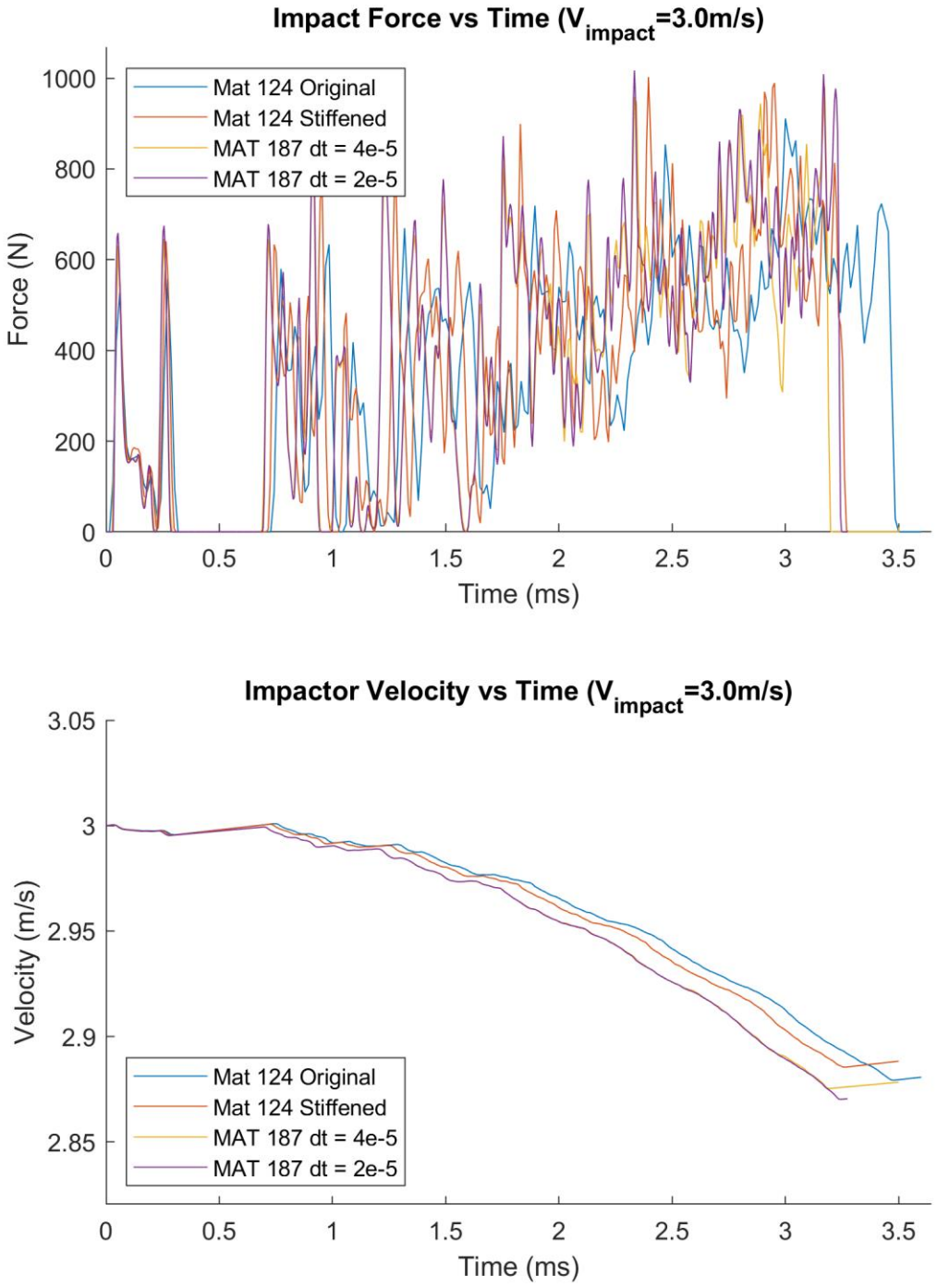

Figure 66. Impact Force vs Time and Impactor Velocity vs time for each material model in the impact tower model with an impact velocity of 3m/s

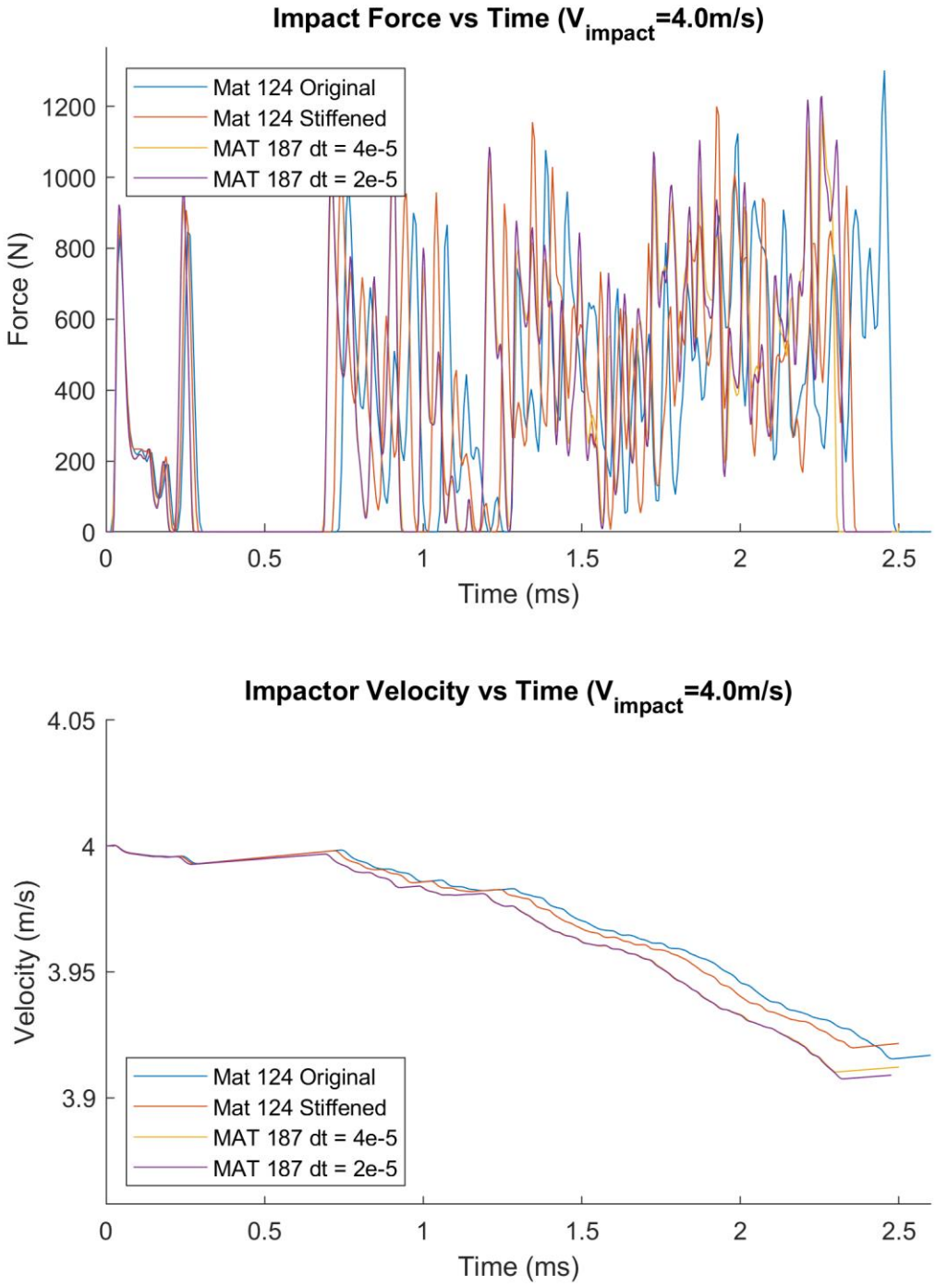

Figure 67. Impact Force vs Time and Impactor Velocity vs time for each material model in the impact tower model with an impact velocity of 4m/s

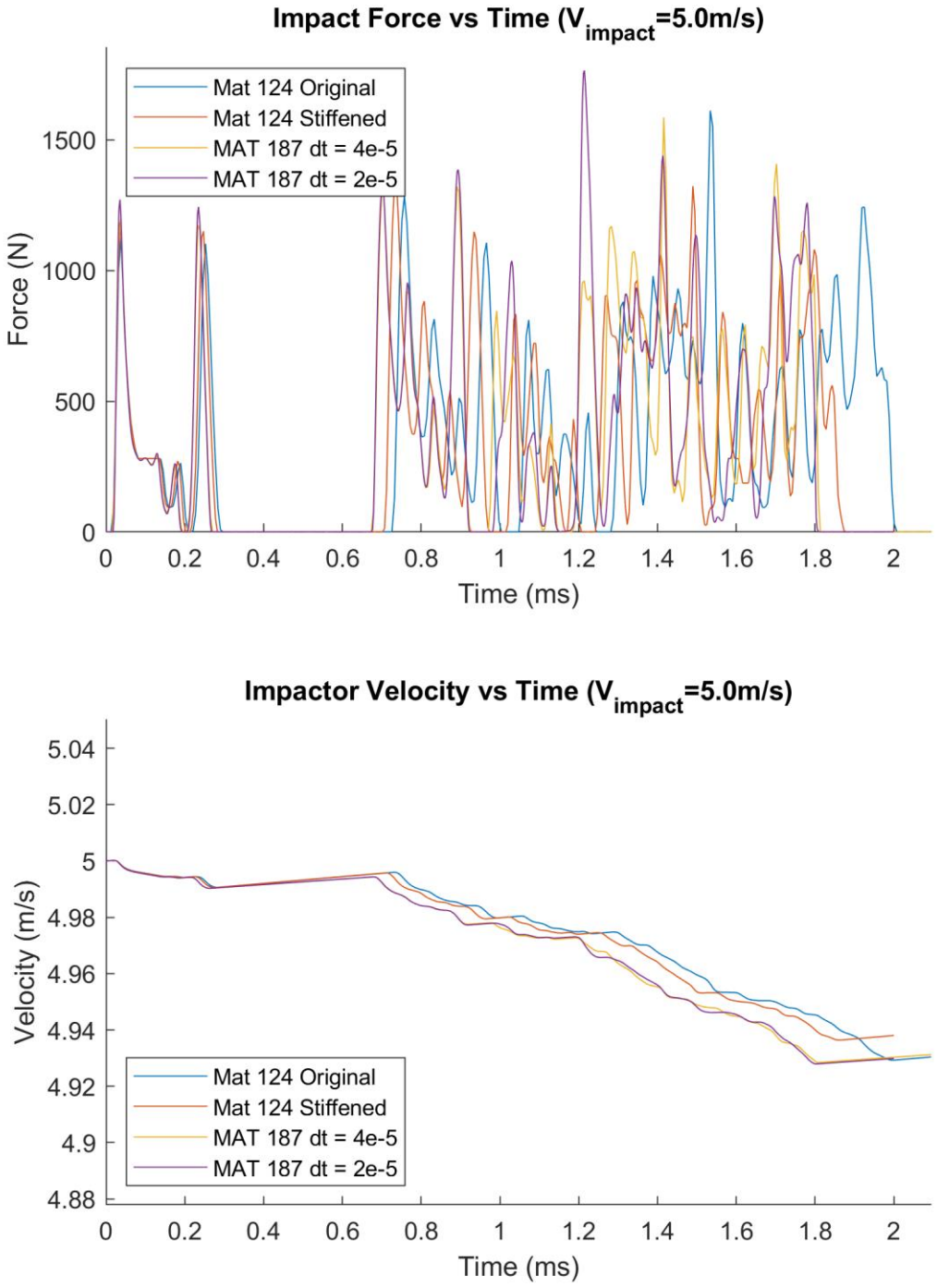

Figure 68. Impact Force vs Time and Impactor Velocity vs time for each material model in the impact tower model with an impact velocity of 5m/s

APPENDIX E

CHARPY V-NOTCH TEST PIECE CERTIFICATE OF ANALYSIS

Institute for Reference Materials and Measurements

ERM European Reference Materials

CERTIFICATE OF ANALYSIS

ERM®- FA014o N°. 23

CHARPY V-notch test pieces (nominal absorbed energy [1] 60 J)		
Parameter	Certified value [2] (J)	Uncertainty [3] (J)
Absorbed energy (KV) at 20 ± 2 °C, according to EN 10045-1 and ISO 148	58.7	1.5

1) The term absorbed energy is defined in EN 10045-1 and ISO 148 and refers to the impact energy required to break a V-notched bar of standardised dimensions.

2) Mean absorbed energy for 5 specimens (delivered as 1 set) of batch ERM®-FA014o. The certified value is traceable, via the Master Batch ERM®-FA014c of the same nominal absorbed energy (60 J), to the Charpy impact test method as described in EN 10045-1 and ISO 148. Therefore, the certified value is valid only for strikers with a 2 mm tip radius.

3) Estimated expanded uncertainty with a coverage factor k = 2, corresponding to a level of confidence of about 95 %, as defined in the Guide to the Expression of Uncertainty in Measurement (GUM), ISO, 1995.

This certificate is valid until February 2010; this validity may be extended as further evidence of stability becomes available.

NOTE

European Reference Material ERM®-FA014o is produced and certified under the responsibility of IRMM according to the principles laid down in the technical guidelines of the European Reference Materials® co-operation agreement between BAM-IRMM-LGC. Information on these guidelines is available on the Internet (http://www.erm-crm.org).

Accepted as an ERM®, Geel, April 2005

Signed:

Prof. Dr. Hendrik Emons
Unit for Reference Materials
EC - JRC - IRMM
Retieseweg 111
2440 Geel, Belgium

ERM
European Reference Materials

DESCRIPTION OF THE SAMPLE

A unit consists of five Charpy V-notch test pieces, which are rectangular steel bars of nominal dimensions 55 mm x 10 mm x 10 mm, with one V-notch, accurately machined to tolerances imposed in EN 10045-1 and ISO 148. The five specimens are packed together in a plastic bag filled with oil to prevent oxidation.

INSTRUCTIONS FOR USE

Samples of ERM®-FA014o correspond with the 'certified BCR test pieces' as referred to in EN 10045-2 (Method for the verification of impact testing machines), as well as with the 'certified reference test pieces' as defined in ISO 148-3 (Preparation and characterisation of Charpy V reference test pieces for verification of test machines). Sets of five of these certified reference test pieces are intended for the indirect verification of impact testing machines with a striker of 2 mm tip radius, according to procedures described in detail in EN 10045-2 and ISO 148-2. Special attention is drawn to cleaning of the specimens. The following procedure is recommended:

1. Wipe excess oil from the specimens with cellulose paper.
2. Immerse the specimens in a clean bath of degreasing solvent for about 5 min.
3. Wipe the specimens with cellulose paper and let dry.
4. Before testing, bring the specimens to the test temperature (20 ± 2 °C). To assure thermal equilibrium is reached, move the specimens to the test laboratory at least 12 h before the tests.

After cleaning, the user must avoid touching the specimens with the fingers (wear clean gloves). Vigorous cleaning methods affecting the roughness of the specimen surface or possibly causing deformation or indentation of the specimen edges should be avoided, as this can result in obtaining erroneous data.

After cleaning, samples need to be broken with an impact pendulum in accordance with EN 10045-1 or ISO 148 standards.

Charpy test pieces sometimes leave debris on the Charpy pendulum anvils. Therefore, the anvils must be checked regularly and if debris is found, it must be removed.

After testing, the user is recommended to inspect the traces/imprints left behind by the anvils and hammer on the two halves of the broken specimen. Asymmetry of these marks can indicate problems with the machine geometry or the positioning of the sample prior to impact. If so desired, broken samples can be stored for later inspection of the anvil and striker marks.

STORAGE

Specimens should be kept at ambient temperature in their original packing until used.

SAFETY INFORMATION

Precautions need to be taken to avoid injury of the operator by broken specimens when operating the Charpy impact pendulum.

METHOD USED FOR CERTIFICATION

Charpy pendulum impact tests in accordance with EN 10045-1 and ISO 148, using strikers with 2 mm tip radius.

ERM
European Reference Materials

PARTICIPANTS

- Cogne Acciai Speciali, Aosta (IT)
- European Commission, Joint Research Centre, Institute for Reference Materials and Measurements, Geel (BE)
- Laboratoire National d'Essais, Trappes (FR)

LEGAL NOTICE

Neither IRMM, its contractors nor any person acting on their behalf:

(a) make any warranty or representation, express or implied, that the use of any information, material, apparatus, method or process disclosed in this document does not infringe any privately owned intellectual property rights; or

(b) assume any liability with respect to, or for damages resulting from, the use of any information, material, apparatus, method or process disclosed in this document save for loss or damage arising solely and directly from the negligence of IRMM.

NOTE

A detailed technical report of the certification is available on www.erm-crm.org. A paper copy can be obtained from IRMM on explicit request.

European Commission – Joint Research Centre
Institute for Reference Materials and Measurements (IRMM)
Retieseweg 111, B - 2440 Geel (Belgium)
Telephone: +32-14-571.722 - Telefax: +32-14-590.406